

UNIVERSITÄT FÜR BODENKULTUR  
INSTITUT FÜR GEOTECHNIK

Peter Mayrhofer

**GEOLOGICAL AND GEOTECHNICAL  
CHARACTERIZATION OF GROUND CONDITIONS IN  
BADONG COUNTY, CHINA**



2013

BETREUER: Prof. Dr.-Ing. Wei Wu  
MITBETREUER: Ao. Univ. Prof. i. R. Ing. Dr. phil. Rudolf Schwingenschlögl

DIPLOMARBEIT NR. 360

# Acknowledgement

This master thesis has been carried out at the Institute of Geotechnical Engineering, University of Natural Resources and Life Sciences, Vienna, since autumn 2012. A number of people deserve thanks for their support and help. It is therefore my greatest pleasure to express my gratitude to them all in this acknowledgement.

I would like to express my gratitude to my supervisor Professor Wei Wu for the valuable comments, remarks and engagement through the process of this master thesis. He gave me the opportunity to research for this thesis in Wuhan, China.

I want to thank Professor Wei Xiang who gave me the opportunity to conduct my study in his research group at the China University of Geosciences (Wuhan), Department of Geotechnics and Engineering Geology, Faculty of Engineering. Without his help in organising both, the field work as well as the tests in the laboratory, this thesis would not have been possible.

I would like to convey my gratitude to my second supervisor Professor Rudolf Schwingenschlögl for his guidance, valuable comments and encouragement from the start until the end of my study.

Many students of the Faculty of Engineering, Wuhan have helped me in the study, being always generous with their time to respond to me whenever I approached them for data, for material and for discussions throughout the four months of challenge on this research in China. Especially I thank student Gong Si Yi who gave a great first introduction into the geology of the Badong area, students Jia Hailiang and Wang Fenghua who accompanied me during the field work, Dr. Jinge Wang and Dr. Cui for their support and valuable suggestions and in Austria PhD student Shun Wang for his help in searching for data, PhD student Miguel Cabrera and Dr. Madhu Sudan Acharya for suggestions in the simulations. I would like to thank Professor Franz Ottner for help in interpretation of the XRD-Test.

I wish to express my gratitude to Jessica Northey and Julie Northey for their linguistic support with regard to the English language. However, I am the only person responsible for remaining errors in the thesis.

I would like to acknowledge the financial, academic and technical support of the University of Natural Resources and Life Sciences, Vienna and its staff, particularly in the award of a Research Studentship that provided the necessary financial support for this research.

Last but not least, all of my friends and family. Each of you can share in this accomplishment, for without your support it would not have been possible.

# Abstract

Relocation activity due to the Three Gorges Project is already completed. However, there are still many construction activities in the area around relocated Badong town. All construction activities take place in the specific geological environment of the Badong area. Therefore slope stability is of great concern.

This thesis presents a preliminary study of the ground conditions around Badong, where small shallow landslides due to anthropogenic activity are often observed. We will focus on slope failures in three characteristic ground conditions. First, there are various ancient landslides around Badong town. Investigation of former sliding surfaces is of great interest to national and international research community. But for shallow landslides/slope failures in these ancient landslides, the properties and the structural pattern of the upper mass is of importance. The second characteristic slopes with high construction activities are those on purple mudstone. The rocks on these slopes are highly weathered, so that the rock has been largely disintegrated into soil. The third characteristic slopes are rock slopes on marlstone and limestone. Though often only moderately weathered, the decay rate rises due to exposure after cutting. Weak interlayers of the rock are a special feature of this type of slope.

Usually foundations on ancient landslide soil have very low strength. A range of  $18^\circ$  to  $28^\circ$  of the friction angle and a range of 24 kPa to over 30 kPa of cohesion can be assumed. The strength parameters of the purple mudstone vary in a high range, where further investigation is recommended. The weak layer in marlstone/limestone possesses steeper dip angle than the slope angle, so an applied surcharge load has only minor influence on the slope stability. A simulated cutting of the rock mass with the ensuing weathering on the surface and along the joints shows a remarkable decrease in the slope stability.

Furthermore, numerical analysis is carried out with the commercial software Geoslope. Admittedly, such analyses are mainly qualitative as the ground conditions may vary significantly from slope to slope. The tests, carried out for this thesis, agree well with data in literature.

# CONTENT

1	INTRODUCTION .....	1
1.1	Badong town .....	2
1.2	Geological Background .....	2
1.2.1	Geology of China .....	2
1.2.2	Geology of Three Gorges Reservoir Area .....	2
1.2.3	Badong Formation .....	5
1.2.3.1	Characteristics of T <sub>2</sub> b <sup>1</sup> .....	6
1.2.3.2	Characteristics of T <sub>2</sub> b <sup>2</sup> .....	6
1.2.3.3	Characteristics of T <sub>2</sub> b <sup>3</sup> .....	6
1.2.3.4	Characteristic of T <sub>2</sub> b <sup>4</sup> .....	7
1.2.3.5	Cleavage structure and Joints .....	7
1.2.3.6	Rock Quality Designation (RQD) Value .....	8
1.2.3.7	Mechanical properties of the Badong group .....	8
1.2.4	Weathering characters .....	9
1.2.5	Hazard of toppling on argillaceous limestone .....	14
1.2.6	Weathering conditions on purple mudstone .....	14
1.3	Climate .....	16
1.4	The Three Gorges Project (TGP) .....	17
1.4.1	Impacts of- and measurements around the TGP .....	17
1.4.1.1	Energy requirement .....	18
1.4.1.2	Hydrological impacts .....	19
1.4.1.3	Ecological impact .....	19
1.4.1.4	Requirement of settlement area and relocation policy .....	20
1.5	Types of slope in Badong County .....	22
1.5.1	Rock slopes .....	22
1.5.2	Soil slopes .....	22
1.6	Landslides .....	23
1.6.1	Historical Landslide Situations .....	26
1.6.2	Causes of shallow landslides: The influence of rainfall and human activity .....	27
1.6.2.1	Rain- induced landslides, an overview .....	27
1.6.2.2	Slope failure on T <sub>2</sub> b <sup>3</sup> .....	28
1.6.2.3	Recent small landslides on ancient landslides .....	29
1.6.2.4	Re- profiling and inappropriate cutting .....	30
1.7	Slope stabilisation and protection methods .....	31
1.8	Slope management .....	31

2	METHODS.....	34
2.1	Selected sites.....	34
2.2	Field Investigation .....	36
2.2.1	Designation of Rock.....	36
2.2.1.1	Particle Size.....	37
2.2.1.2	Determination of the hardness (scratch hardness).....	37
2.2.1.3	Determination of the rock strength (Schmidt Hammer).....	37
2.2.1.4	Calcium carbonate content .....	38
2.2.1.5	Colour .....	38
2.2.1.6	Odour.....	38
2.2.1.7	Condition of Rock .....	38
2.2.2	Designation of mineral soil.....	40
2.2.2.1	Particle size.....	40
2.3	Laboratory tests.....	41
2.3.1	Water Content Test .....	41
2.3.2	Density Core Cutter Method .....	41
2.3.3	Triaxial test .....	42
2.3.3.1	Specimens preparation and saturation .....	42
2.3.4	Unconsolidated undrained triaxial test.....	42
2.3.5	Quick Shear test within the weak layer.....	44
2.3.6	X-Ray Diffraction Test .....	45
2.4	Rock quality designation index (RQD), Rock mass rating (RMR).....	46
2.4.1	Rock quality designation index (RQD) .....	46
2.4.2	Rock mass rating (RMR).....	47
2.5	Stability analyses .....	49
2.5.1	Factor of safety calculation method Morgenstern Price.....	49
3	RESULTS.....	51
3.1	Foundations on ancient landslide mass .....	51
3.1.1	Investigated site .....	51
3.1.2	Field Investigation .....	52
3.1.2.1	The grain distribution .....	53
3.1.3	Laboratory Tests .....	54
3.1.3.1	Water content $w$ , dry density $\rho_d$ : .....	54
3.1.3.2	Unconsolidated undrained triaxial test.....	54
3.1.4	Former published results.....	56
3.1.4.1	Shear parameter of the Huangtupo sliding mass.....	56
3.1.5	Simulation of slope stability under different boundary conditions .....	57
3.1.5.1	Simulation: Excavation on ancient sliding mass on Xirangpo .....	57

3.2	Foundations on $T_2b^2$ .....	60
3.2.1	Investigated site .....	60
3.2.2	Field Investigation .....	61
3.2.2.1	Rock foundation versus soil foundation.....	62
3.2.3	Laboratory Tests .....	63
3.2.3.1	XRD-Test .....	63
3.2.4	Former published results.....	63
3.2.5	Simulation of slope stability under different boundary conditions .....	64
3.2.5.1	Input parameter .....	64
3.2.5.2	Simulation: Excavation on $T_2b^2$ highly decayed rock.....	65
3.3	Foundation on $T_2b^3$ .....	68
3.3.1	Investigated site .....	68
3.3.2	Field Investigation .....	69
3.3.2.1	Artificial opening profile.....	69
3.3.3	Laboratory tests.....	73
3.3.3.1	Shear test of weak zones between the layers.....	73
3.3.3.2	XRD-Test .....	75
3.3.3.3	Mineral content of the weak layer .....	75
3.3.3.4	Watercontent w: .....	76
3.3.4	Rock mass rating (RMR).....	76
3.3.5	Simulation of slope stability under different boundary conditions .....	77
3.3.5.1	Simulation: Excavation on $T_2b^3$ slightly weathered rock.....	77
4	DISCUSSION AND CONCLUSIONS.....	86
4.1	Ancient landslide soil.....	86
4.2	Decayed rock and soil on geological environment of $T_2b^2$ .....	87
4.3	Rock on geological environment of $T_2b^3$ .....	88
5	LITERATURE.....	90
6	FIGURES .....	93
7	TABLES.....	97
8	ANNEX.....	98
8.1	Triaxial test data .....	98
8.2	Shear test data .....	102
8.3	Schmidt Hammer records.....	102
8.3.1	Records and conversion of $T_2b^3$ .....	102
8.3.2	Records and conversion of $T_2b^2$ .....	103
8.3.3	Conversion table.....	103
8.4	Table of Schnell (Smoltczyk et al. 2001, p. 122).....	106

# 1 Introduction

The area around Badong town is highly affected by the project of the Three Gorges Dam. The maximal level of the river is now 175 m.a.s.l.<sup>1</sup> The prefilling level was 70 m.a.s.l. (Wang et al. 2013, p. 3). Relocation activity due to the impoundment is already finished. However, there are still many construction activities. Generally, the Three Gorges Project (TGP) enhanced trading activities and therefore the demand for infrastructure, e.g. currently a road under construction which connects the Huangtupo Slope with new Badong Town. Additionally the slope of Huangtupo (an ancient landslide), which was formerly considered as stable, showed moderate movements. About 18,000 people had been relocated onto this slope in the 1980s and now have to be relocated again. For this new houses will be built on the north side of the river. All these individual construction activities take place in the geological environment of the Badong area, therefore slope stability is of great importance. This thesis presents a preliminary study of the characteristic ground conditions of this environment. During the field inspection small shallow landslides due to anthropogenic activity were often observed. We will focus on these landslides. Particularly after heavy rainfall, the number of landslides increases. This, combined with inappropriate cutting of slopes for foundations and application of external loads, leads to an increasing risk of slope failures.

This thesis considers three characteristic ground conditions and the corresponding risk of slope failures. Characteristics in respect of subsidence are not studied, as data of deeper ground conditions were not available. First, there are various ancient landslides around Badong town. Investigation of former sliding surfaces, to assess the risk of reactivation, is of great interest to national and international researchers. But for shallow landslides/slope failures on these ancient landslides, the properties and the structural pattern of the upper mass is of importance. The second characteristic slopes with high construction activities are those on purple mudstone. The rocks on these slopes are highly weathered, so that the rock has been largely disintegrated into soil. The third characteristic slope is a rock slope on marlstone and limestone. Though often only moderately weathered, the decay rate rises due to exposure after cutting. Weak interlayers of the rock are a special feature on this type of slope.

The thesis describes these characteristics through performed field investigation and laboratory tests. The data obtained are compared with data from previous investigations. Furthermore, numerical analysis is carried out with Geoslope software. However, such analyses are mainly qualitative as the ground conditions may vary significantly from slope to slope.

---

<sup>1</sup> Meter above sea level

## 1.1 Badong town

Badong town is a new immigration residential area in the Three Gorges Reservoir. It is located on the south side of the Yangtze River and it is seriously affected by landslides (Chai et al. 2012, p. 1). It is the transition area between the Xiling Gorge and the Wu Gorge. The town is divided into five districts and the borders are defined by gullies (see Figure 1). These five districts are from west to east: Xirangpo, Yuntuo, Baituo, Daping and Huangtupo. The area is composed of valleys and low mountains.



Figure 1: Overview of Badong Town (Google Earth 2005)

## 1.2 Geological Background

### 1.2.1 Geology of China

China is located at the junction of the circum-Pacific tectonic region and Himalayan tectonic region. The main geodynamic source of mainland China is the subduction of the Pacific plate, an extrusion activity of the Indian Oceanic plate (in relation to the Pacific plate). Two tectonic regions create the tectonic framework and basic topographical configuration of China. This is the Qinghai-Tibet Plateau and the Himalayan Mountains, formed at the edge of the Indian Oceanic plate and Asian plate (Wang 2009, p. 21).

### 1.2.2 Geology of Three Gorges Reservoir Area

Geological research has shown that at Qutang Gorge in Fengjie County the ancient Chuanjiang River was merged with the Xiajiang River, to form today's Yangtze River. Before this, the Chuanjiang River flowed west and the Xiajiang River flowed east. Both rivers eroded headward in direction of the Wushan Qiyueshan area. After the Yangtze was formed, three dynamic water forces acted in a short

time: the “water saw” undercut the Chuanjiang river<sup>2</sup> on the top of the watershed, the Xiajiang River eroded headward, and an earthquake occurred, induced by underwater river collapse or karst collapse. These three forces reshaped the bank structure. Surface collapse and landsliding contributed to this process and overlapped with the alluvial-diluvial actions (Wang 2009, p. 21). Also in Fengjie the regional sedimentary faces divide, into the west, which is mostly Jurassic red beds, and the east, mostly Triassic carbonate rock (Wang 2009, p. 15).

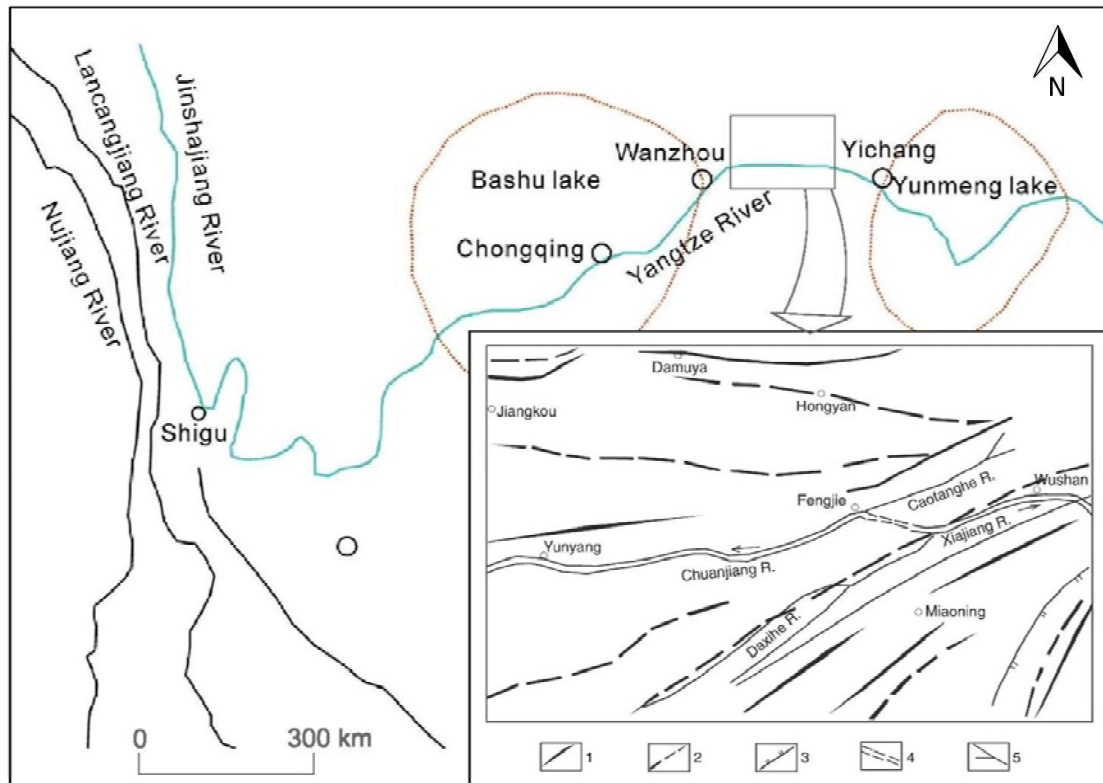


Figure 2: Three rivers (Jinshajiang, Lancangjiang(Mekong) and Nujiang(Salween river)) flow to the north until Jinshajiang turns towards east to form the Yangtze River (Wang 2009, p. 22); Small Figure: Structural outline map in the connected area between Chuan and Xiajiang rivers. 1 Anticline; 2 syncline; 3 faults; 4 Qutang Gorge at present; 5 water system (Wang 2009, p. 16)

In the area around Badong the river flows along the Guandukou syncline. The slopes are made up of a monoclinical mountain and some small-scale relaxed folds or fold distortion, with strong extrusion in some parts. It is a broad and relaxed syncline with an axial plane inclined slightly to the south. The dip angle of the north wing is 10°-25° and the south wing between 20° and 48° (Wang 2009, p. 25). Therefore all layers dip towards the river according to the natural slope. This implies a hazard of downhill-sliding, upon human activities combined with water-influence (Figure 3).

<sup>2</sup> Often named as Sichuan river

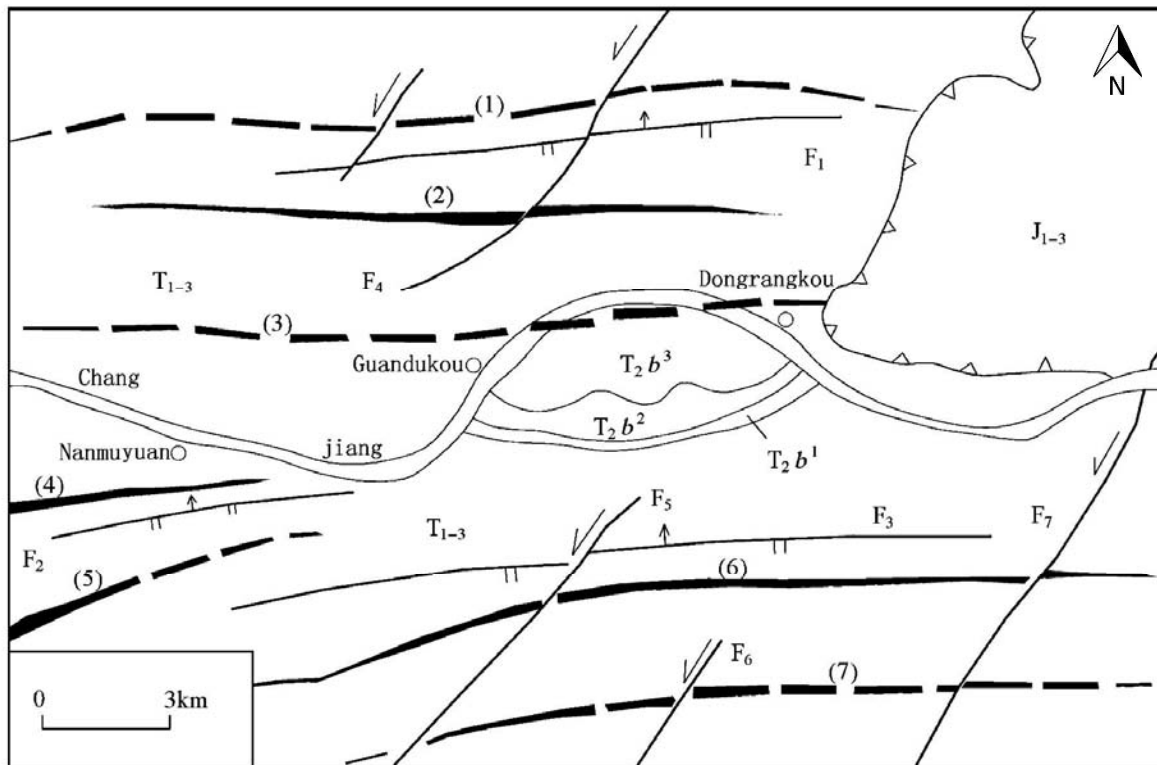


Figure 3: Areal structure sketch of Badong slope in the Three Gorges of the Yangtze River; 1-Jurassic System; 2-Triassic System; 3-continental deposit basin; 4-anticline structure axis; 5-syncline structure axis; 6-reversed fault; 7-shift fault  
 (1)-Huofeng syncline; (2) Xiaogaoshan anticline; (3)Guanducou syncline;(4)Namuyuan anticline; (5)Duping syncline; (6)Baifuping anticline; (7)Fengcuiya syncline.  
 F<sub>1</sub>-Fuangyintang fault; F<sub>2</sub>-Bingshuijing fault; F<sub>3</sub>-Maluchi fault; F<sub>4</sub>-Gongqiao fault; F<sub>5</sub>-Yeluchi fault; F<sub>6</sub>-Meiziya fault; F<sub>7</sub>-Niukou fault (Wang 2009, p. 26)

The tectonic formation around the Badong area belongs to the Fengji-Wushan-Badong structural belt (Qi et al. 2009, p. 933), it is located at the interlocking site of the Daba Mountain arc fold belt . The Qiyueshan fracture belt and a series of compact folds are found there too. The Yangtze River valley passes parallel to most structure lines or intersects at small angles. The total area is bedded into the middle of the Yantze pseudo-platform (Wu et al. 2011, p. 2). The geology of Badong is a site made up of six members which have different layers. The Badong geological formation originates from the middle Triassic system (Qi et al. 2009, p. 933).

### 1.2.3 Badong Formation

The upper levels of members five and six are mostly eroded and therefore not relevant for the problems in concern of the Badong area. The most common members are therefore one to four and will be considered here.

The Badong Formation is described by the following abbreviation:

T:..... Triassic

Number<sub>2</sub>: ..... Second epoch of the Triassic period

B:..... Badong

Numbers<sup>1,2,3...</sup>: ... The (1<sup>th</sup>, 2<sup>nd</sup>, ...) Member of the Badong Formation

Depending on the region, various strata and thickness of the Badong Formations can be observed.

The following figure shows the stratigraphical structure with different thicknesses in Changhan (left) and Dawoshan (right) regions of Badong.

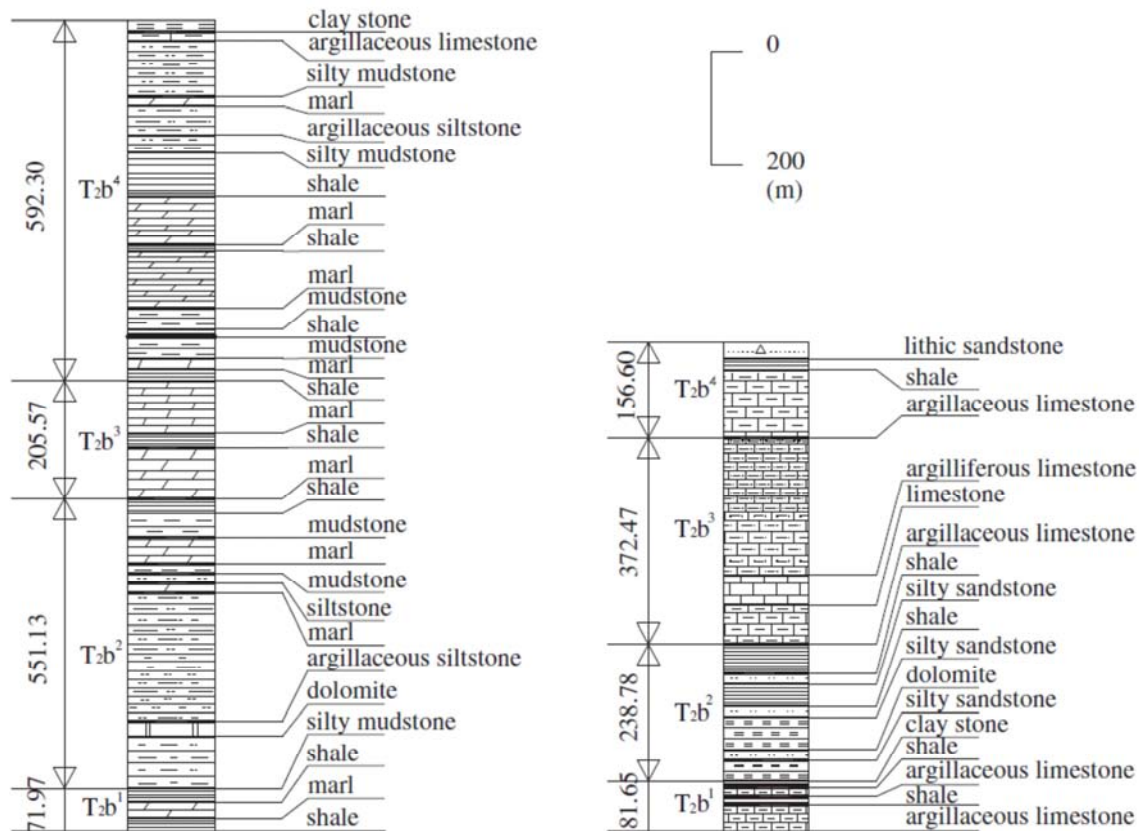


Figure 4: Two typical stratigraphic columns showing the group of argillaceous limestone rocks (Qi et al. 2009, p. 933)

The following sections give the general information about the main characteristics of the Badong Formation. These characteristics however are not definite values, as aspects such as the thickness are variable in respect of the location.

### **1.2.3.1 Characteristics of $T_2b^1$**

- About 80 m thick
- Major content: grey, grey-yellow and yellow green marl, argillaceous limestone, some clay bearing limestone and thin layer of calcareous shale (Qi et al. 2009, p. 934)

### **1.2.3.2 Characteristics of $T_2b^2$**

- From 100 to 241 m thick
- Composed of purplish red mudstone
- Small amount of grey yellow, grey green mudstone, patches of sandy claystone, silty claystone and calcareous claystone interbedding with various thick siltstone, fine grain sandstone and calcareous sandstone (Qi et al. 2009, p. 934)

### **1.2.3.3 Characteristics of $T_2b^3$**

- Over 300 m thick
- The thickness of the predominant layer varies from middle-thick to thin
- The lower part:
  - grey to grey- black limestone, clay bearing limestone and marl with intercalated calcareous shale and calcareous clay stone which can result in weak layers
  - consists mainly of hard rock
- The middle part:
  - grey yellow to grey green siltstone, silty claystone and calcareous shale
- The upper part close to  $T_2b^4$ :
  - grey clay bearing limestone, marl and calcareous shale interbedding with purple red calcareous siltstone, grey green calcareous siltstone and calcareous claystone with various thickness
  - Consists of hard rock interlayered with soft rock like marl-stone (Qi et al. 2009, p. 934)

The soft interlayers of  $T_2b^3$  which represent the weak zones can be classified into three types (Chai et al. 2012, p. 5ff.):

#### Type 1 Clay interlayer

The main mineral composition is clay with more than 50%, mostly illite and chlorite (Chai et al. 2012, p. 5ff.). This weak layer can display a very low shear strength, which means a very low cohesion and

friction angle. Analyses from the terrain of the weak zone of the Badong Formation show that the cohesion can be as low as 5 kPa, and the lowest measured internal friction angle is about  $10.3^\circ$  (Wang 2009, p. 95). The mineral contents of incompetent beds of  $T_2b^3$  are similar to those of landslide slide zones (Chai et al. 2012, p. 11). Another character is the weak expansibility. It is very likely to be weathered and eroded; it would form a cavity if it is set out, or would be transformed into a muddy interlayer if the weathering takes place underground.

#### Type 2 Crushed beds

Crushed beds are often found at the interface of soft and hard rock masses which are formed under multi-stage tectonic compression. Under long-term corrosion by groundwater, these crushed beds would transform into gravelly clay, as their clay content would increase. These crushed beds are located over the groundwater table (e.g. after river incision) and can be re-cemented with calcite. If the beds are wide enough and there is influence of compression and displacement, a tectonic fracture zone can be formed.

#### Type 3 Groundwater corrosion zone

Groundwater corrosion zones are often composed of marl, with characteristics of weathering and corrosion. The zones are often discontinuous argillaceous bands, because the corrosion generates along the surfaces of layers, joints and fractures.

#### **1.2.3.4 Characteristic of $T_2b^4$**

- about 110 m thick
- purple red mudstone with middle to thick thickness is predominant
- small amount of argillaceous limestone with intercalated calcareous shale (Qi et al. 2009, p. 934)

#### **1.2.3.5 Cleavage structure and Joints**

The cleavage structure of Badong's geological formation is dense in development and occurs often in strata. It is an important factor for the stability of slopes. The cleavages are nearly vertical to the fold core. The angle between the cleavage and stratum are between  $72^\circ$  and  $90^\circ$  in the third member and between  $36^\circ$  and  $60^\circ$  in the second member of the Badong group (Wang 2009, p. 90). The cleavage spacing of the second and the fourth member are in a range of mm to cm whereas in the third member it can reach to tens of centimetre levels. It is also observed that thinner strata develop better, that a higher content of mud has more cleavages than a lower content and that the upper stratum develops better than the lower stratum (Wang 2009, p. 91).

There are several joints in the Badong area. The east-west joint is often found from the riverfront to the core of the Guandukou syncline. It is probably formed as a result of stress in the south-north direction. The south-north joint can be divided into shear joints and tension joints. The first is steep, level, regular and reaches from tens to hundreds of metres, with spacing of 500-600 meters. The tension joint, mainly in hard rock mass, has an irregular, nonlinear face and normally extends for tens of metres. Most tension joints have a branch end and the gap is filled by calcite. The predominant direction is nearly vertical to the cleavage side. North- northeast and north- northwest joints are in the pattern of conjugate joints and appear in different lithological sections. Normally they have a range of several cm to about 20 m. So the main direction of the pressure stress in conjugate joints is northeast (Wang 2009, p. 93).

### 1.2.3.6 Rock Quality Designation (RQD) Value

Of a block diameter 0.1 m, the mean RQD of various surveying points in the Badong formation is remarkably high of more than 90%. On a larger block diameter of 0.5-0.7 m the RQD is lower. It is mainly around 60% and among the different samples the scatter is very high. So the structure of the rock mass is designed by its pattern of layers or the layered fracture patterns (Wang 2009, p. 94).

### 1.2.3.7 Mechanical properties of the Badong group

On the basis of various existing data from indoor shear tests and considering factors such as geological and structural properties of various rock masses in the area of Badong, the strength parameters can be determined. The Mohr- Coulomb criteria are elaborated by the estimation method of Hoek- Brown (Wang 2009, p. 98) as displayed in Table 1 and Table 2.

	$T_2b^4$	$T_2b^3$	$T_2b^2$	$T_2b^1$	$T_{1j}^3$	$T_{1j}^2$	$T_{1j}^1$
Density $\rho(\text{g/cm}^3)$	2.55	2.63	2.55	2.35	2.68	2.68	2.66
Deformation modulus $E_m(\text{GPa})$	2.0	4.0	3.0	1.5	10.0	9.0	7.0
Poisson's ratio $\mu$	0.3	0.25	0.3	0.35	0.2	0.2	0.25
Uniaxial stress strength $\sigma_{mc}$ (MPa)	0.8	2.5	1.0	0.15	5.0	4.5	4.0
Uniaxial tension strength $\sigma_{mt}$ (MPa)	0.03	0.50	0.05	0.01	0.5	0.45	0.4
Shear strength $C_m$ (kPa)	240	400	260	165	1100	1100	1000
$\phi_m$ ( $^\circ$ )	28	38	30	22	41	41	39

Table 1: Recommended parametric values for mechanical calculation of rock masses (Wang 2009, p. 98)

Type of structure plane	Shear Strength	
	$c_j$ (kPa)	$\phi$ (°)
T <sub>2</sub> b <sup>3</sup> mudstone layer	60	31
T <sub>2</sub> b <sup>3</sup> mudstone cleavage plane	40	30
T <sub>2</sub> b <sup>2</sup> calcareous muddy siltstone plane	20	31
T <sub>2</sub> b <sup>2</sup> calcareous muddy siltstone cleavage plane	8	30
T <sub>2</sub> b <sup>1</sup> marlite plane	8	25
T <sub>1j</sub> pelmicrite plane	30	32

Table 2: Recommended parametric values for calculation of structure planes (Wang 2009, p. 98)

#### 1.2.4 Weathering characters

There are three minerals dominating in the Badong group:

1. carbonate minerals
2. clay minerals
3. detrital minerals

The members of the Badong formation can be grouped according to their mineral characteristics.

Mineral characteristics of T<sub>2</sub>b<sup>1+3</sup>:

- Carbonate minerals such as calcite (55-95%)
- Clay minerals as their secondary minerals (Qi et al. 2009, p. 934)

Mineral characteristics of T<sub>2</sub>b<sup>2+4</sup>:

- Clay minerals (85-90%)
- Calcite as a secondary mineral (Qi et al. 2009, p. 934)

The carbonate mineral content can be ranked as shown below.

$$T_2b^3 > T_2b^1 > T_2b^4 > T_2b^2$$

It shows that member  $T_2b^{2+4}$  and member  $T_2b^{1+3}$  have similar mineral and chemical characteristics.

According to the chemical content, the different strata can be divided into two groups (Figure 5):

Group A:

$SiO_2, Al_2O_3, F_2O_3$

Group B:

$CaO, MgO$

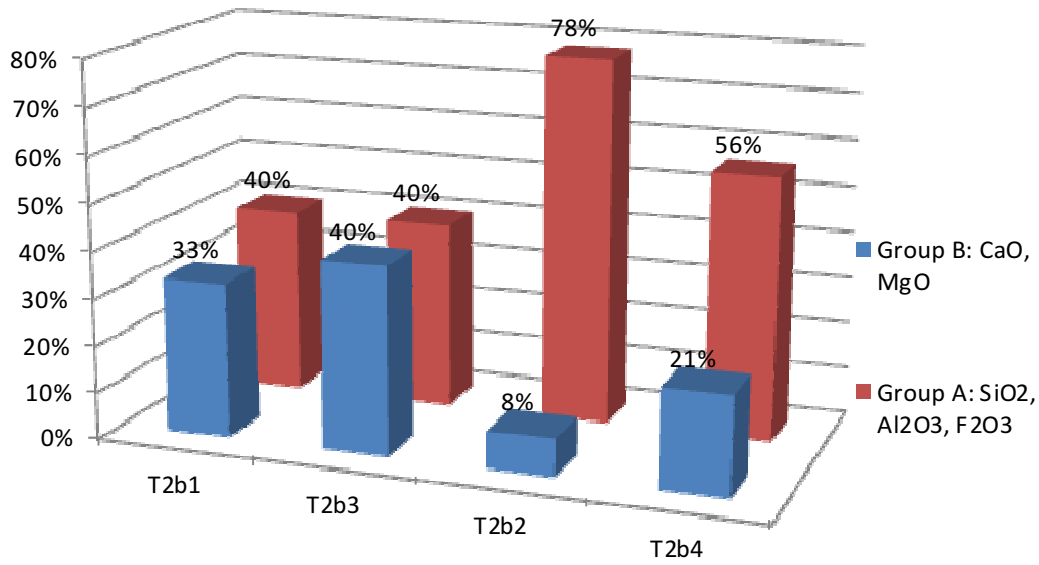


Figure 5: Mineral contents of different members of the Badong formation

$T_2b^2$  and  $T_2b^4$  have 78% and 56% amounts of group A and 8% and 21% of group B, respectively.  $T_2b^1$  and  $T_2b^3$  have 40% amounts of group A and little less of group B (Qi et al. 2009, p. 934). According to the mobility orders of  $CaO > Na_2O > MgO > Fe_2O_3 > Al_2O_3 > SiO_2$  (Polynov 1937, quoted in Qi et al. 2009, p. 934) it can be deduced that  $T_2b^{1+3}$  are more soluble than  $T_2b^{2+4}$ .

Investigations with drilling cores revealed that the topography, rock type and rock mass structure is highly related to the weathering depth. The inclination of the slope has a significant influence on the thickness of the weathering layer. On a steeper slope the depth of weathered rocks is less than 15 m thick, whilst on a slope with less inclination the depth of weathered rocks is 50-60 m of thickness (Qi et al. 2009, p. 934).

The residual soil of  $T_2b^3$  is brownish red, yellow grey or apricot coloured. It is particularly the apricot argillite layer in the residual soil which tends to cause slope instabilities. If the rock is in completely weathered conditions, it appears as buff coloured stratified soil or bedded disintegrated rock blocks (see left side of Figure 6).



Figure 6: Transitional zone between residual soil of  $T_2b^3$  (left) and  $T_2b^2$  (right) (Photo: Mayrhofer 2012)

Figure 7 and the right side of Figure 6 reveal a  $T_2b^2$  purple red mudstone, decomposed into soil. The soluble compositions are dissolved so that thickly dotted pores (see Figure 8) appear (Qi et al. 2009, p. 934).



Figure 7:  $T_2b^2$  decomposed into soil (Photo: Mayrhofer 2012)



Figure 8: Thickly dotted pores of  $T_2b^2$  (Photo: Mayrhofer 2012)

The highly weathered argillaceous limestone rock was believed to be suitable as in-situ geomaterial for building foundations and cut slope. Ground investigations showed that despite the high weathering conditions, they have adequate strength for slope and building foundations. After excavation the already weathered limestone was easily decomposed into soils. Geohazards like sink holes and landslides occurred a few years after the excavations for the new town of Fengjie. So programmes were implemented to investigate, re-design and re-construct the ground stabilization measures, to prevent disasters in newly built towns in the Three Gorges area (Qi et al. 2009, p. 931).

Figure 9 and Figure 10 show highly weathered argillaceous limestone. After cutting, cracks form easily, due to solubility and unloading. Joints are densely developed and cut the rock into small pieces. The occurrence of toppling and falling stones is frequent (Qi et al. 2009, p. 934).



Figure 9: Highly weathered  $T_2b^3$  (Photo: Mayrhofer 2012)



Figure 10: Highly weathered  $T_2b^3$  (Photo: Mayrhofer 2012)



Figure 11: Weak layer in  $Tb3$  (Photo: Mayrhofer 2012)

Figure 11 shows a 20 cm thick layer of intercalated calcareous clay-stone which is highly decomposed. Due to chemical weathering, the strong limestone with a  $\text{CaCO}_3$ -content of 90% changes its composition. However, with slight weathering the limestone changes to a  $\text{CaCO}_3$ - content between 65 and 70% (Qi et al. 2009, p. 935). So the name changes to mudstone, as illustrated in Figure 12.

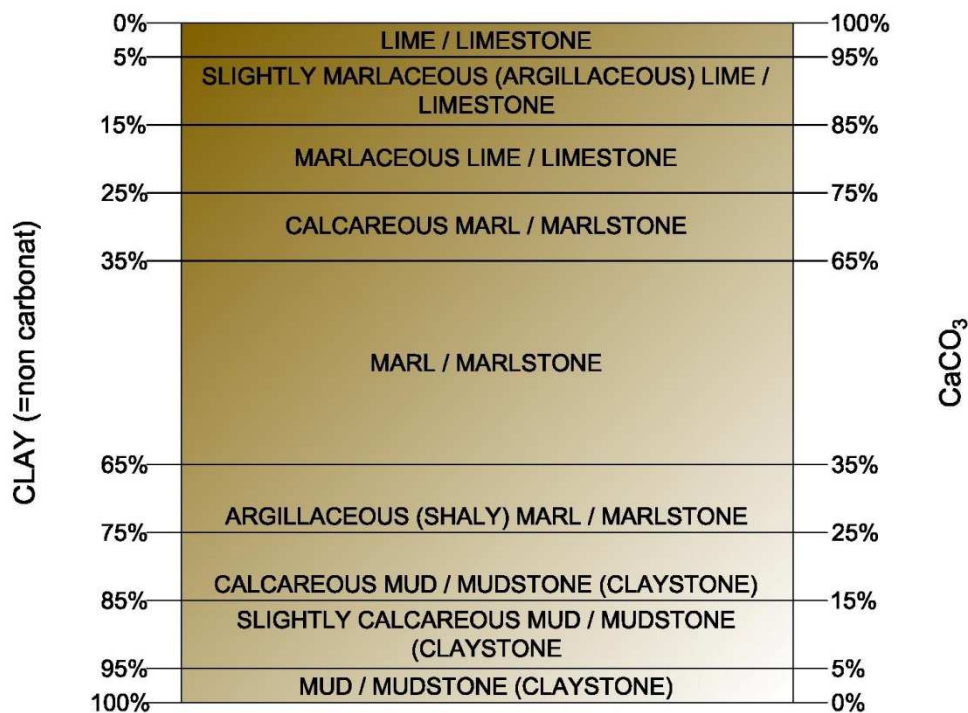


Figure 12: Distinction of claystone, marlstone and limestone by means of content of clay- and CaCO<sub>3</sub>

Within the weathering process the colour changes in the following steps: dark grey, grey, grey-green, yellow-green, yellow or brownish red (because more Fe<sup>2+</sup> is oxidized to Fe<sup>3+</sup>). Joints build channels for the infiltrating water, so the weathering can be deep. Strength and deformation modules decrease fast with the decrease of CaCO<sub>3</sub>-content. Results of mechanical tests show that a fresh argillaceous limestone rock has a uniaxial compressive strength of about 105 MPa, and deformation module of 16 GPa. But a highly weathered rock has the strength of about 57 MPa and a deformation modulus of 4 GPa see (Figure 13) (Zhang 2004, quoted in Qi et al. 2009, p. 934). Also the shear strength changes. For example, on unweathered bedrock a peak shear strength of 28° is common, while with weathering, the shear strength of these strata decreases so that the critical strength is 15°-18° with a residual strength as low as 8°-12° (Qi et al. 2009, p. 198). This is significant in terms of changes in shear strength in steep slopes with high overburden pressures. The progressively weakened mud-rock strata are squeezed out towards the natural slope face, so that the thick limestone bands lose their original support and they dip increasingly outward.

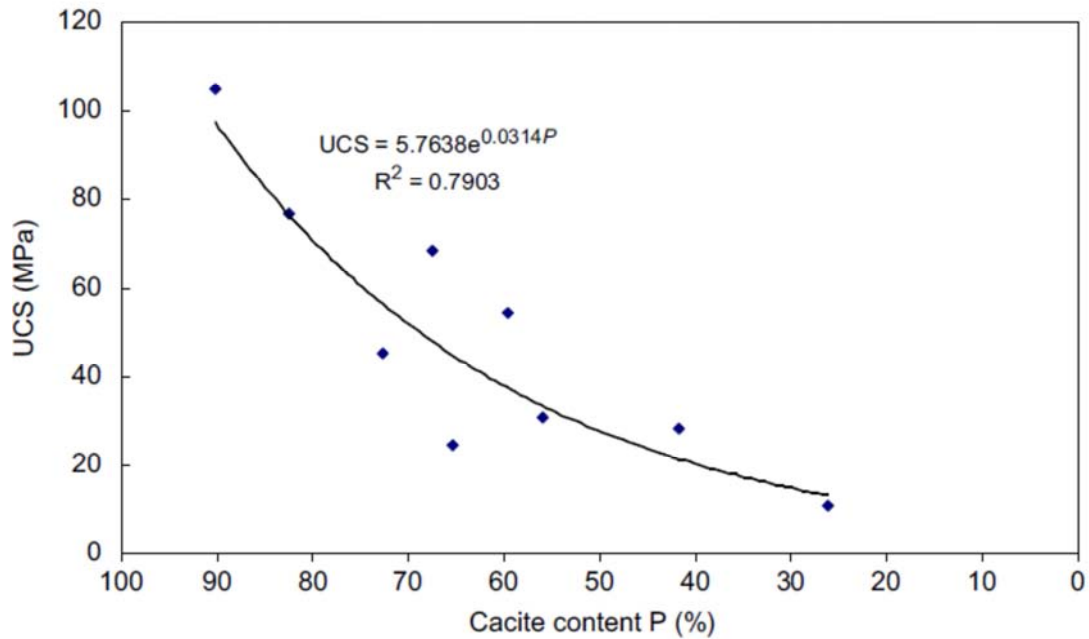


Figure 13: Relationship between uniaxial compressive strength (UCS) and calcite content of weathered argillaceous limestone rocks (Qi et al. 2009, p. 938)

### 1.2.5 Hazard of toppling on argillaceous limestone

As described in Chapter 1.2.4, the still strong limestone and mudstone will weaken once exposed to the external environment. An example of this is the highway construction in the Yangtze area. The rock-slope of dominantly calcareous strata with some inter-bedded mudstone was cut at angles of 70°-90°. It was not expected that the near surface angle of the bedding was much lower (or even outward dipping) than that seen in the outcrops in the gullies and hence the potential for problems was not foreseen. The gravitation force from the centroid of the block may extend beyond the lower edge of the block, so the whole block becomes unstable and topples. Initially the topple movement may be inhibited by frictional forces between the rear of the block and the blocks behind. But with further weathering by roots of plants the blocks can move down (Qi et al. 2009, p. 199).

### 1.2.6 Weathering conditions on purple mudstone

Mudstone in particular is easily decayed and very soft. Readily it develops structural, diagenetic and decayed cracks. Under changes of temperature and moisture conditions, the physical decay rate of purple mudstone is very high. It has been estimated that the decay rate of exposed purple mudstone in the field is about 15,800 t km<sup>2</sup>\*yr<sup>-1</sup>. (He 2003, quoted in Zhang et al. 2012, p. 8). Water plays an important role. This concerns the dissolution of cementing carbonate and clastic feldspar, crystallization of salt minerals and the formation and transformation of ferric oxide and ferric hydroxide, as well as increasing pore pressure and capillary tension, and reducing frictional and fracture energy. Crack growth depends mainly on water content in the rock (Zhang et al. 2012, p. 16).

To understand the weathering characteristics of surface layers in the purple mudstone sloping fields of the Three Gorges Reservoir area of China, the following parameters are important:

1. oxide content of major elements
2. composition of clay minerals

The difference in weathering characteristics of surface layers under different slope gradients (as discussed before on rocks of  $T_2b^3$ ) is an important factor in understanding and predicting the weathering conditions of the soil under foundations. With an increase of slope gradient, the relative diffraction peak for kaolinite at weathered layers decreases, and on slopes between  $50^\circ$  and  $60^\circ$  it disappears altogether (Jiang et al. 2006, p. 50). Thus the pedogenesis on less steep slopes is higher than on steep slopes. The major chemical compositions of purple mudstone are Si, Al, and Ca oxides which are 60-70% in total. The  $CaO_3$  content in particular is relatively high, which can be explained by the fact that the strata of the Badong Group is of the Middle Triassic, which was mostly formed in a shallow sea environment, with the clay itself having a high content of Ca. Another aspect is that the surface biochemistry process is very complicated, with dissolved  $Ca^{2+}$  being re-deposited. A measuring of the clay mineral content at the same slope gradient and no change within an increasing depth, was observed in this study. This shows that the age of the weathering layer was very young and pedogenesis was weak. So in total the weathering layer is becoming weaker and weaker within the slope angle and the erosion is becoming stronger. It is common that a gentle slope is less vulnerable to erosion than steeper slopes, and so weathering deposits too are easier retained in the weathering layer. To some extent, the degree of weathering can be estimated through different slope angles. These were the findings of a previous study (Jiang et al. 2006, p. 54). However the limited depth was an obvious restricting factor.

#### 1.2.6.1.1 Leaching factor

It is reported that soluble salts in weathered red mudstone are dramatically dissolved and leached by rain. Soluble salts play a very important role in cementing clayey soil particles, because physico-chemical forces among clay particles lower with the decrease of salt concentration. This is because of the cation-exchange in clay mineral layers and due to inward diffusion of salt or inward osmotic flow into spaces among clay particles, causing changes in the thickness of the double layer of clay particles. This also leads to disaggregate particles coarser than clay, as their double layer is thick (Wen et al. 2012, p. 61). After samples were leached 6 times with deionized water, the residual shear strength was reduced up to 65% and the  $\varphi_{\text{residual}}$  went down to 62%. So the drop of shear strength through lixiviation (also because of artificial irrigation) should be also considered, when estimate future slope stability (Wen et al. 2012, p. 63).

### 1.3 Climate

The climate is mostly affected by the Asian monsoon system. A main characteristic is a seasonal alternation between a warm and wet summer monsoon, and a cold and dry winter monsoon. Between the upper and the lower stream of the Yangtze there is a slight difference in the precipitation. The upper mainly gets the rainfall from the south Asian monsoon. The annual rainfall decreases from the upper to the lower eastern streams. Westwards it is about 1,000 mm and in the lowlands it is about 700 mm in the Sichuan Basin. But it can rise to over 1,700 mm on the eastern flanks of the central Longmen Shan. In the west of the Longmen Shan, precipitation decreases along the plateau, from 600 mm in the middle reaches of the Yalong Jiang (Jiang= river) to about 400 mm at the top of the Jinsha Jiang.

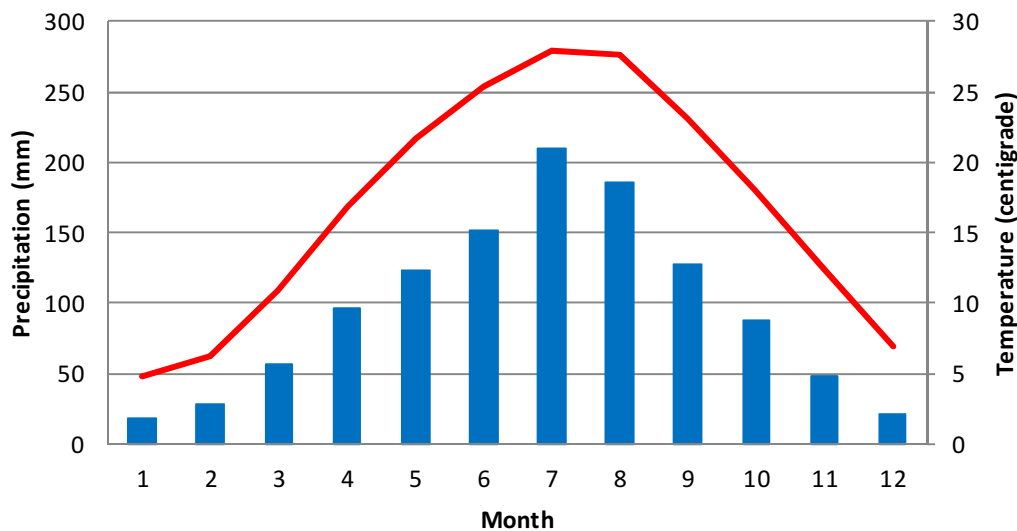


Figure 14: Climate graph of Yichang (Data from: NOAA<sup>3</sup> Station Id: PC57461; Latitude: 30°42'N; Longitude: 111°18'E; Elevation: 133m)

The temperatures in the summer are warm along the Yangtze River catchment. Especially in the eastern lowlands in the region of Wuhan, the temperatures in July can exceed 30 °C. In the eastern lowlands and the Sichuan Basin the winter is mild to cool and on the plateau it is very cold and dry with sub-zero temperatures. The mountains of the Longmen Shan are with snow throughout the year (He et al. 2012, p. 2).

<sup>3</sup> National Oceanic and Atmospheric Administration

## **1.4 The Three Gorges Project (TGP)**

The high construction activity in Badong is obviously closely connected with the project of the Three Gorges Dam. The dam is located in the middle section of the Xiling Gorges, near a small Town Sandouping in the Yichang County. In 1979 this dam site was selected because the crystalline rock area appeared favourable, and the greater width offered greater flexibility for general layout and structure and for good construction conditions (Deji 1999, p. 184). The dam is 2,309 m long, 84 m wide and rises 185 m from the riverbed. Since 2009 the reservoir reached the ultimate height of 175 m.a.s. (Alberts et al. 2004, p. 586). The amount of concrete utilized to perform this project is 26.43 million m<sup>3</sup>. The controlled drainage area is of 1 million km<sup>2</sup>, with an average annual runoff of 451 billion m<sup>3</sup>. 32 turbines generate 22.4 GW: this contributes to one- ninth of China's total output. The total cost was 180 billion RMB (25 billion USD), this was 20 billion RMB less than the original budget (Liu et al. 2013, p. 233).

The slope of the two chambers of the five step ship lock is cut into weathered and fresh granites, which are 1,607 m long and 50- 170 m in height. The ship lock facilitates the passage of fleets of 10,000 ton capacity and an additional ship lift handles ships with 3,000 tons (Sheng et al. 2002, p. 165). The reservoir length measured by Landsat images is 699 km (Wang et al. 2013, p. 8) or 663 km (Wang et al. 2005, ) at a water level of 175 m.a.s. The difference is mainly a result of different measurement methods and different backwater conditions through hysteresis. The water level changes over the year according to a certain regime. In January the level is lowered until it reaches the flood control level of 145 m.a.s. in June. In October the level reaches 175 m.a.s. again.

### **1.4.1 Impacts of- and measurements around the TGP**

The project of the Three Gorges Dam has different impacts on its environment. There are many aspects which could be classified as either negative or positive. This remains subjective and depends on the point of view of the observer.

Positive aspects could be displayed as significant benefits in electric power generation, in flood control and in shipping traffic enhancement; negative ones are an adverse impact on migration, on flood control and on cultural issues (Dai Huichao 2005, quoted in Dai Huichao 2010, p. 15).

### 1.4.1.1 Energy requirement

Energy is an indispensable factor for a country to develop. The issue is which resources are used to meet this requirement. Comparing the Gross domestic product (GDP) growth of the European Union, China, Austria and the World, it is remarkable that China could maintain an annual growth of 9% (World-Bank 2013) even throughout the world economic crisis. In Europe especially, there is the promoted policy to reduce energy consumption via saving. Contrasting Europe with China, and considering the energy use per capita<sup>4</sup>, it is evident that China has still very low energy consumption per capita, compared to western countries (compare Figure 15).

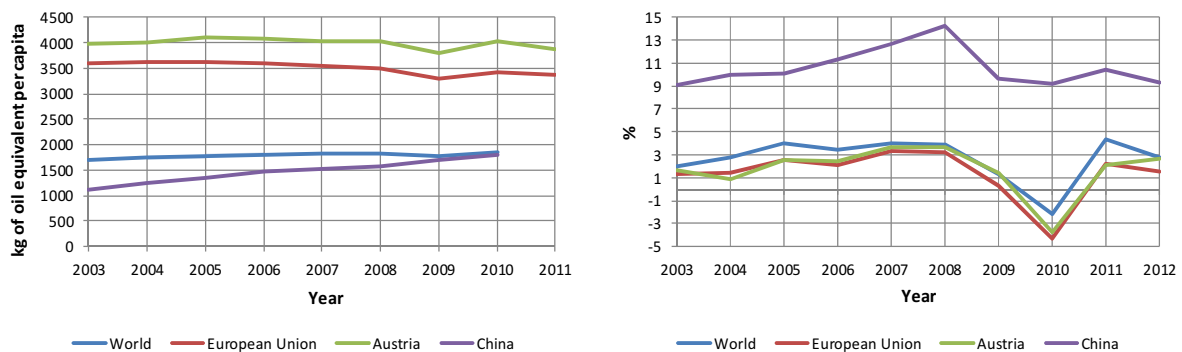


Figure 15: Energy use per capita and GDP growth (World-Bank 2013)

By the end of October 2009, the turbines of the TGP had generated 364.4 billion kWh. This is equivalent to 137 million-tons of standard coal equivalent. So it can be deduced that 312 million tons of CO<sub>2</sub>, 3.7 million tons of SO<sub>2</sub> and 1.6 million tons of NO<sub>x</sub> were reduced from the TGP (Liu et al. 2013, p. 234). However, energy requirements are still mostly satisfied by fossil resources. By the total energy consumption of 2.91 billion tons of standard coal equivalent in 2008, fossil fuels remain the dominant sources of primary energy, ranging from 88% to 92% (Statistics-China 2008, quoted in Liu et al. 2013, p. 231).

<sup>4</sup> Energy use refers to use of primary energy before transformation to other end-use fuels, which is equal to indigenous production plus imports and stock changes, minus exports and fuels supplied to ships and aircraft engaged in international transport.

#### **1.4.1.2 Hydrological impacts**

There was also the fear that waves induced by landslides could affect the dam. Calculations on generated waves showed that if the next possible landslide 26 km upstream rushed into the river the wave height would be only 2.7 m in front of the dam (Deji 1999, p. 6). But the changes have great influence on sediment deposition and erosion, riverbed geometry, flow velocity and flow conditions. In the whole area of the Three Gorges Reservoir, there are 45 observation stations employed to work on research. Their observations and analyses have found that the effect of the sediment and of the change of the riverbed in the reservoir is small and can be controlled (Sun et al. 2011, p. 377). At the time of the field study, the research centre in Badong was no longer in service, so the very latest data could not be obtained; however silt accumulation on the dam site is faced by sluice gates at a height of 90 m.a.s and 75 m.a.s. respectively, whilst the generator intake is on 108 m.a.s. (Alberts et al. 2004, p. 589). However, the accumulation of coarse material like gravel is still a problem as this is too heavy to be flushed.

Flood control is one of the major functions of the TGP. Former floods over the last century resulted in the death of over 300,000 people (Jackson et al. 2000). The last serious flood happened in 1998 and caused over 4,000 deaths, inundated 25 million hectares of cropland, and cost in excess of US\$ 36 billion, in damages to property and infrastructure (Tullos 2009, p. 209). The completion of the project reduced the flood peak of 15,000 m<sup>3</sup>/s, which also alleviated the flood control pressure of the downstream of the dam. The flood-control protects 15 million people. In the dry season the dam discharge about 12 billion m<sup>3</sup> water to the downstream of the river, so the demands from navigation, manufacturing and local people are better satisfied. The navigation cost is cut down to 1/3 and the navigation energy consumption is reduced to 46% of the former costs (Liu et al. 2013, p. 235).

#### **1.4.1.3 Ecological impact**

Between 2002 and 2005, a monitoring of key ecological factors shows that the concentration of total phosphorous and nitrogen increases, so algae cell density and the number of algae species increase significantly after impounding the reservoir. The water regime of the Yangtze River changes greatly, which means that the permanent water level raises significantly and thus the flow slows down. This lowers the turbulent motion and the capacity for dispersion and extends the residence time in bays and branches (Dai Huichao 2010, p. 16). Before impoundment, the Yangtze River had a natural current. The water level fluctuation used to be from 30 m up to 50 m over one year. During the flood season the water level could rise 10 m during a single day. The average water surface slope was 0.002 and could reach 0.01 at rapid current. Surface velocity was 3-4m/s and was up to 6-7m/s in flood period. These are not suitable conditions for the majority of algae species and those which

were adaptable to higher velocities could not develop, because the earthy content hindered their growth because of reducing light. After the impoundment the condition for algae improved, due to the slowdown of surface velocity and the drop of earthy material in the water, to a level which favours photosynthesis. So the risk of water eutrophication rises (Dai Huichao 2010, p. 22).

39.2 billion RMB were invested in water pollution prevention and control in the Three Gorges Reservoir and its upstream. From 2002 to 2010, 28 sewage water treatment plants and 20 garbage treatment plants were built to treat solid waste and waste water before going into the reservoir. Up to the present day, 1,959 enterprises have had to close because of a risk of serious pollution, as their technology wasn't "state of the art". 1,012 enterprises are planned to be closed if they cannot meet the required standard to protect the environment (Liu et al. 2013, p. 234).

Fish in the Yangtze River basin are seriously affected by barriers like the Three Gorges Dam. The four major carp species<sup>5</sup>, which are typical migration fish, dwindled by more than 50%, their fry resources were reduced more than 90%. This effect could have been mitigated through human-made flood peaks during the spawning season (Yi et al. 2010, p. 1952). However, in 2008, some rare species, such as 129,300 Chinese sturgeons, 2,000 Yangtze sturgeons and 418,600 Chinese suckers were released into the Yangtze River. National natural reserves (total river area of 33,174.2 Ha) have been established to protect rare species of animals and fish (Liu et al. 2013, p. 235).

#### **1.4.1.4 Requirement of settlement area and relocation policy**

Social issues like relocation of people and their compensation, especially, found worldwide attention and were discussed intensely. Every large scale project requires space and inevitable impinges on the wealth of affected persons. Wealth can be grouped in three different broad classes of wealth (Mulder et al. 2009, p. 685):

1. Embodied wealth, which a person represents by their capabilities (knowledge and experience)
2. Material wealth like land livestock and household goods
3. Relational wealth represented by social and physical infrastructure

Material wealth is easy to measure, and therefore compensation is mostly limited to material wealth. Embodied wealth, such as agricultural skills can be lost if this person cannot use the skills under new conditions, but a large project like the TGP also creates a new prosperous local market, where new trading activities may increase opportunities for related skills and possibly even generate a higher income. Relational wealth is difficult to measure. Economic/social/cultural networks which have been built over many years can be in danger after relocation, however it can also bring opportunities,

---

<sup>5</sup> Black carp (*Mylopharyngodon piceus*); grass carp (*Ctenopharyngodon idellus*); silver carp (*Hypophthalmichthys molitrix*); big-head carp (*Aristichthys nobilis*)

as construction of infrastructure may make people better able to build a larger social network and to have better access to education and healthcare resources (Wang et al. 2013, p. 133). China's compensation policy can be characterized in three epochal transitions (Wang et al. 2013, p. 3):

1. The "reform and opening –up policy" in 1978, in which the government recognized the legitimacy of private claims regarding property. Individuals were no longer forced to sacrifice their wealth without compensation.
2. The "market- oriented reform" in 1994 expanded compensation. Negotiations between citizens, government and state-owned companies engaged in dam construction became common. Quasi-private enterprises were also involved, and this strengthened the ability of displaced people to make compensation claims.
3. The internet, after 2000 and the rise of civil society expanded transparency, participation and accountability. Not only material wealth, but also embodied and relational wealth is taken into consideration.

The Three Gorges Reservoir submerged the homes and environs of 726,000 people; however, according to official documents of 2010, 1,397,000 people had been relocated, directly affecting 20 counties in Chongqing City and Hubei Province. Compensation was largely based on the market price of houses and land forfeited by relocated people. A document issued by the Central Government on August 1993, "The Three Gorges Project Development- oriented Resettlement Regulations" implied that compensation should be fair, so that the relocated people could maintain or even improve their original standards of living (Wang et al. 2013, p. 6). In respect of material wealth, relocated people were given houses and newly-cleared farmland. In addition to this, monetary compensation at a rate many times their annual income was given. But there were also deficits in the implementation of the "developmental- oriented resettlement strategy". Very few training programs were provided, and after relocation a large percentage of people were unemployed. Hospitals, schools and other infrastructure projects were built in newly created villages, but in most cases the investments did not meet the needs of the villagers (Xinhua-News-Agency 2003). So the previous embodied and relational wealth of relocated people was still larger than the compensations they received (Wang et al. 2013, p. 6). However, including construction of housing, roads and other infrastructure, the government of China had invested, by September 2009, more than 71 billion RMB for the resettlement of residents in the Three Gorges Reservoir areas (Liu et al. 2013, p. 234).

## 1.5 Types of slope in Badong County

Due to geological climatic characteristics as well as human actions, the Badong area displays different types of slopes. Especially due to the need for new locations due to the Three Gorges project, human activities created new engineered slopes around the reservoir. The number is about 2800 new engineered slopes. Cutting slopes can be differentiated between soil slopes and rock slopes (Wu et al. 2011, p. 314).

### 1.5.1 Rock slopes

**Clastic structure rock slopes:** Geological disturbance or weathering forms a severely broken structure. Especially the argillaceous limestone of Badong County is severely broken under long term weathering, erosion, and disturbance by slope unloading through cutting. Failures like structural collapses leading into scattered accumulation are common (Wu et al. 2011, p. 316).

### 1.5.2 Soil slopes

**Residual soil slopes:** These slopes mainly consist of marlite and sand slime rock. The following slope-failures are often observed due to the conditions of the residual soil. On slopes without vegetation surface scouring is very likely. Spots with loose broken soil and low cohesion display rather superficial layer collapses. Superficial landslides are mostly on the basis of deep weathering (Wu et al. 2011, p. 314).

**Colluvial accumulation slopes:** Due to the limitations of the geological environment, colluvial soil is reformed and reused for new constructions. Excavation changes the stability and initial field stress, so rock falling, collapse and sliding failure are likely.

**Artificial earth fill slopes:** By construction of new towns, the cutting away of earth in the highland often implies refilling on the slope in lowland areas. Failures like uneven subsidence or deep slippage can follow. This failure causes deformation and damage to buildings. Cracks on the ground surface are a common sign of this kind of failure (Wu et al. 2011, p. 316).

## 1.6 Landslides

The Three Gorges area is, due to its adverse landform and geological setting, very prone to landslides (Li 2002, quoted in Wen et al. 2007, p. 83). On July 13 2003, a landslide of about 20,000,000 m<sup>3</sup> happened just about six weeks after water impoundment had started. 24 people lost their lives (Wen et al. 2007, p. 155). The metallic silicon factory, the shale brickyard plant and in total four plants in the town of Shazhenxi were completely destroyed. This size of impact meant the destruction of the industrial base of the town. Also farmland of 711,000 m<sup>2</sup> was destroyed. The landslide changed the industrial and agricultural economy of the town and it was difficult to recover (Wang 2009, p. 195). As a result, the Chinese Government has set measures and approved a project named “comprehensive geological hazard mitigation for landslides and rockfalls in the Three Gorges dam area” (GHMLRTG). A systematic investigation of landslides and potentially unstable slopes, the possibility of reactivation and their failure mechanisms, monitoring and stabilization of significant landslides and unstable slopes took place. Through this program, which was implemented in several steps until 2009, landslides in the whole area affected by the dam were investigated through several institutions and more than 200 significant landslides have been stabilized (Dam et al. 2006, quoted in Wen et al. 2007, p. 83).

Landslides in mountain- river reservoirs are mainly caused by the rise and fall of reservoir levels as interaction to compensate the new conditions. Rainfall and other causative factors are driving this compensation which is executed by a cumulative deformation through long-term and wide- ranging gradual destruction. The deformation happens along slopes which are sensitive to hydrodynamic influence. Thus due to different slope structures, landslides in the Three Gorges Reservoir can be classified into the following four categories (Wang 2009, p. 155):

**Ancient landslide revivification:**

Through reservoir impoundment formerly stable or almost stable sliding slopes reactivate and slide partially or collapse (see Figure 16).

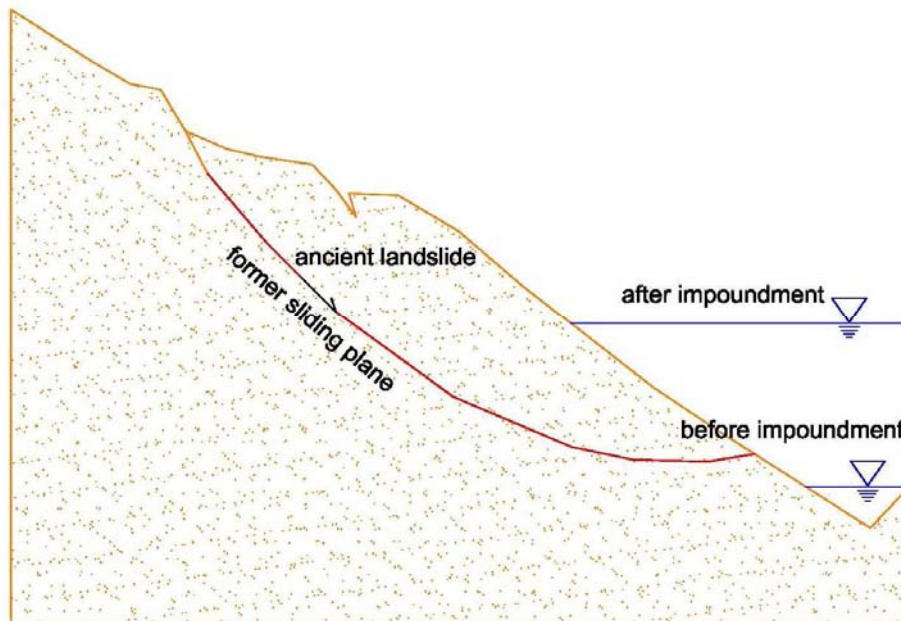


Figure 16: Sketch of ancient landslide revivification (Wang 2009, p. 151 modified by the author)

**Surficial slip of the thick loose deposit:**

Parts of some stable or almost stable thick accumulations become unstable by the sliding of the plane layer of the superficial part of this loose deposit. This loose deposit can be classified due to different causes such as collapse and slide deposit, slope wash deposit, proluvial deposit, artificial storing and so on. This mass creeps downward and deforms, or the front edge partially becomes unstable through sliding (see Figure 17).

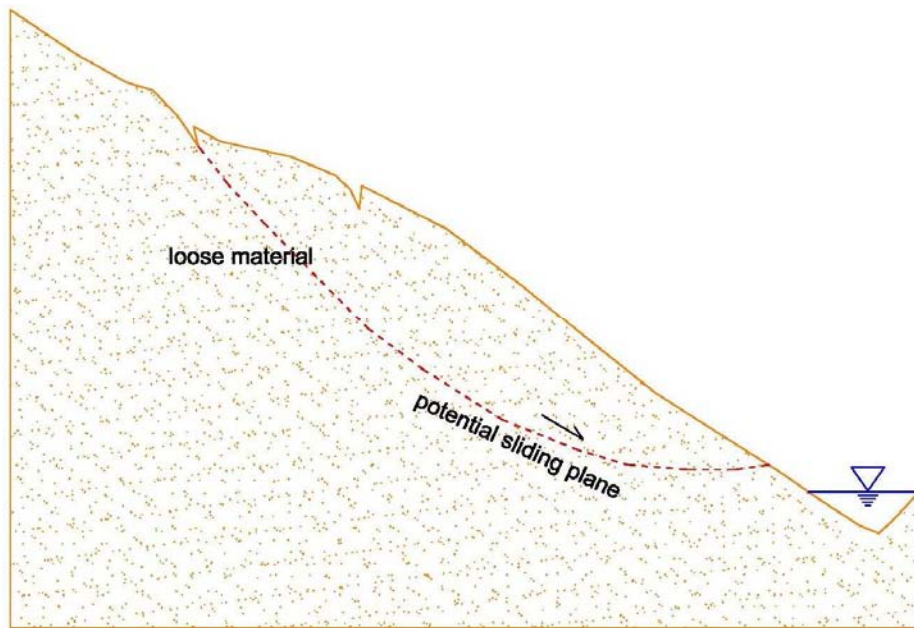


Figure 17: Sketch of surficial slip of thick loose deposit material (Wang 2009, p. 151 modified by the author)

#### Sliding along the bed- deposit interface:

This occurs commonly on a deposit which is not thick and the depth of the bed-deposit interface is not high. The accumulation moves as a whole along the bed-deposit plane (see Figure 18).

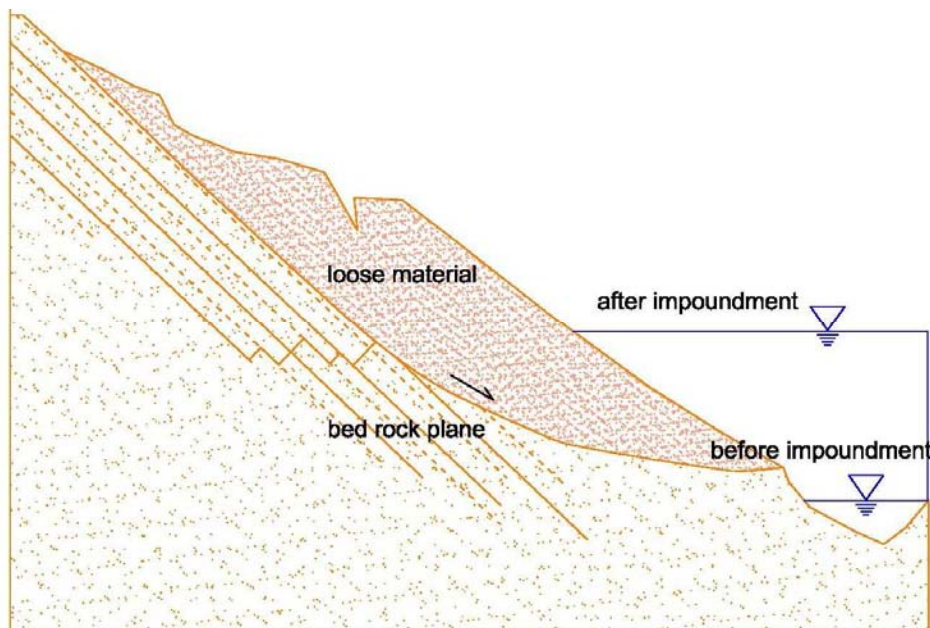


Figure 18: Sketch of a slide along the bed- deposit interface (Wang 2009, p. 151 modified by the author)

#### Bed rock sliding along the weak accordant layer:

A bed rock with a moderately low dip angle is the basis of a weak interlayer like sandstone-mudstone interbedding, or an argillized interlayer between limestone and marlite strata ( $T_2b^3$ ). This weak layer destabilizes after cutting the slope or after immersion through storage impoundment due to

reduction in shearing resistance greatly. The whole landslide mass along the weak layer moves. Especially if the upper part of the accordant slope is precipitous and the lower part inclined to slide, according to the principle of effective stress ( $\sigma'$ ), the gently slanting toe of the slope, though with original friction, will slide as a whole, as the skid resistance through the immersion is reduced. The aforementioned Qianjiangping Landslide in Zigui County of Hubei Province in July, 2003 and the tragic Vajont Landslide in Italy are examples of this type of landslide.

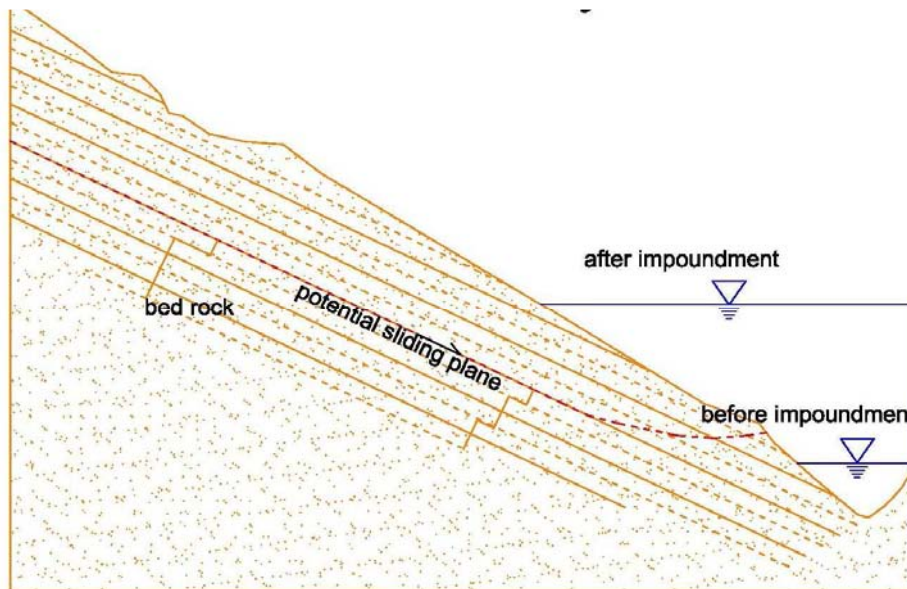


Figure 19: Sketch of bed rock sliding along the weak accordant layer (Wang 2009, p. 151 modified by the author)

### 1.6.1 Historical Landslide Situations

Reported historical landslides in Zigui County, which neighbours Badong County, show that geological disasters of landslides occurred frequently in the past. Historical documents in the County records and local records reveal that as many as 18 officially recorded destructive landslides occurred in Xintan.

According to the “Guizhou Records” on a rainy day of May 20, 1561, thousands of government buildings as well as the residential houses were destroyed. This was the reason why the Zigui City had to be moved back to the town of Guizhou. “Come to Sichuan” written by Luyou in Southern Song Dynasty, described how Badong was formerly situated in the north coast and then moved to the south coast as a result of the big landslide on the northern bank side. It can be seen that such situations were common in the history of the Three Gorges area. In general, after a landslide, the farmers have to move due to the loss of natural flat and rich land. They re-settle a short distance up the sloping land which is steep, barren and exposed for soil erosion which results in a lower income resulting in serious social problems. But there are also some positive effects of landslides. In the Ming and Qing dynasties, due to the hindrance of shipping, Xintan and Xinglong became the

commodity collection and distribution centres as well as the transit port in the upper part of the Yangtze River. This led to more commercial activities and better living standards for local residents of Lingtan, Fangtan and Jiaotan. Also the flat areas created by the landslide are often good places for the people to settle after a while (Wang 2009, p. 194ff.).

**1.6.2 Causes of shallow landslides: The influence of rainfall and human activity**

The rainfall and human activity are an important factor to understand slope failures. Strength parameters, such as the effective cohesion and friction angle of the soil do influence mostly the timing of failure, but not the failure mechanism itself. The slope topography (as shown above) and rainfall history impact the slope failure mechanism to a great extent (Borja et al. 2010, p. 248).

**1.6.2.1 Rain- induced landslides, an overview**

Small shallow landslides in particular are induced by rainfall. Table 3 shows that the correlation between monthly rainfall and small shallow landslides is significant. Landslides happen when the monthly rainfall reaches 50-100 mm and daily rainfall is above 50 mm. When the monthly rainfall is above 150 mm and the daily rainfall is above 100mm, the number of landslides rises significantly (Keqiang et al. 2009, p. 1928).

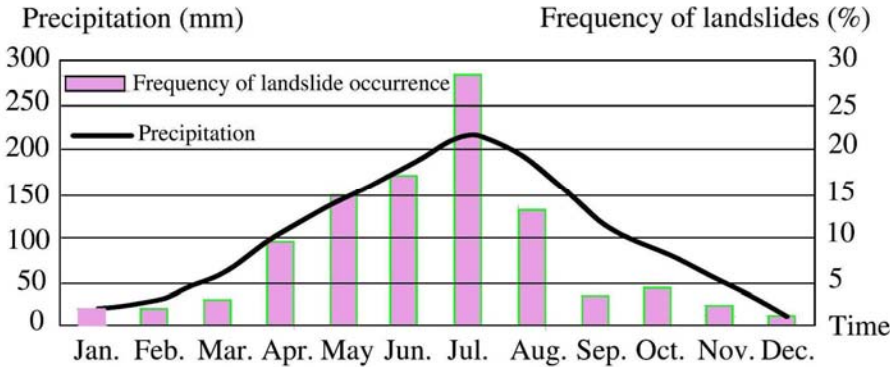


Table 3: Relationship of frequency landslide occurrence with precipitation in the Three Gorges Reservoir (Figure by Keqiang et al. 2009, p. 1928)

Landslides happen with a certain delay after a peak of rainfall; mostly several hours or days after the heavy rain peak. The reactivation of mostly old landslides is related to the overall saturation and natural water content of soil. Soil is less pervious and absorbent; it needs time for the process of saturation and with this come remarkable changes of hydrodynamic conditions (Keqiang et al. 2009, p. 1928). In other conditions, the water also needs time to migrate to a weak layer, before it can trigger a slope failure.

**1.6.2.2 Slope failure on  $T_2b^3$**

The following case of a shallow landslide was observed in Badong in early November 2012, during the field research (see Figure 21). The last recorded rainfall was on 29.10.2012 (compare Figure 20) of just nearly 7 mm on this day. So rainfall was not considered to be a major triggering factor, as the slide occurred on the 2<sup>nd</sup> of November 2012 in Badong.

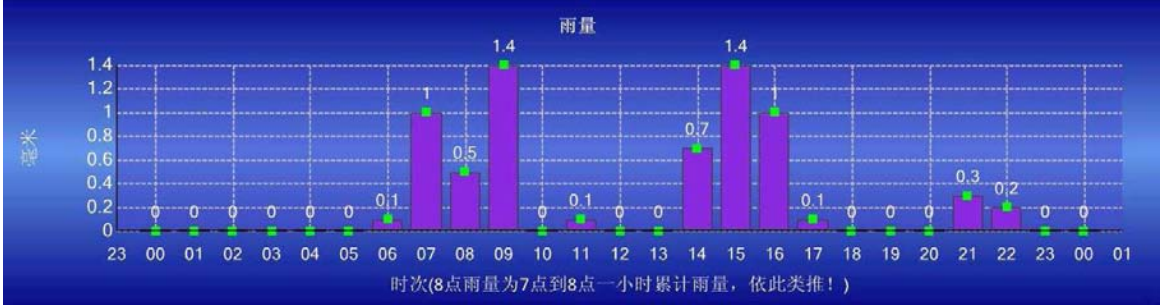


Figure 20: Hourly rainfall at 29.10.2012 in millimetre in Badong (Meteorological-Services-section 2013)

In this case, the calculation of the weak layers underneath the constructions, which resulted as sliding surface, had (according to on-site discussions with Chinese experts) been incorrectly estimated. This layer had been thought to be horizontal with no dip angle. Both the higher dip angle than presumed and the lack of support of the former building (which was taken away) caused the serious slope failure. No one was injured but an important traffic connection in Badong had to be closed for weeks. However, the fact is that this small landslide happened because of human activity namely the instalation of an additional external load (crane) and removal of resistance forces (old house was removed to build a new one).



Figure 21: Slope failure in urban area of Badong (Photo: Mayrhofer 2012)

### **1.6.2.3 Recent small landslides on ancient landslides**

There were two small characteristic landslides on the Huangtupo slope in 1995. The first, Erdaogou landslide (see Figure 22), which was about 90 m wide, 100 m long, 5-13 m thick, and had a volume of about  $6.7 \times 10^4 \text{ m}^3$ , occurred on the side of a ravine on June 10. It is not considered as a reactivation of a small part of the ancient Huangtupo landslide. The original cause was human activity, or more exactly the trigger force is considered to be the additional municipal waste and drainage to the back of the landslide.



*Figure 22: Example of a small landslide on the site of an ancient landslide: Erdaogou landslide developed in the debris accumulation (June 10, 1995)(Wang 2009, p. 368)*

In the same year, another comparably small landslide, the Sandaogou landslide, 100 m wide 200 m long and approx.  $20 \times 10^4 \text{ m}^3$  volume happened west on the Huangtupo slope. In this case rainfall and change of water level of the Yangtze River were thought as main triggering factors (Wang 2009, p. 367).

#### **1.6.2.4 Re-profiling and inappropriate cutting**

An often reported reason for slope failures is inappropriate cutting, but a systematic classification of failure patterns is missing. Re-profiling increases the safety factor of the cut slope but it reduces the safety factor of a natural slope. Little money is spent on ground investigation for cut slopes in China, so the investigated area is limited and the potential for larger landslides along deeper slip surfaces is often neglected (Sun et al. 2012, p. 1103). Rock slopes are often classified by geological conditions developed from the Rock Mass Rating (RMR) classification. This uses the summation of weighted contributing factors. It should be used carefully, because the failure of slopes is not just a question of one factor and the slope normally not only contains rock but is also covered with loose deposits. A deep seated landslide often covers a large area, so the geological conditions can change within the location. So case histories of the setting can give a better overview than just rely on sophisticated methods like Slope Mass Rating (SMR). But it is mandatory to describe the zonation of rock units, the existence of a plane of weakness, to assess possible failure patterns and describe and interpret the weathering conditions of the rock units in a rational manner (Sun et al. 2012, p. 1107). Cutting into a passive section of a slope with deposits of merely 3 m thick may increase the risk of a landslide enormously. The underground water is normally active at the interface between loose deposits and bedrock, as the permeability of these materials is different. The self-weight, the flow of groundwater, a large amount of fine particles and organic matters can create a second slip face (Sun et al. 2012, p. 1107). So the toe is a sensitive part of the slope e.g. in Austria, this was neglected during constructing the motorway “Phyrn” and due to a small excavation the expressway was pushed outward (Fuchsberger 2008, p. 1).

Discontinuities exposed during excavation deserve special attention. Faults, joints, schistosity and contact interfaces form together a complex structure and the mechanical properties vary significantly. Before the excavation, potential discontinuities may be not recognized. The time of setting the reinforcement is also vital. It is effective to put first the reinforcement and follow with the cutting, or at least carry out the reinforcement during the cutting, as re-profiling reduces the stability of the slope above the excavation line (Sun et al. 2012, p. 1107).

## 1.7 Slope stabilisation and protection methods

Various engineering techniques for stabilising and protecting the slopes at the Three Gorges area are used (Wu et al. 2011, p. 4):

**Shotcrete anchor bar supporting:** This is used to prevent the surface from weathering. Applicable for intact rock slopes, as a low cost measure.

**Frame beam protection:** Mostly carried out as vertical rib beam frame structure or as rectangular mesh structure. Usually the frame beam is fixed with an anchor bolt (wire). It is suitable for soil or rock slopes with good reinforcement results.

**Retaining wall:** Especially for loose cracked rock and soil slopes or as toe protection of a landslide combined with other slope protection measures. There are various kinds, such as mortar rubble masonry retaining walls, mortar boulder strip masonry retaining walls, reinforcement concrete retaining walls, and complex structures of anti-slide piles and baffle plates.

**Slope stabilizing piles and sheet pile:** If the rock and soil mass are loose and broken, anti-slide piles, together with cast-in-situ concrete baffles or prestressed anchor bolts (wires), are used. This forms pile-walls or pile-anchor structures. It is for high slopes, where the retaining wall is not economic, due to its large cross section. Deep slippages require sheet pile walls, as this is the option with the smallest cross section. But on very high slopes over deflection of sheet-pile walls, uneven internal forces in the pile bodies and large burial depth of the anchorage segments should be taken into account; thus anchorage sheet-pile walls are often used to solve the aforementioned problems.

**Flexible protection:** To minimize weathering and peeling of the soil masses on the slope, flexible grids are used. This method is mostly used for areas with less dense population, to mitigate the impact of toppling rocks. It is a low cost measure, simple in construction and easy to maintain.

## 1.8 Slope management

The proper management of slopes is a key factor to mitigate or even prevent disasters. Almost every endangered slope can be stabilized but the budget is a restricting factor. However, limited budget also can be a driving force for innovation. Observing projects it seems that innovation and budget are connected with a constant. As more budgets is available, as less innovation exists, and vice versa. Several methods are presented to face slope instability.

In general a hazard of disequilibrium of a slope is faced by increasing resisting forces by strengthening earth materials and/or decreasing driving forces by reducing the mass weights within potential sliding mass. Stabilization measures include draining surface and underground water from the potential sliding area, excavating and redistributing sliding mass and installing retaining facilities.

The base of measurements are the factor of safety, if the factor exceeds 1.0 then the slope is considered to be stable (Bernhard Pipkin 2008, quoted in Zuoan et al. 2006, p. 2). But the Factor of safety cannot completely include the effects of some control measures even these have great effects on landslide control. Ground water drainage measures are important and effective, but cannot be completely included in the Factor of safety (Zuoan et al. 2006, p. 3). So instead of starting to mitigate a potential slide of a foundation or even a whole slope with all conventional methods on the basis of a Factor of safety  $<1$ , a dynamic approach could be considered. This means the control measure are executed dynamically and at the same time its effects are monitored and evaluated. Usually any landslide control treatment is designed only based on stability analysis based on the first analysis results. So, the design for landslide control is complex and expensive. The shear strength in the sliding surface is gradually developed with deformation and sliding loads are progressively applied. Due to this progressive development not all treatments are effective immediately. So the dynamic comprehensive control method also uses updated monitoring information. As more available data obtained, as more the problem is understood. The investment for the control at different stages is small (Zuoan et al. 2006, p. 4). The Shijiapo landslide, a small landslide opposite Badong Town in its initial status was assessed and due to stability analysis stabilizing piles were used (see Figure 23). So the first slip zone was stabilized and the sliding surface developed gradually deeper down to another weak zone which was not revealed by drilling (see Figure 24 and Figure 25). The mass which slid down was even bigger than it would have been before. A gradual development and further assessment could have brought the slope in equilibrium again.



*Figure 23: Shi-jia-po landslide; black line: row of stabilising piles foundation (Photo: Mayrhofer 2012)*

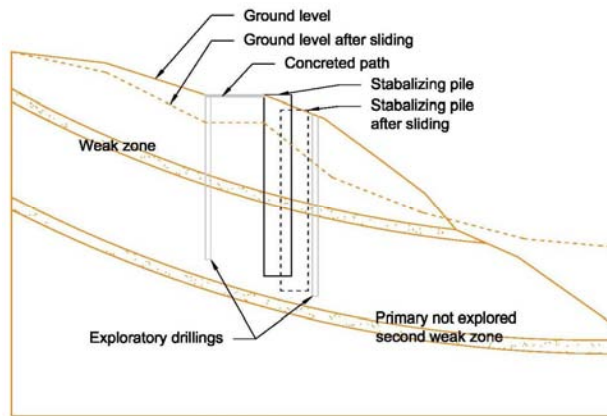


Figure 24: Sketch of the Shijiapo landslide



Figure 25: Shijiapo landslide (rest of concreted path and stabilising pile (Photo: Mayrhofer 2012)

Another example is a case study on an open pit landslide (Zuoan et al. 2006, p. 5). After an earthquake and rainstorms a u-shaped landslide were formed and tension cracks observed. Geotechnical investigation showed that it was a pre-existing landslide and the movement was closely connected with rainfall. After a stability analysis the slope was in its critical state. Economical and technical merits were assessed and the dynamic control scheme was adopted (see Figure 26 and Figure 27) (Wei 2003, quoted in Zuoan et al. 2006, p. 7). A monitoring net was installed, draining dykes along sliding boundaries were built, cracks on the slope were backfilled and tamped to mitigate the effects of rainfall. Monitoring showed that the sliding movement became slower. The next rainfall sliding rate increased and an adverse plump lentoid area was found in the slope abdomen. Based on information on ground and underground water a deep drainage system was constructed in the dry season. The slope displacement slowed down in slow changing displacement rates. A scheme of stabilizing piles was expensive and risky as the sliding depth increases with the development of landslides, so jambs along the landslide toe were made as a retaining wall and by calculation on the limit equilibrium method it improved the factor of safety to 1.03 (Zuoan et al. 2006, p. 8).

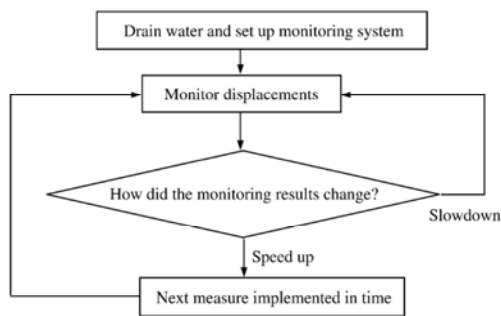


Figure 26: Control measures for landslide control (Zuoan et al. 2006, p. 9)

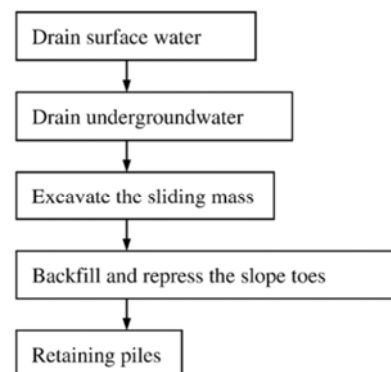


Figure 27: Design procedures for landslide control (Zuoan et al. 2006, p. 9)

## 2 Methods

The following sections outline the methods used for the field investigations and laboratory tests on the soil and rock of the three different slopes in the Badong area. First the selection criteria for the three sites are described and then the methods for field investigations and laboratory tests are specified.

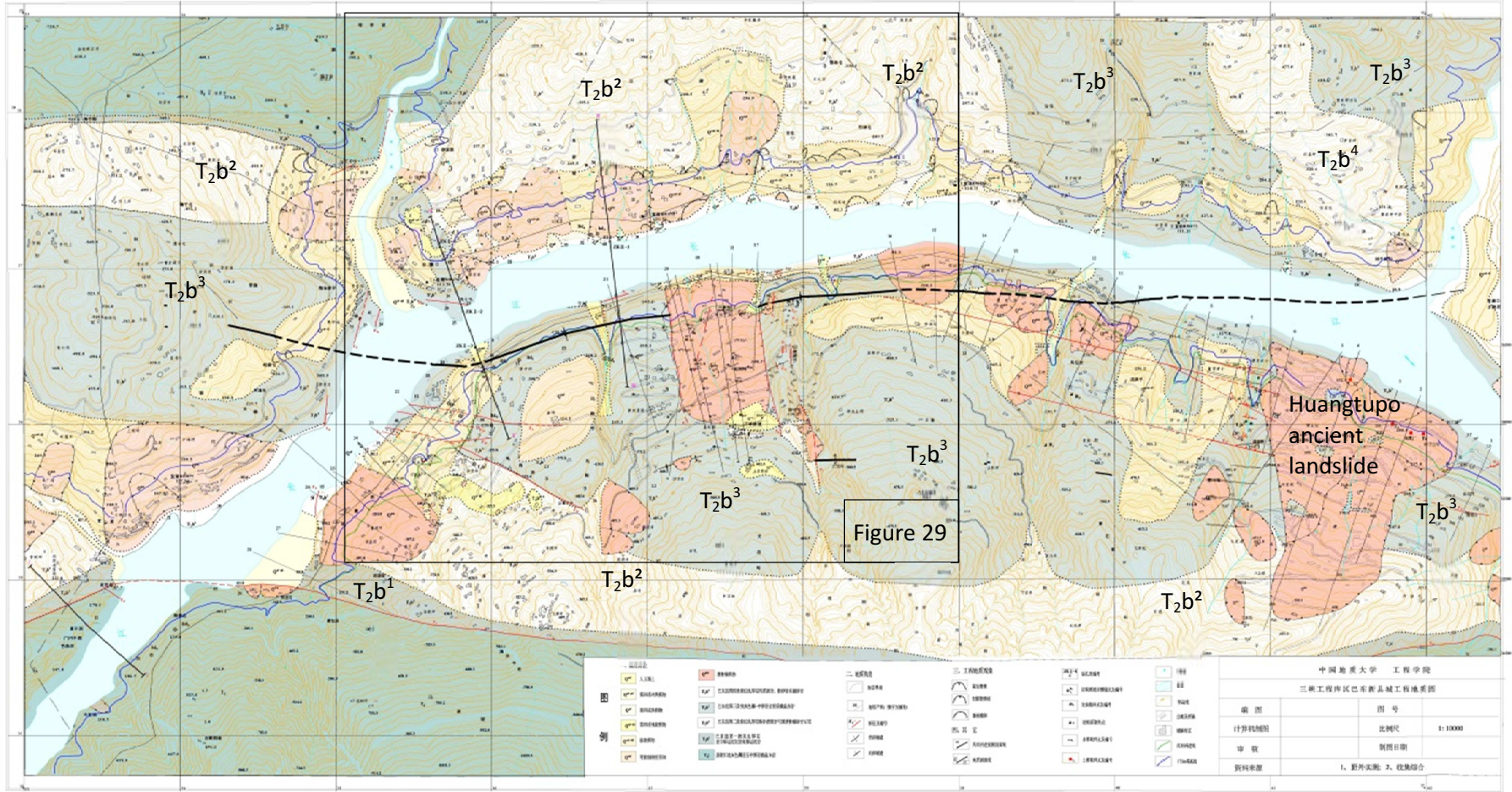
### 2.1 Selected sites

For this research, some general information of the area around the representative outcrop was collected. The geological map in Figure 28 is the base topographic information of Badong area. The areas in which the construction activities are high were defined. It appears that primarily in areas under the influence of the geological formation of  $T_2b^2$  and  $T_2b^3$  and the slopes of ancient landslides are the most affected areas by new constructions. During field study on both sides of the Yangtze River, it appeared that the geological conditions of the different geological members of the Badong formation and Quaternary deposits on ancient landslides are similar within each category. For example, any area with  $T_2b^3$  has similar characteristics such as dip angle, strata, mineral content and weathering conditions. In Figure 29 the three selected sites are shown. The selection criteria are the quality of an outcrop which means the accessibility and freshness and the existence or potential of human activity in this area. In the area of  $T_2b^2$  only highly weathered outcrops were met as the weathering depth is very deep. In the area of the geological formation of  $T_2b^3$  a fresh excavation exposure was found. In areas of ancient landslides no accessible fresh opening was available so this site is assessed by data from the surrounding area and by samples taken at shallow depth.

Figure 28: Geological map of Badong area (China University of Geosciences, Wuhan)

# 三峡工程库区巴东新县城工程地质图

比例尺: 1: 10000



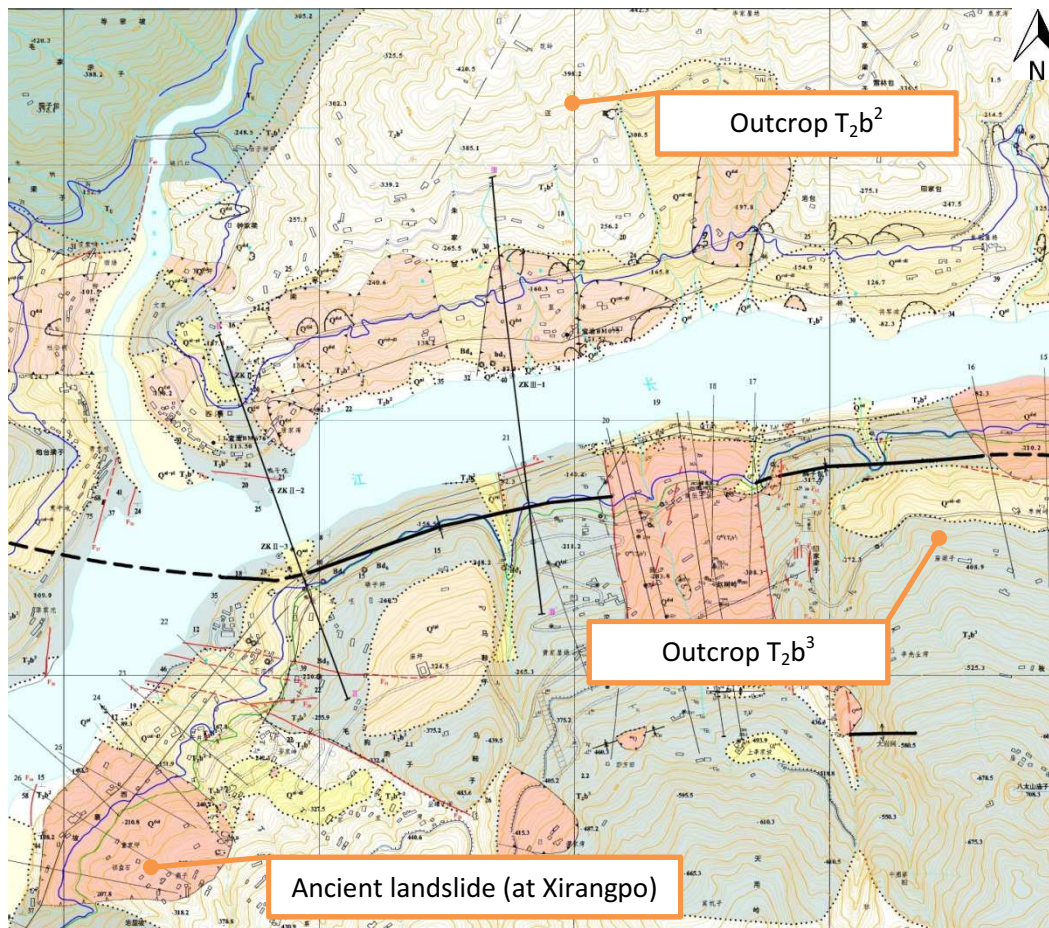


Figure 29: Mapping of the selected sites (China University of Geosciences, Wuhan)

## 2.2 Field Investigation

The ÖNORM B4401 (Austrian-Standard 1981) covers the geotechnical investigation carried out in the field work in Badong. The in this thesis used terms and symbols are defined in ÖNORM B 4490 (Austrian-Standard 1981). The following sections outline the different tests carried out both in the field and on the samples taken.

### 2.2.1 Designation of Rock

The following designations are not meant to describe the type of rock in a petrographic context but to assess the engineering properties, their rock mass and especially their joint faces which are important to carefully evaluate.

### **2.2.1.1 Particle Size**

The size of the components of minerals was assessed:

To distinguish between:

- Coarse grained rock (macro crystalline)
- Fine grained rock (fine- crystalline)
- Dense Rock (micro- crystalline)

The particle size differs within their type since coarse grained sandstone overlaps with fine grained conglomerate. To display the size in mm is recommended.

### **2.2.1.2 Determination of the hardness (scratch hardness)**

A clear determination of the hardness is only possible on minerals. Therefore the designation should be executed on the largest possible single grains. Dense rock (such as lime stone, basalt) can also be assessed on the fracture surface.

The following degrees of hardness were determined:

- 1-2 with finger nails able to scratch
- 3 with knife easy to scratch
- 4 with strong pressure of a knife still able to scratch
- 5 with knife hardly but with a file able to scratch
- ≥6 produces sparks if hit by steel and scratches window glass

### **2.2.1.3 Determination of the rock strength (Schmidt Hammer)**

A determination of the rock strength is possible through taking measurements using the Schmidt Hammer. Such measurements were taken in the investigated site of  $T_2b^2$  and  $T_2b^3$ . For each value 16 readings were taken, dropping the three highest and the three lowest. Then the average of the ten remaining was taken. A table of the manual handbook of the Schmidt Hammer (Type ZC3-A) was used to then convert the metered value of the readout scale (see Figure 30) into the rock strength (see annex 8.2.). The used column of the Table is 0.0 (0.0 mm calcification). However, this method doesn't give a direct measurement. It is used to give an indication based on surface properties (Proceq 2013).



Figure 30: Readout scale of the Schmidt hammer (Photo: Mayrhofer 2012)

#### 2.2.1.4 Calcium carbonate content

The calcium carbonate content of a rock can be estimated by an air dried sample. Hydrochloric acid (water to hydrochloric acid 5:1) is dropped on a sample. It is to distinguish between:

- Non calcareous: no reaction (non effervescent)
- Calcareous: slight to clear reaction, but not persisting (e.g. argillaceous marl, clayey marl, clay marl, shaly marl)
- High calcareous: highly persisting effervescent (e.g. limestone)

Pure limestone dissolves residue-free. Marl leaves muddy residuals. Dolomite needs an undiluted hydrochloric acid and has to be pulverized before.

#### 2.2.1.5 Colour

The colour is immediately determined after the sample is taken. Differences between fresh fractures and old joint faces were recorded.

#### 2.2.1.6 Odour

The smell on fresh broken samples is determined (e.g. an earthy smell indicates argillaceous rock).

#### 2.2.1.7 Condition of Rock

##### 2.2.1.7.1 Weathering conditions

The weathering conditions of the rock samples were assessed to determine the:

- Characteristics of not weathered rock: intact rock mass, bright sound during knocking, fresh colours, reflecting fracture planes; and
- Characteristics of weathered rock: weak rock mass, dull colour, earthy staining, sanding, and further friable between fingers.

#### 2.2.1.7.2 Type and grade of tectonic decomposition

On taken samples or exposed rocks, the following was determined:

- free of cracks
- joints
- cracks
- brecciated
- sheared
- crushed or triturate (Myolinit)
- glass seam
- slawm

#### 2.2.1.7.3 Description of separation plane structure

Types of separation plane like bedding plane, cleavage plane, joint plane (ss, sf, k)

Facing of the separation plane: dip direction and the dip angle measured with geological compass.

Condition of the separation plane:

- even or uneven
- rough – plain (e.g. slickenside)

Filling between the separation plane

Weathering conditions on separation planes:

- colouring
- weakening
- solution process

## 2.2.2 Designation of mineral soil

Field work carried out in Badong included several tests on the mineral soils. A number of tests concerning the density measurement, plate loading and shear vane were planned by the author but unfortunately impossible to carry out in the time frame of the field work. However, tests concerning the soil foundation provide the most useful data for the results concerning the soils. Missing data was also obtained from previously existing research carried out in the Badong area. Photographic evidence was taken of the mineral soils to provide an overview and in order to document the findings.

### 2.2.2.1 Particle size

The classification of soils is subdivided into coarse grain and fine grain components.

The coarse grain components with a diameter  $>0.063$  mm are subdivided into:

- Boulder (Y)       $>200$  mm
- Stones (X)       $>63$  mm –  $200$  mm
- Gravel (G)       $>2$  mm –  $63$  mm
  - Subdivided into coarse,- medium,- and fine gravel
- Sand (S)         $>0.06$  mm –  $2$  mm
  - Subdivided into coarse,- medium,- and fine sand

The coarse grain components were designated through visual classification.

The fine grain components with a diameter  $\leq 0.006$  mm are subdivided into a grading fraction of:

- Silt (U)          $>0.002$  mm –  $0.6$  mm
- Clay (T)         $<0.002$  mm

The particle size of clay and silt are under the visibility limit of the naked human eye. Manual methods are necessary.

Crushing the soil between the hands a silty soil appears soft and floury. The dry particles on the fingers are to be blown away. Clayey soils feel soapy and greasy and even when the particles are dry it is not possible to take it off without washing. Further test of plasticity were carried out.

**2.3 Laboratory tests**

The methods of laboratory investigation were carried out according to the National Standard of the People’s Republic of China (China National Standard 1999).

**2.3.1 Water Content Test**

The water content test was carried out in accordance with the following steps:

1. 10- 30 g representative specimen was weighed in a cutting ring (see Figure 31) Then the mass of the box and the wet soil were weighed.
2. Then the box was put in an oven and dried at the constant temperature of 105- 110°C. The drying time, for the clay and silt, was over the standard of 8 hours minimum. After the required time the box was put in a dry container cooling it to room temperature. Then the mass of the box and the dry soil was weighed.
3. The water content of the specimen was calculated according to the following formula accurate to 0.1%.

$$w_0 = \left(\frac{m_0}{m_d} - 1\right) \times 100$$

Whereas:

$m_d$ .....mass of the dry soil (g)

$m_0$ ..... mass of the wet soil (g)



Figure 31: Cutting ring (Photo: Mayrhofer 2012)

**2.3.2 Density Core Cutter Method**

This test method is applicable to the fine-grained soil. The dimension of the cutting ring inner diameter was 61.8 mm with a height of 20 mm.

The cutting edge was placed on the soil specimen and depressed vertically. At the same time, the soil knife was used to cut the soil specimen along the outer side of the cutting ring until the soil specimen was higher than the cutting ring. Then the fret saw or soil knife was adopted to level off the soil specimen at the ends of the cutting ring. Finally, the outer walls of the cutting ring were scrubbed and the total mass of the cutting ring and the soil weighed. The representative specimen was taken from the remaining soil to measure the water content.

The wet density of the specimen was calculated according to the following formula:

$$\rho_0 = \frac{m_0}{V}$$

Whereas:  $\rho_0$ .....wet density of the specimen (g/cm<sup>3</sup>)

The dry density of the specimen was calculated according to the following formula:

$$\rho_d = \frac{\rho_0}{1 + 0.01w_0}$$

Three parallel measures were made in this test and the measured difference didn't exceed 0.03 g/cm<sup>3</sup> and the mean value of these measured values was taken.

### 2.3.3 Triaxial test

#### 2.3.3.1 Specimens preparation and saturation

The diameter of the specimen used in this test was 35 mm and the specimen height was 2 times that of the specimen's diameter. The allowed maximum particle size of specimen met the requirements of Table 4.

Specimen diameter	Allowed maximum particle size
< 100	1/10 of specimen diameter
> 100	1/5 of specimen diameter

Table 4: The maximum particle size of specimen soil grain (mm)

As the particle size did not fit, the soil was prepared like disturbed soil according to the maximum particle size of soil grain.

After preparing the specimen according to the scheduled dry density and water, the specimen of the disturbed soil was thumped tightly layer by layer (from 5 to 8 layers) in a sample hitter. The earth material quantity of each layer was equal.

To saturate the sample the air exhaust saturation was carried out. The sample was exposed to a vacuum for two hours and saturated with water for eight hours before the test.

#### 2.3.4 Unconsolidated undrained triaxial test

The specimen was sheared in the following steps:

1. The shear strain rate was 0.5% - 1.0% of strain per minute.
2. When the peak value appeared at the numerical reading of load meter, the shearing was carried out until the axial strain was 15% (see Figure 34).

(For complete data see annexe 8.1)



Figure 32: Prepared sample for triaxial test (Photo: Mayrhofer 2012)



Figure 33: Fixed sample on the triaxial device (Photo: Mayrhofer 2012)

Output data from the test device are:

- height of specimen
- diameter
- confining pressure  $\sigma_3$
- load speed
- axial displacement
- axial strain
- axial force
- axial stress
- $\sigma_1$



Figure 34: Sheared sample at an axial strain of 15% (Photo: Mayrhofer 2012)

Cohesion and shear angle were read and taken out of diagrams of drawn Mohr's circles (by linear equation).

### 2.3.5 Quick Shear test within the weak layer

The test was repeated with different vertical pressures.

The shear velocity was 0.8 mm/min until the test was finished; the specimen was cut and destroyed in 3- 5 min (see Figure 36)



Figure 35: Device for quick shear test (Photo: Mayrhofer 2012)



Figure 36: Specimen after shearing (Photo: Mayrhofer 2012)

The shear stress was calculated according to the following equation:

$$\tau = \frac{C * R}{A_0} * 10$$

Whereas:

T.....bared shear stress of specimen (kPa)

R.....numerical reading of dynamometer

A relation curve of shear stress and shearing displacement was drawn up as shown in the example in Figure 37. The peak value of shear stress on the curve serves as the shearing strength. When there is no peak value, the shear stress corresponds to 4 mm of shearing displacement which serves as the shearing strength.

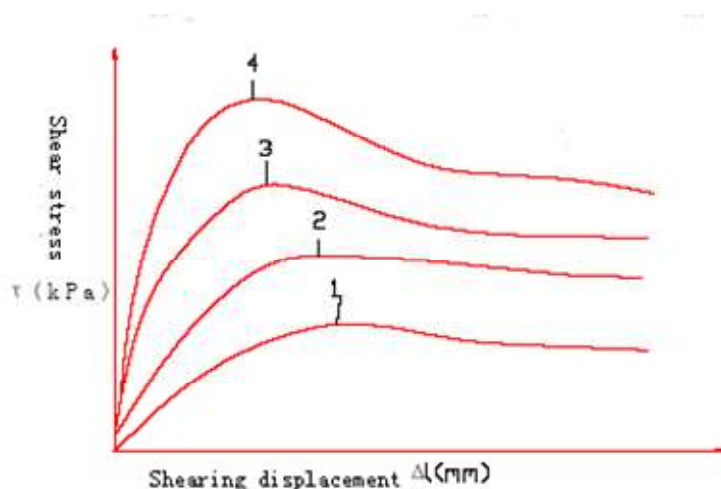


Figure 37: An example of a relation curve of shear stress and shearing displacement (China National Standard 1999)

Relation curves of shearing strength and vertical pressure were drawn. The slope angle of the straight line represents the sliding- angle, the intercept of straight line on the ordinate is the cohesive force as shown in the example of Figure 38.

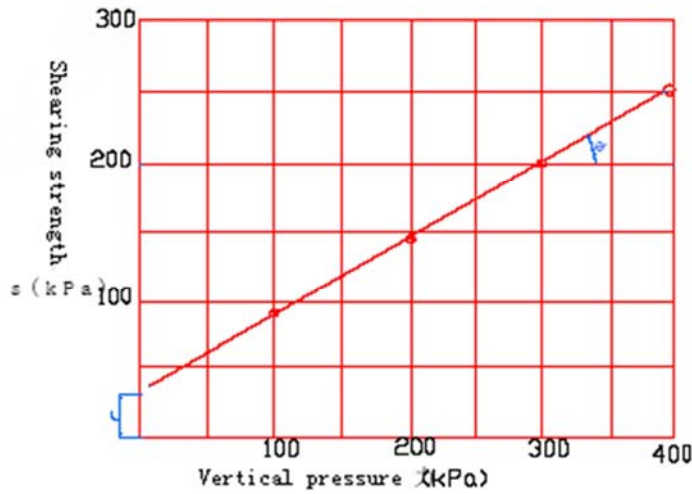


Figure 38: Relation-curve of shearing strength and vertical pressure (China National Standard 1999)

### 2.3.6 X-Ray Diffraction Test

The X-Ray Diffractometer (Type: X'Pert pro Dy2198) of the University of Geosciences of Wuhan was used (see Figure 41 and Figure 42). It is possible to describe about 95% of all solid materials as crystalline and hence the atoms are arranged in a regular pattern. X-rays interact with the crystalline substance and a diffraction pattern appears. The diffraction pattern of a pure substance can be considered as a fingerprint of the substance (Scintag 1999).

The soil is dried at 70 degrees Celsius, so that the clayey part does not lose the absorbed intermediate layer water. The samples (rock and soil) are ground down to particles of 0.002 mm cross section. Then the sample is pressed between two small glass plates, in order to obtain the required smooth flat surface (see Figure 39 and Figure 40).



Figure 39: Ground sample (Photo: Mayrhofer 2013)

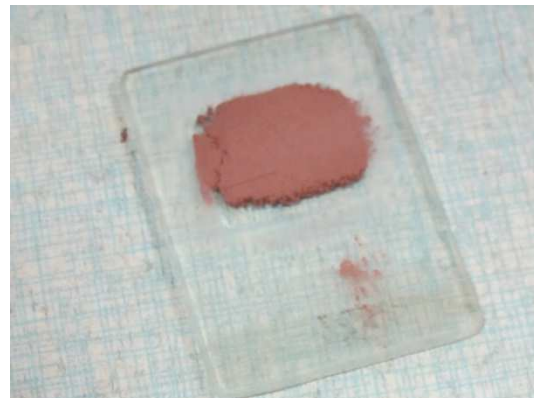


Figure 40: Sample between two small glass plates (Photo Mayrhofer: 2013)

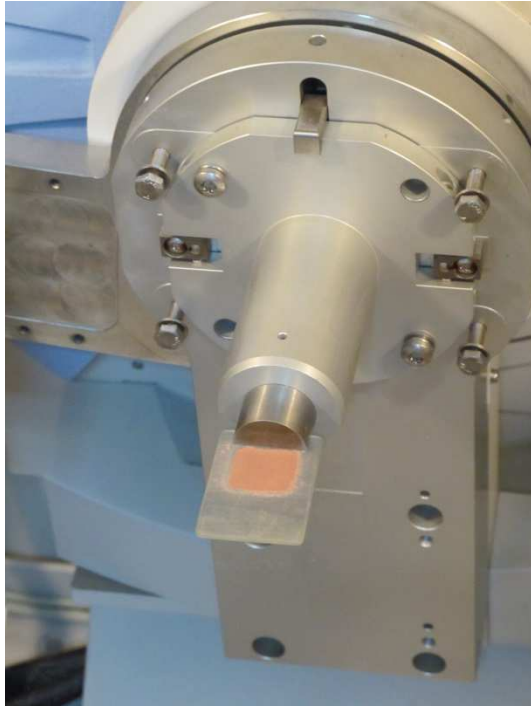


Figure 41: Sample holder of the X-Ray Diffractometer (Photo: Mayrhofer 2013)



Figure 42: X-Ray Diffractometer of China University of Geoscience (Photo: Mayrhofer 2013)

Then the sample is pressed into the sample holder of the X-Ray Diffractometer. The plot of the diffraction spectrum was analysed by the Team of the Laboratory of the China University of Geoscience of Wuhan and the results were sent via mail.

## 2.4 Rock quality designation index (RQD), Rock mass rating (RMR)

Efforts to find a constitutive law of rock mass has a long history, but until now there is no satisfying model found. So the rock and the rock mass respectively are best described through its structure, such as separation planes. Most of the parameters are obtainable during fieldwork (Schwingenschlögl 1991).

### 2.4.1 Rock quality designation index (RQD)

The rock quality designation index was first developed by Deere (Deere D.U. 1967) to provide a quantitative estimation of rock mass quality from drill core logs. Palmström (Palmström A. 1982) recommended that, when no drilling core is available, but the discontinuities are visible on surface exposures, the RQD can be estimated by the number of discontinuities per unit volume.

The suggested formula for clay-free rock masses is following:

$$RQD = 115 - 3.3 J_v$$

Whereas:

$J_v$ .....sum of the number of joints per unit length for all joint (discontinuity) sets known as the volumetric joint count (Rock-science 2013).

#### **2.4.2 Rock mass rating (RMR)**

Rock mass has obviously a lower strength than the intact rock. To estimate the strength of rock masses a system of rock mass classification called the Geomechanics Classification or the Rock Mass Rating (RMR) system was developed by Bieniawski in 1976 and refined until 1989 (Bieniawski 1994). However, there is still no published satisfying determination system for estimation the strength of rock masses. Six parameters are used to classify a rock mass using the RMR system:

1. Uniaxial compressive strength of rock material
2. Rock Quality Designation (RQD)
3. Spacing of discontinuities
4. Condition of discontinuities
5. Groundwater conditions
6. Orientation of discontinuities

The Rock Mass Rating system is presented in Table 5. The rating of each parameter is listed. The summed ratings give the value of RMR. Of this value the rock mass classes and strength parameter can be deducted as illustrated in section C and D of Table 5 (Rock-science 2013).

A. CLASSIFICATION PARAMETERS AND THEIR RATINGS									
Parameter			Range of values						
1	Strength of intact rock material	Point-load strength index	>10 MPa	4 - 10 MPa	2 - 4 MPa	1 - 2 MPa	For this low range - uniaxial compressive test is preferred		
		Uniaxial comp. strength	>250 MPa	100 - 250 MPa	50 - 100 MPa	25 - 50 MPa	5 - 25 MPa	1 - 5 MPa	< 1 MPa
		Rating	15	12	7	4	2	1	0
2	Drill core Quality RQD		90% - 100%	75% - 90%	50% - 75%	25% - 50%	< 25%		
	Rating		20	17	13	8	3		
3	Spacing of discontinuities		> 2 m	0.6 - 2. m	200 - 600 mm	60 - 200 mm	< 60 mm		
	Rating		20	15	10	8	5		
4	Condition of discontinuities (See E)		Very rough surfaces Not continuous No separation Unweathered wall rock	Slightly rough surfaces Separation < 1 mm Slightly weathered walls	Slightly rough surfaces Separation < 1 mm Highly weathered walls	Slickensided surfaces or Gouge < 5 mm thick or Separation 1-5 mm Continuous	Soft gouge >5 mm thick or Separation > 5 mm Continuous		
	Rating		30	25	20	10	0		
5	Groundwater	Inflow per 10 m tunnel length (l/m)	None	< 10	10 - 25	25 - 125	> 125		
		(Joint water press)/ (Major principal $\sigma$ )	0	< 0.1	0.1 - 0.2	0.2 - 0.5	> 0.5		
	General conditions		Completely dry	Damp	Wet	Dripping	Flowing		
	Rating		15	10	7	4	0		
B. RATING ADJUSTMENT FOR DISCONTINUITY ORIENTATIONS (See F)									
Strike and dip orientations			Very favourable	Favourable	Fair	Unfavourable	Very Unfavourable		
Ratings	Tunnels & mines		0	-2	-5	-10	-12		
	Foundations		0	-2	-7	-15	-25		
	Slopes		0	-5	-25	-50			
C. ROCK MASS CLASSES DETERMINED FROM TOTAL RATINGS									
Rating	100 < 81		80 < 61	60 < 41	40 < 21	< 21			
Class number	I		II	III	IV	V			
Description	Very good rock		Good rock	Fair rock	Poor rock	Very poor rock			
D. MEANING OF ROCK CLASSES									
Class number	I		II	III	IV	V			
Average stand-up time	20 yrs for 15 m span		1 year for 10 m span	1 week for 5 m span	10 hrs for 2.5 m span	30 min for 1 m span			
Cohesion of rock mass (kPa)	> 400		300 - 400	200 - 300	100 - 200	< 100			
Friction angle of rock mass (deg)	> 45		35 - 45	25 - 35	15 - 25	< 15			
E. GUIDELINES FOR CLASSIFICATION OF DISCONTINUITY conditions									
Discontinuity length (persistence)	< 1 m		1 - 3 m	3 - 10 m	10 - 20 m	> 20 m			
Rating	6		4	2	1	0			
Separation (aperture)	None		< 0.1 mm	0.1 - 1.0 mm	1 - 5 mm	> 5 mm			
Rating	6		5	4	1	0			
Roughness	Very rough		Rough	Slightly rough	Smooth	Slickensided			
Rating	6		5	3	1	0			
Infilling (gouge)	None		Hard filling < 5 mm	Hard filling > 5 mm	Soft filling < 5 mm	Soft filling > 5 mm			
Rating	6		4	2	2	0			
Weathering	Unweathered		Slightly weathered	Moderately weathered	Highly weathered	Decomposed			
Rating	6		5	3	1	0			
F. EFFECT OF DISCONTINUITY STRIKE AND DIP ORIENTATION IN TUNNELLING**									
Strike perpendicular to tunnel axis				Strike parallel to tunnel axis					
Drive with dip - Dip 45 - 90°		Drive with dip - Dip 20 - 45°		Dip 45 - 90°		Dip 20 - 45°			
Very favourable		Favourable		Very unfavourable		Fair			
Drive against dip - Dip 45-90°		Drive against dip - Dip 20-45°		Dip 0-20 - Irrespective of strike°					
Fair		Unfavourable		Fair					

\* Some conditions are mutually exclusive. For example, if infilling is present, the roughness of the surface will be overshadowed by the influence of the gouge. In such cases use A.4 directly.

\*\* Modified after Wickham et al (1972).

Table 5: Rock Mass Rating System (Bieniawski 1979)

## 2.5 Stability analyses

Limit equilibrium software makes it possible to handle increasing complexity within an analysis. It deals with complex stratigraphy, highly irregular pore water pressure conditions, various linear and nonlinear shear strength models, almost any kind of slip surface shape, concentrated loads, and structural reinforcement (Geo-Slope 2012, p. 1).

Following components for stability analyses were taken from the results:

- Geometry: description of stratigraphy and shapes of potential slip surface
- Soil strength: parameter are based on the Mohr Coulomb failure criterion
- Reinforcement: anchors and piles as these are often used in Badong area
- Imposed loading: simulating external loads like buildings

### 2.5.1 Factor of safety calculation method Morgenstern Price

For calculation of the factor of safety the Morgenstern Price method was used. Two factor of safety were considered; the moment- and force equilibrium.

The determination of these factors of safety of a sliding body of any shape is made with varying shear strength parameters and pore pressures. Also an assumption must be made, regarding the distribution of internal forces by choosing the function (Morgenstern et al. 1965, p. 92.)

This method allows choosing between a constant function for interslice forces and half-sine function. The half- sine function was used to calculate estimated circular slip surfaces and the constant function is used for planar slip surfaces, because the interslice resultant force is constantly declined. The calculation with constant function conforms in this case to the Spencer method. Plane slip surfaces are assumed along weak layer like a clay layer in  $T_2b^3$ .

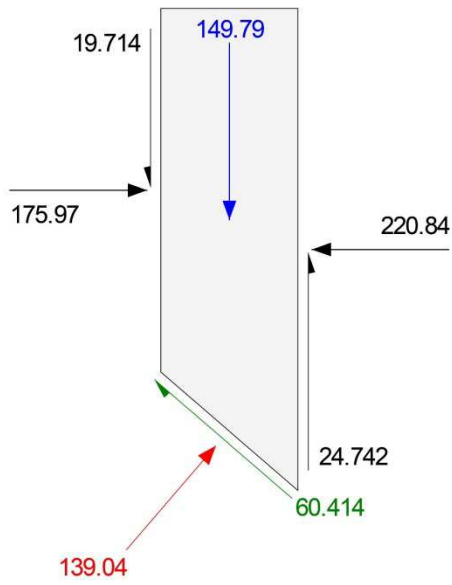


Figure 43: Free body of constant function (Geo-Slope 2012, p. 40)

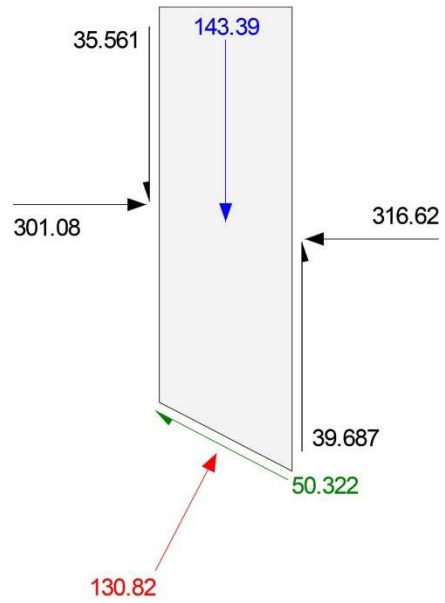


Figure 44: Free body of half- sine function (Geo-Slope 2012, p. 42)

As aforementioned with a constant function the ratio of shear- and normal forces are the same (see Figure 43). On the left side the ratio is  $175.97/19.714= 8.93$ , and on the right side the ratio is  $220.84/24.742= 8.93$ .

### 3 Results

The following sections outline the results found from the field investigations and laboratory tests. These assessments were carried out on the soil and rock formation in the three selected sites in Badong as identified in Figure 29 (see chapter 2.1), respectively the ancient landslide, the  $T_2b^2$  opening and the  $T_2b^3$  exposure.

#### 3.1 Foundations on ancient landslide mass

Whilst big landslides, like Huangtupo, are already well researched and assessed, the field investigation in the Badong area revealed that several small slope failures on ancient landslides like the aforementioned Erdaogou landslide (see Chapter 1.6.2.3, Figure 22) still occur. They are mostly triggered by earth moving during construction.

##### 3.1.1 Investigated site

The investigated site on the ancient landslide at Xirangpo is located south west of Badong Town on the south wing of the Guangdukou syncline. Its toe is about 100 m.a.s.l. and it reaches an altitude of 325 m.a.s.l. If the water impoundment of the Yangtze reaches its maximum of 175 m.a.s.l (October – January), almost half of the regarded area is submerged under the water. The mean dip angle of the surface is about 18°. The area is mostly used by farmers. The farming areas are cut into a series of successively receding flat surfaces. The few houses are built on shallow foundations of about one meter depths. Due to the low habitat density, there is a potential for new housing, although it should be taken into consideration that the area is intensively used for farming, which generates the income for the few farmers living there. There are no reported recent landslide activities. But because of the potential for new housing and therefore a possible increase of human activity, it is an interesting site in which to investigate slope stability under different external conditions, like external loads or earth movement, and under given internal conditions like the present soil properties.

The map in Figure 45 shows, that the mass of the slope consists mostly of quaternary age residuals, mostly demise residuals on the top ( $Q^{del}$ ).

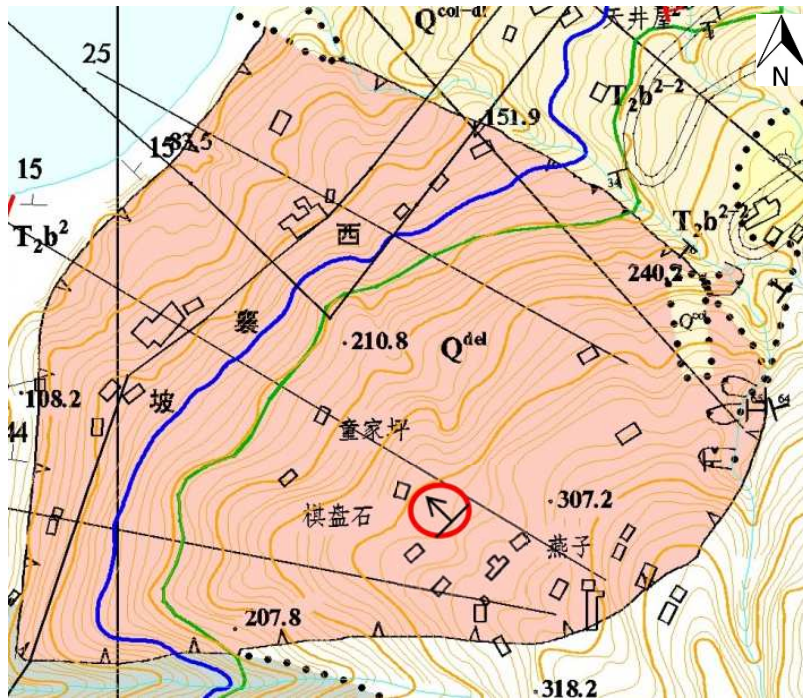


Figure 45: Geological map of the ancient landslide at Xirangpo (pink area) (China University of Geosciences, Wuhan); the red circle indicates the investigated site; the blue line indicates the water level at 175 m.a.s.l.

No existing cross section of this slope is available to give information on the underground.

### 3.1.2 Field Investigation

The samples are taken right under the rear edge of the slope (red circle in Figure 45). Due to limited tools for digging, the samples are taken at just one metre depth. The colour of the soil is red, as the slope is situated on the second member of the Badong formation.

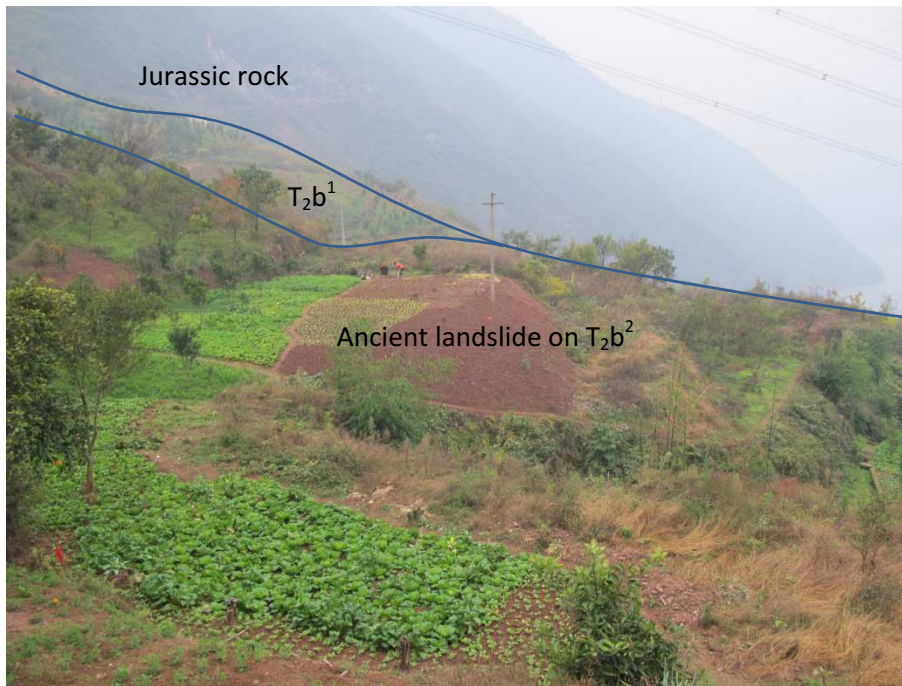


Figure 46: Setting of the investigated ancient landslide (Photo: Mayrhofer 2012)

### 3.1.2.1 The grain distribution

The soil consists mostly of gravel and silt. The fine material blasts the skeleton of the gravel. The consistence is found to be moist-wet and semi-solid. Some organic additions like roots are found up to 1 m depth.

There are no possibilities such as wells to measure the ground water level, but it is expected to be about 20- 50 m under the ground level, as two ravines are cutting the side edge of the slope. Exploratory drilling records are not available.

Additionally the shear parameter of the table by Schnell (Smoltczyk et al. 2001, p. 122; see annex 8.2) was assessed. The categories to choose differ between blasting and not-blasting the skeleton. In this case the soil properties of the following category are taken: gravel, sandy, with silt and clay content which are blasting the skeleton of the gravel. This category suggests shear parameter of  $\varphi$  28°-35° and  $c$  30 kPa-10 kPa. As the content of silt appears very high the assumed parameter are  $\varphi$  28° and  $c$  30 kPa. The associated unit weight is 20 kN/m<sup>3</sup>.

### 3.1.3 Laboratory Tests

#### 3.1.3.1 Water content $w$ , dry density $\rho_d$ :

Cutting ring No.	Wet soil mass (g)	Dry soil mass (g)	Wet density (g/cm <sup>3</sup> )	Water ratio (%)	Dry density (g/cm <sup>3</sup> )	unit weight (kN/m <sup>3</sup> )
1049	132,406	112,710	2,207	17,5%	1,879	
99	135,216	115,241	2,254	17,3%	1,921	
<b>Mean</b>	<b>133,8</b>	<b>114,0</b>	<b>2,23</b>	<b>17,4%</b>	<b>1,90</b>	<b>21,88</b>

Table 6: Density and water ratio of the ancient landslide soil (Dec. 2012)

The parameters are similar to the upper part of the landslide mass of the Huangtupo landslide. The water ratio is 17.4%. One day prior to the taking of the samples there was a recorded rainfall of 2 mm (Meteorological-Services-section 2013).

#### 3.1.3.2 Unconsolidated undrained triaxial test

In the Laboratory of CUG Wuhan, the triaxial device for UU- tests (unconsolidated undrained- test) is available. This simulates conditions of high pore pressure, as it would be after the reservoir level is lowered. New buildings are not permitted close to the Yangtze, so it is not of priority interest in this thesis. However, the results are demonstrated to give an insight into the situation on the bank area of the Yangtze River. Soil samples taken from the selected site were subjected to the triaxial test device. In cooperation with Chinese colleagues, an excel file was developed to analyse the data (see annexe 8.1). After drawing the Mohr-circle, total strength parameter  $\varphi$  of 22.71° and cohesion of 48.44 kPa are measured. This data allows a comparison of similar tests taken on the Huangtupo slope. As the reported test results from the mass of the upper part of the Huangtupo slope (see Table 7) are similar to the tests on the selected site at the Xirangpo slope, it is possible to take further properties of the Huangtupo slope to estimate the properties of deeper existing layers. However, a limiting factor remains, in that the strength parameters of the Huangtupo slope are not clearly defined as total- or effective strength. The Mohr circles should be equal in size and with an increase of the axial load of the specimen the circle normally moves along the abscissa axis. In this triaxial test the radii of the circles increase within the increasing  $\sigma_1$  (see Figure 48). This can be explained by the fact that the samples might not been fully saturated, so the results do not display a fully undrained behaviour. However, the results do display an almost undrained behaviour, but for a foundation on this site it is only the undrained effective shear strength that is relevant, so calculating with the results of the present triaxial test means calculating on the safe side.

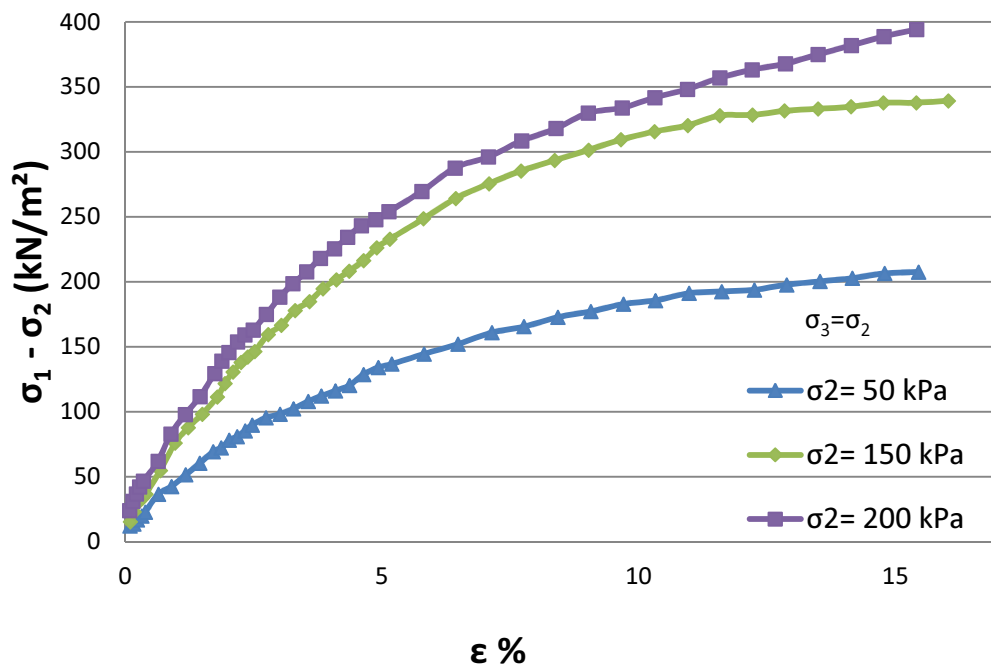


Figure 47: Triaxialtest (2012)

The results of the sample of 100 kN/m<sup>2</sup> confining pressure were not taken into the calculation of the shear strength, as the sample did not compress along the axis, but moved sideward. It is known, that undrained samples can hardly be controlled as they collapse with bulging by skeleton decay (Gudehus 2011, p. 642). In addition, the values are not coherent to the trials of the other samples with different confining pressures.

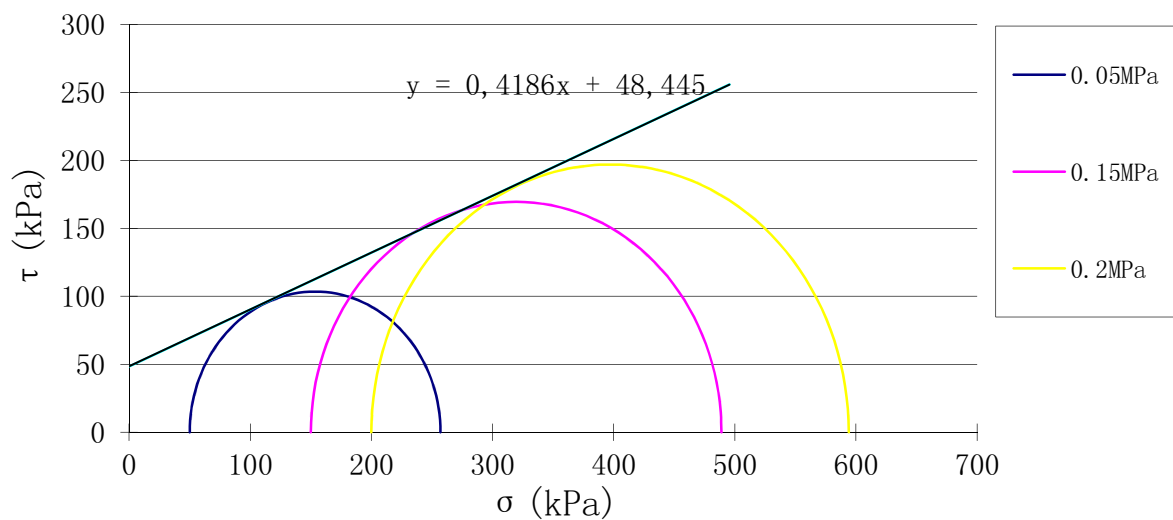


Figure 48: Mohr circles of the triaxial tests

### 3.1.4 Former published results

#### 3.1.4.1 Shear parameter of the Huangtupo sliding mass

Since the executed Triaxial test alone would be too uncertain to be taken without control, the data from the Investigation report of Huangtupo landslide in Badong county (see Table 7) are compared with the present Triaxial test results. The sliding mass of the middle and upper part are under similar conditions as the site where the samples of the Xirangpo slope were taken. The friction angle of the Xirangpo slope ( $\phi=22.7^\circ$ ) is situated between the results of the Huangtupo Sliding mass ( $\phi = 23^\circ$  (middle part) and  $18^\circ$  (upper part)).

Material		Unit weight $\gamma$ (KN/M <sup>3</sup> )	Deformation modulus E (MPa)	Poisson's ratio $\mu$	Shear strength		Residual strength	
					C MPa	$\phi$ (°)	$C_r$ MPa	$\phi_r$ (°)
Bedrock	Siltstone, sandstone T <sub>2</sub> b <sup>2</sup>	27	16300	0.31	0.98	44.2	0.40	32
	Limestone T <sub>2</sub> b <sup>3-1</sup>	27	51000	0.21	0.7	54	0.30	35
	Pelitic limestone T <sub>2</sub> b <sup>3-2</sup>	26	37600	0.23	0.42	48	0.26	33
Sliding zone	Sliding zone (upper part)	22	25.66	0.34	0.019	14.0	0.013	12.5
	Sliding zone (under part)	22	16.13	0.35	0.017	14.0	0.011	12.0
Sliding mass	Sliding mass (under part)	21.5	1960	0.29	0.027	18.0	0.021	16.1
	Sliding mass (middle part)	21	2560	0.28	0.031	23.0	0.024	16.7
	Sliding mass (upper part)	20	1210	0.31	0.024	18.0	0.019	15.2

Table 7: Data from "Investigation report of Huangtupo landslide in Badong County" Hubei geo-hazard prevention and investigation institute, December, 2011

**3.1.5 Simulation of slope stability under different boundary conditions**

**3.1.5.1 Simulation: Excavation on ancient sliding mass on Xirangpo**

**Material Properties:**

Ancient Sliding Mass

Cohesion: .....31 kPa  
 $\phi$ : .....23°  
 Unit Weight: .....20 kN/m<sup>3</sup>

} orange

T<sub>2</sub>b<sup>2</sup> Bedrock

Cohesion: .....260 kPa  
 $\phi$ : .....30°  
 Unit Weight: .....25 kN/m<sup>3</sup>

} red

**Setting:**

Analysis Type: ..... Morgenstern-Price  
 PWP-Condition: ..... From Pizeometric Line  
 (blue dotted line)  
 Side Function: ..... Half-sine-function  
 Slip surface Option: ..... Entry and Exit

The thickness of the ancient sliding mass is estimated at about 50 m. The simulated foundation is situated on a slope with a dip angle of 18.4°, downhill of the foundation the slope dip angle increases to 25.3°. This displays steeper angles than the mean angle of the observed area to generate a high risk area. The ground water is assumed to be approximately 25 m under the surface. As the two ravines cut deep on both flanks of the slope, the level of the groundwater is expected to be deeper, but the simulated conditions display the condition prevalent in the rain season.

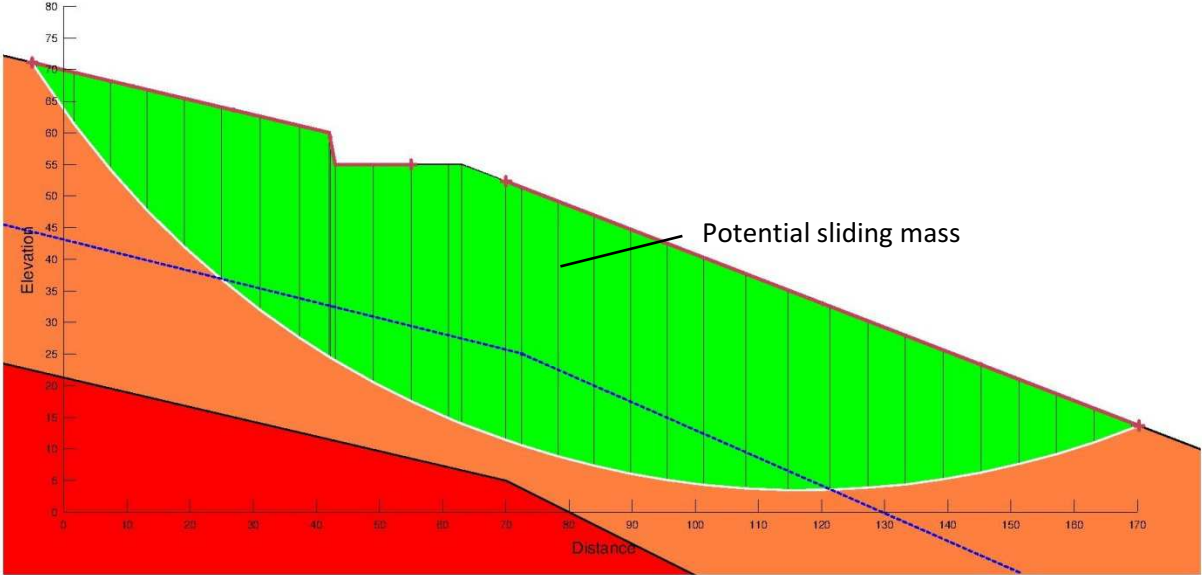


Figure 49: Simulation: Slide mass of ancient landslide on Xirangpo; FOS: 1.699

The simulation shows a factor of safety of 1.699 (Figure 49). The range was set for small landslides, but as the weakest slip surface is on the boundary of the possible slip surface exit range, the more unstable parts of the slope are outside of this range.

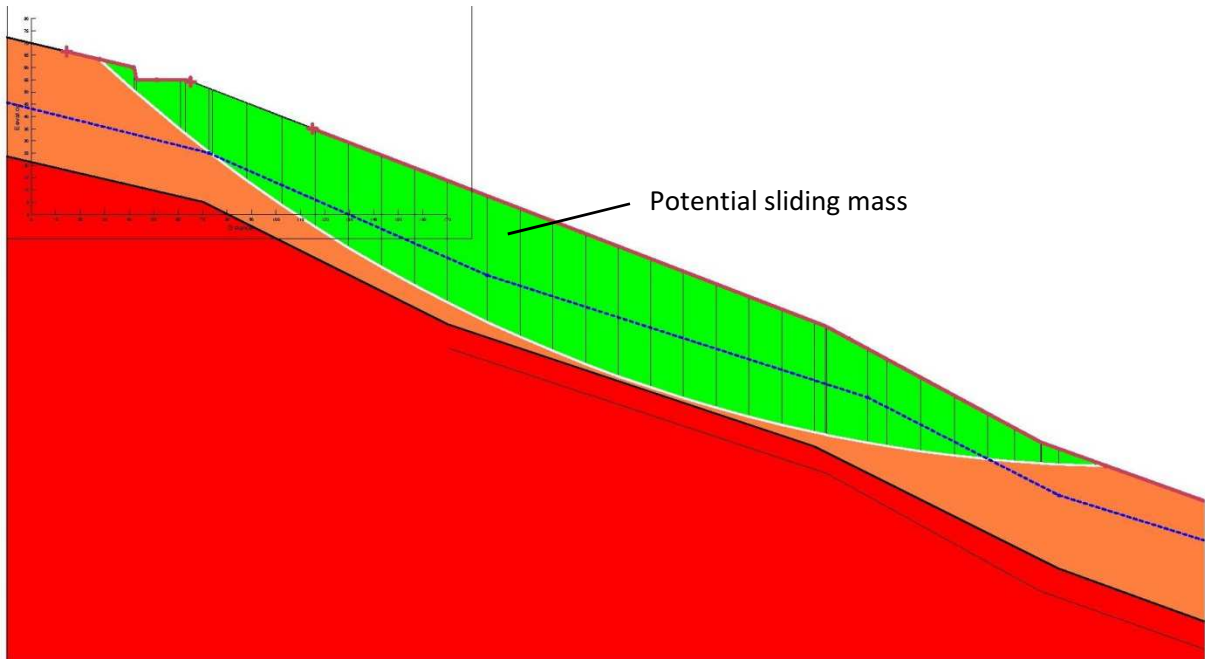


Figure 50: Simulation: Slide mass of ancient landslide at Xirangpo with wide entry-exit ranges; FOS: 1.022

Figure 50 shows a simulation with a wide range of the possible slip surface. The factor of safety decreases (1.022), but the whole slope is stable.

The simulation of a building in form of a surcharge load of (450 kN/m<sup>2</sup>) was added. A nine floor building like the new houses for the people of the Huangtupo slope (as showed in Figure 57) would be this dimension. The factor of safety reduces (compare Figure 51 and Figure 49) and the weakest found slip surface is small and shallow, but the slope is stable.

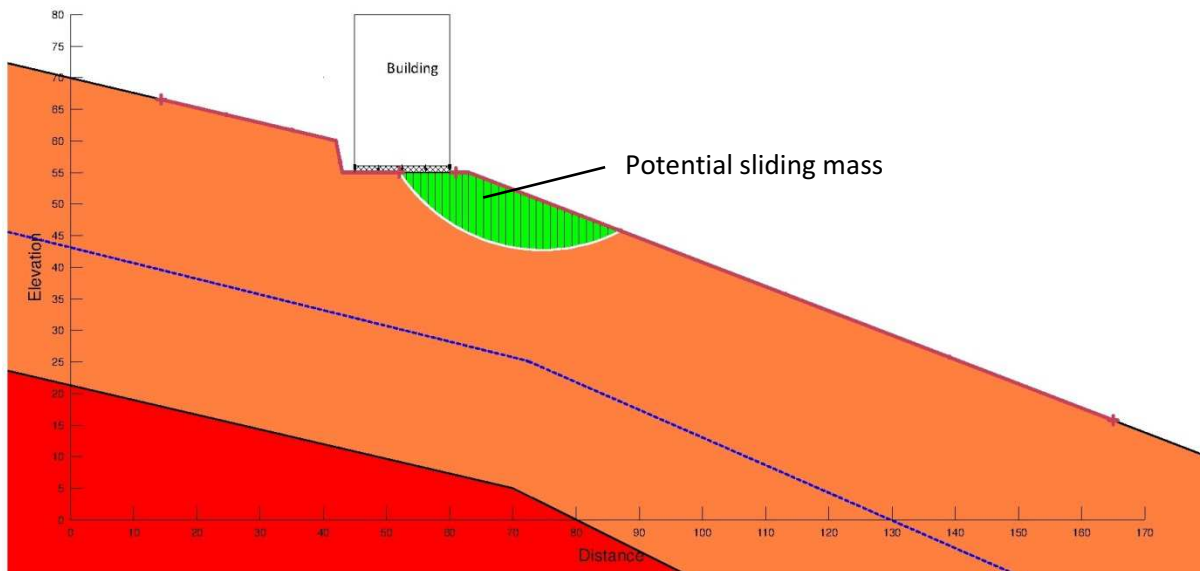


Figure 51: Simulation: Building on slide mass of ancient landslide on Xirangpo; FOS: 1.341

A simulation of stabilization piles increases the factor of safety (compare Figure 52 and Figure 51). However, due to limits of the used software, these piles cannot be calculated as pile foundation, which distributes the load of the house along the pile through the carcass friction. So the calculated effect on these stabilisation piles is the uptake of the shear forces in the underground.

**Pile reinforcement settings:**

Length:.....15 m

Spacing: .....3 m

Shear force: .....1500 kN

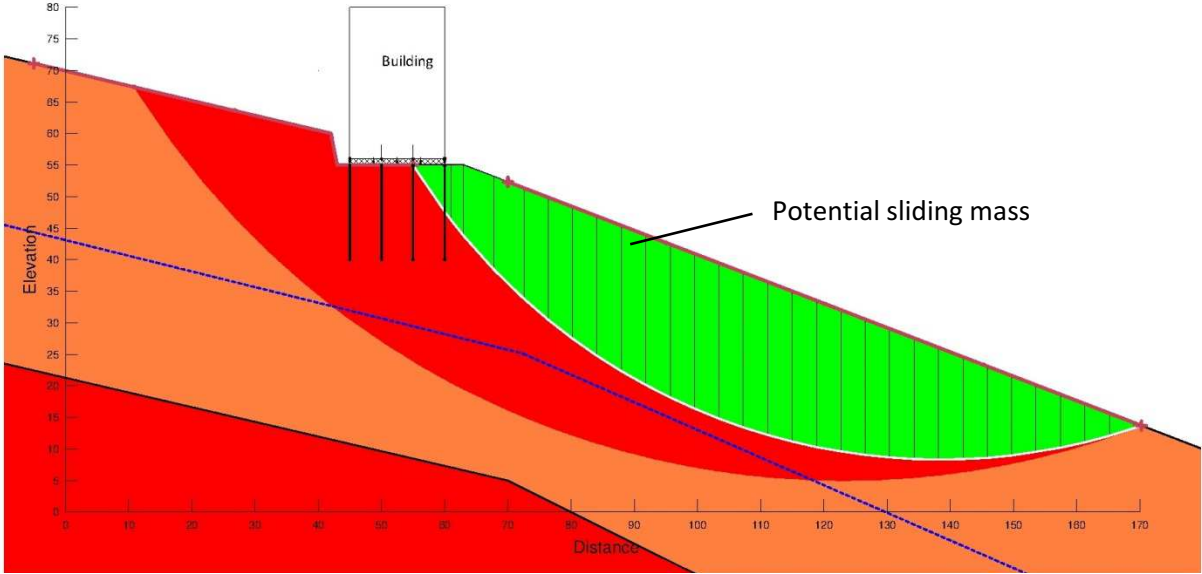


Figure 52: Simulation: Building and stabilisation piles on slide mass of ancient landslide at Xirangpo; FOS: 1.605

## 3.2 Foundations on $T_2b^2$

A further main surface for new houses is that of  $T_2b^2$ . The purple mudstone is well known for its high decay rate and the weathering degree of the subsurface is difficult to predict.

### 3.2.1 Investigated site

The characteristic opening of the second member of the Badong formation is situated in the north of Badong town, on the north wing of the Guandukou syncline. This area is called Tong gu bao. The global position is N 31° 04'E 110° 20' altitude 416 m. It is an artificial opening, made for the new settlements to be provided for the people of the Huantupo slope/landslide. As the following map shows, the investigated area is situated on geological conditions of  $T_2b^2$ , about 1 km north from the Yangtze River.

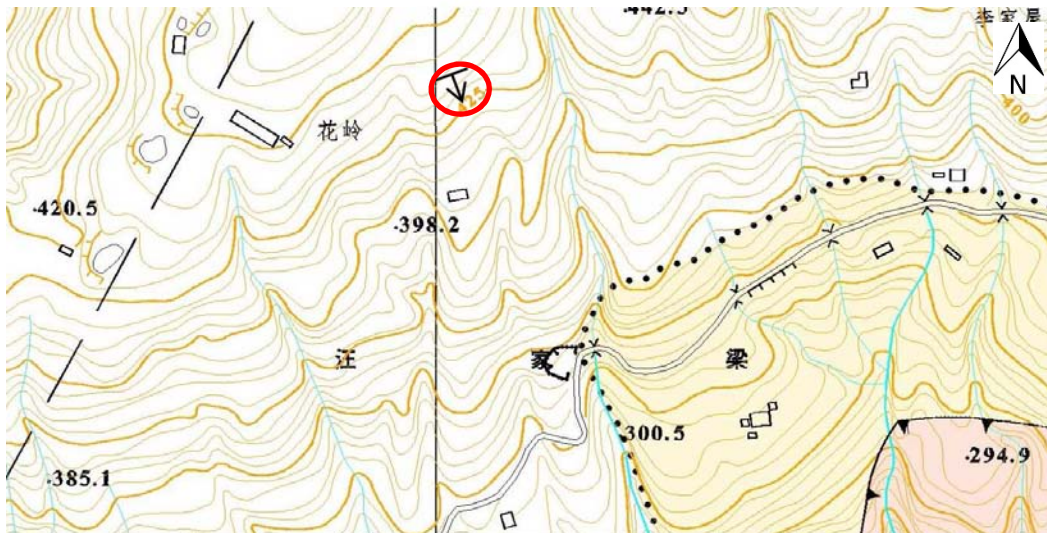


Figure 53: Geological map of  $T_2b^2$  (China University of Geosciences, Wuhan); the red circle indicates the investigated site

### 3.2.2 Field Investigation

The field investigations in the T<sub>2</sub>b<sup>2</sup> site show that the rock is decomposed and weak (see Figure 54). It is weathered into angular stones and gravel.



Figure 54: Exposure of T<sub>2</sub>b<sup>2</sup> (Photo: Mayrhofer 2012)

It consists mostly of red mudstone with white grey inclusions, but also white grey bed sets with locally a smooth transition into red or a boundary as a separation plane (see Figure 55).



Figure 55: Red calcareous mudstone with grey bed sets (Photo: Mayrhofer 2012)

The rock is full of cracks and joints, these are often filled with plastic clay and silt (loam). No ground water is found until approx. 20 m under the initial ground surface. There are some small wet spots underground, however at the same depth, of six meter distance there was no water. These were recorded during field inspections of a hole made for pile foundations for new housing on the selected

site. The dull red mudstone is dark red on its fresh fracture. In parts it appears with black spots (see Figure 56).



Figure 56: Black spots on red mudstone (Photo: Mayrhofer 2012)

The scratch hardness is 2 and the fracture plane is natural cleft. After comminuting the particles appear like clay. The hydrochloric acid test displays a delayed reaction and after the test mud residual stays. After wetting it develops a slightly muddy smell.

The bedding planes of different spots of the site are taken (n=6). The dip direction differs between 210° and 245° and the dip angle between 40° and 45°, neglecting one of 60° which was highly weathered and decomposed. This contradicts the reported dip angle of the north wing of the Guandukou syncline, which should be between 10°-25° (Wang 2009, p. 25).

The strength of the rock differs within its weathering conditions. Rocks with multiple cracks and fillings of clay display a strength of about 10- 30 MPa. Those with less weathering influence such as rocks protected from water, reach strength of 56 MPa.

The silty clay stone of a white greyish colour has a rougher, coarse grained fracture plane. Comminuted material appears like silt and the hydrochloric acid test does not display any reaction.

### **3.2.2.1 Rock foundation versus soil foundation**

The degree of weathering is highly advanced. So in this case the attributes of rock foundation are not satisfied any more. In this case the foundation's performance is more like soil. As mentioned before, it was possible to investigate a hole of approx. 20 m under the former surface. The classification of the lifted material was X, G, u', t. The amount of the fine material was not able to blast the granular skeleton of the gravel. The table by Schnell (Smolczyk et al. 2001, p. 122; see annex 8.2) differs between: *blasting, and not-blasting the skeleton*. In this case the soil properties of the following category are taken: gravel, sandy, with silt and clay content which are not blasting the skeleton of the gravel. This category suggests shear parameters of  $\varphi$  35°- 43° and c 10 kPa- 0 kPa. As the assessed gravel on the slope is angular, the assumed parameters are  $\varphi$  38° and c 8 kPa. The associated unit weight is 22 kN/m<sup>3</sup>.

### 3.2.3 Laboratory Tests

#### 3.2.3.1 XRD-Test

A XRD- Test was carried out in the Laboratory of the China University of Geoscience, Wuhan. The results match with reported results of purple mudstone in this area and display no new features (see Table 8).

	Montmorillonite	Clinochlore	Illite	Kaolinite	Quartz	Feldspar	Calcite	Dolomite	Hematite
样品编号	蒙脱石	绿泥石	伊利石	高岭石	石英	长石	方解石	白云石	赤铁矿
RS 1	20	15	10	0	30	6	15	0	4
RS 3	15	10	10	0	36	14	13	0	2
RS 5	20	10	10	5	32	4	15	0	4

Table 8: XRD-Test of  $T_2b^2$  rock

#### 3.2.4 Former published results

A regional report on purple red mudstone had following results on the grain distribution:

Particle size (粒径) mm	>10	10-5	5-2	2-1	1-0.5	0.5-0.25	0.25-0.075	0.075-0.05	0.05-0.01	0.01-0.005	<0.005
Soil name (土名)											
Purple red soil(gravel) 紫红色含砾土	8.45	3.63	17.23	11.13	2.89	5.71	2.80	13.14	8.59	3.9	22.55

Table 9: Grain distribution after sieving ( Zhou et al. 2001)

The soil appears like the visual assessed soil of the field work, but with already higher decayed particles. As there is no current grain distribution of this thesis, a direct comparison is not possible.

Number 编号	Name 土名	Water content 含水量 w (%)	Density 密度 $\rho$ (g/cm <sup>3</sup> )	Mohr Parameter			
				c (kPa)	$\varphi$ (°)	c' (有效) (kPa)	$\varphi'$ (°)
1	Fine particle 含细粒土	11.9	1.87	10	14	3	27
2	Gravel(soil) 碎石土	/	1.37	2	24	/	/

Table 10: Results of a large scale triaxial test of weatered material on  $T_2b^2$  (Zhou et al. 2001)

The parameter varies in a great extent (Table 10). The gravel has lower  $\varphi$  than the effective  $\varphi'$  of the fine particle.

			Shear parameter	
			c (kPa)	$\varphi$ (°)
$T_2b^2$	Nr. 1	Purple silty mudstone ( $235^\circ \angle 11^\circ$ )	110	38
$T_2b^2$	Nr 2.	Purple silty mudstone ( $15^\circ \angle 68^\circ$ )	105	38

Table 11: Strength parameter of joints in  $T_2b^2$  (Zhou et al. 2001)

In another study, the strength parameters on rough joint-planes display  $\varphi$  of  $38^\circ$  (Table 11). However, the high cohesion is due to intact material bridges in the joint.

### 3.2.5 Simulation of slope stability under different boundary conditions

#### 3.2.5.1 Input parameter

The decay rate of the present soil is hard to predict. Data from existing triaxial tests of this soil are not obtainable. For the simulation, the properties of the fine particles of the highly weathered rock are also considered to demonstrate the long-term situation, because in the future the rock will be further decayed and will consist of finer particles. Schnell's table satisfies this requirement and the parameters, mentioned in Chapter 3.2.2.1, are taken.



Figure 57: New Houses for people of Huangtupo slope, under construction (on  $T_2b^2$ ) (Photo: Mayrhofer 2012)

### 3.2.5.2 Simulation: Excavation on $T_2b^2$ highly decayed rock

#### Material Properties:

##### Weathered Soil

Cohesion: .....8 kPa  
 $\varphi$ : .....38°  
 Unit Weight: .....22 kN/m<sup>3</sup>

} pink

##### $T_2b^2$ Bedrock

Cohesion: .....260 kPa  
 $\varphi$ : .....30°  
 Unit Weight: .....25 kN/m<sup>3</sup>

} red

#### Setting:

Analysis Type: ..... Morgenstern-Price  
 PWP-Condition: ..... From Pizeometric Line  
 (dotted blue line)  
 Side Function: ..... Half-sine-function  
 Slip surface Option: ..... Entry and Exit

For reasons of comparison the same slope angle- and further geometric slope conditions of the ancient sliding mass are taken. The strength parameters of the material of the weathered soil of  $T_2b^2$  are higher. The factor of safety (2.316) shows that the slope is not in danger of sliding (Figure 58). Here also the range was set for small landslides. The weakest slip surface is on the boundary of the possible slip surface exit range. So the more unstable parts of the slope are outside of this range.

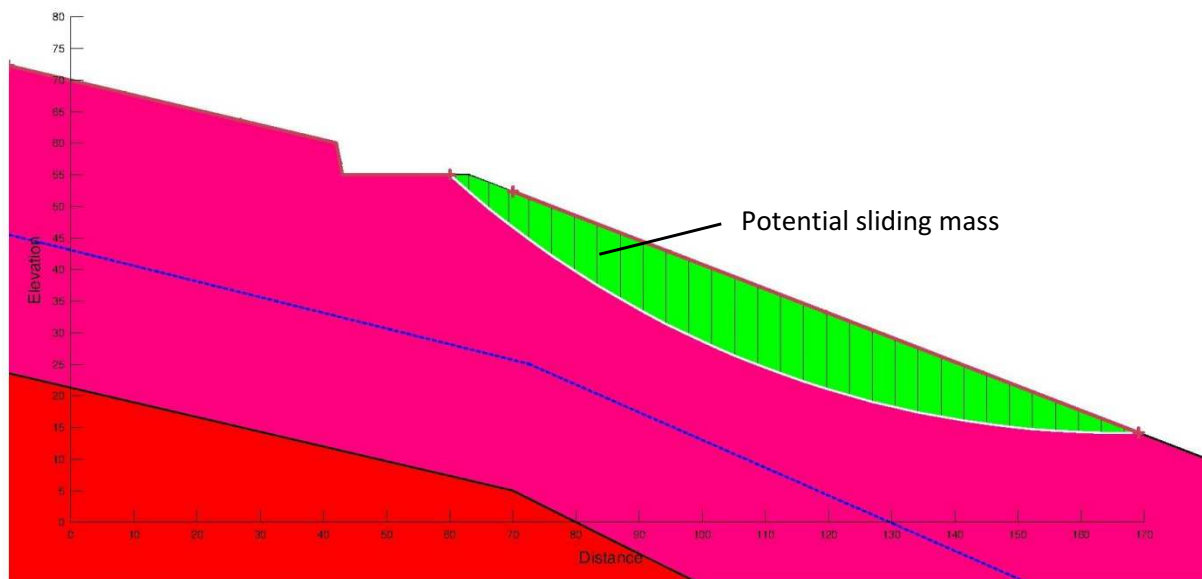


Figure 58: Simulation:  $T_2b^2$  highly decayed rock; FOS: 2.316

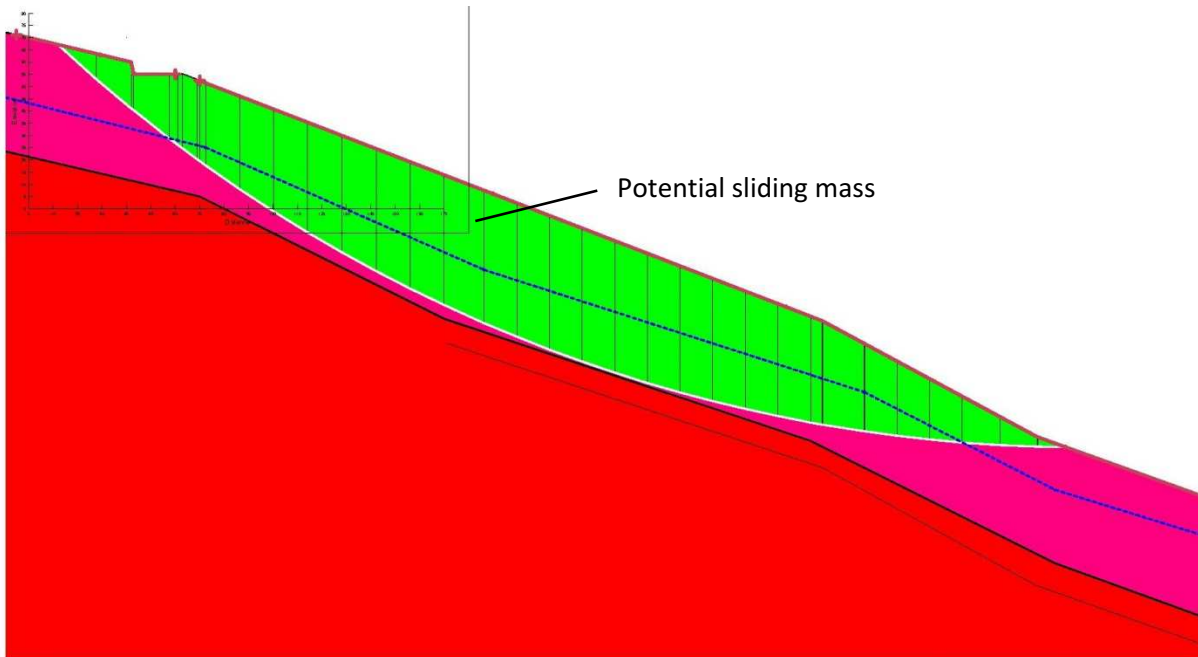


Figure 59: Simulation:  $T_2b^2$  highly decayed rock with wide entry-exit ranges; FOS: 1.728

A simulation with a wide range reveals, that the factor of safety decreases (1.728), but that the whole slope is stable (Figure 59).

Applying a load like a building (see Figure 60), the factor of safety decreases (compare Figure 58 and Figure 60), however, a factor of safety of 2.225 shows, that the skeleton of the gravel is well able to carry the load into the ground. No further simulation with a wider range is made, as the stability of the whole slope is already proven.

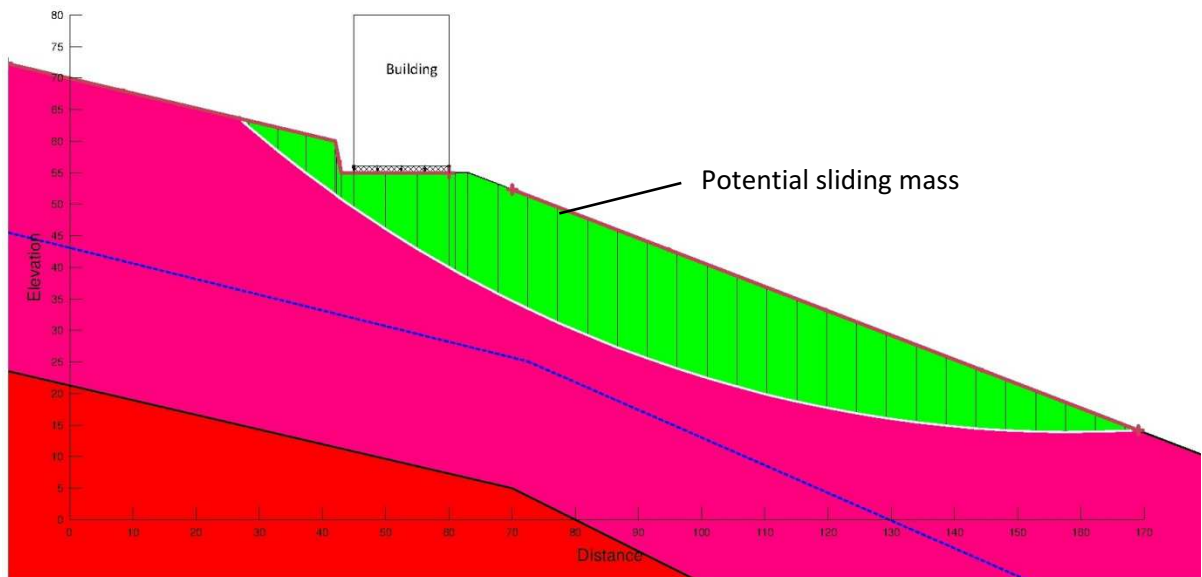


Figure 60: Simulation: Building on  $T_2b^2$  highly decayed rock; FOS: 2.225

Stabilisation piles, as illustrated in Figure 61, would be not necessary on this slope angle. However foundation piles to minimize subsidence should be taken into account and might be necessary.

**Pile reinforcement settings:**

Length:.....20 m

Spacing: .....3 m

Shear force: .....1500 kN

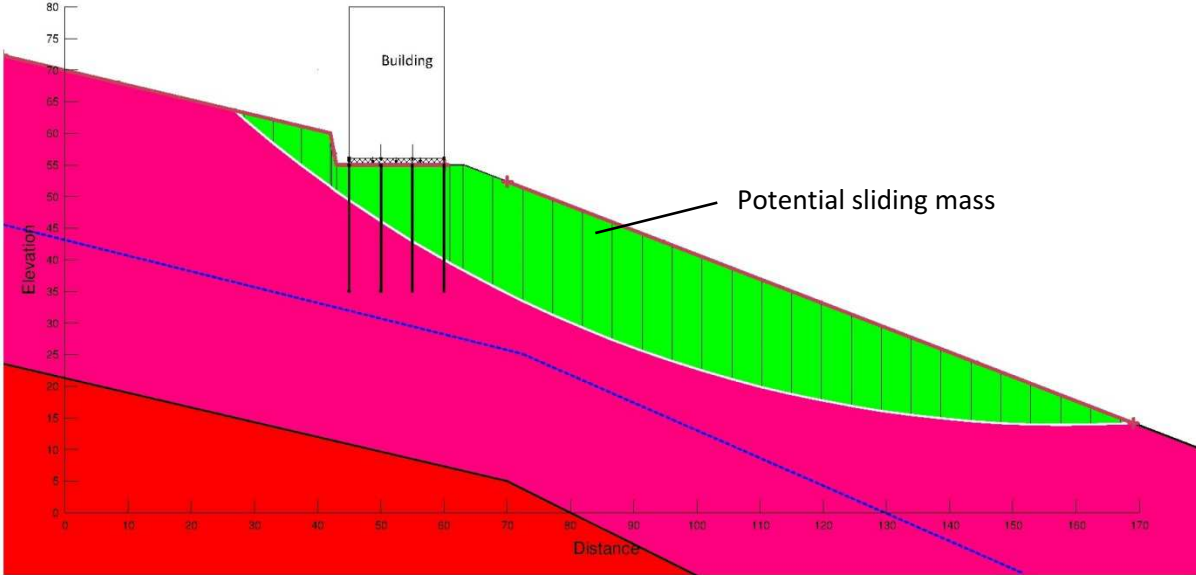


Figure 61: Simulation: Building with stabilisation pile on  $T_2b^2$  highly decayed rock; FOS: 2.396

### 3.3 Foundation on $T_2b^3$

#### 3.3.1 Investigated site

The site of the artificial opening is situated on the Baitupo- slope on the South wing of the Guandukou syncline. The global position is  $31^{\circ} 2'52.89''N$ ;  $110^{\circ}21'21.10''E$  altitude 386 m.a.s.l. It is an existing construction site in the middle of an urban developed area.

As the map in Figure 62 shows, the investigated area is situated on geological conditions of  $T_2b^3$ . The zone of the assessed artificial opening is marked with a red circle.

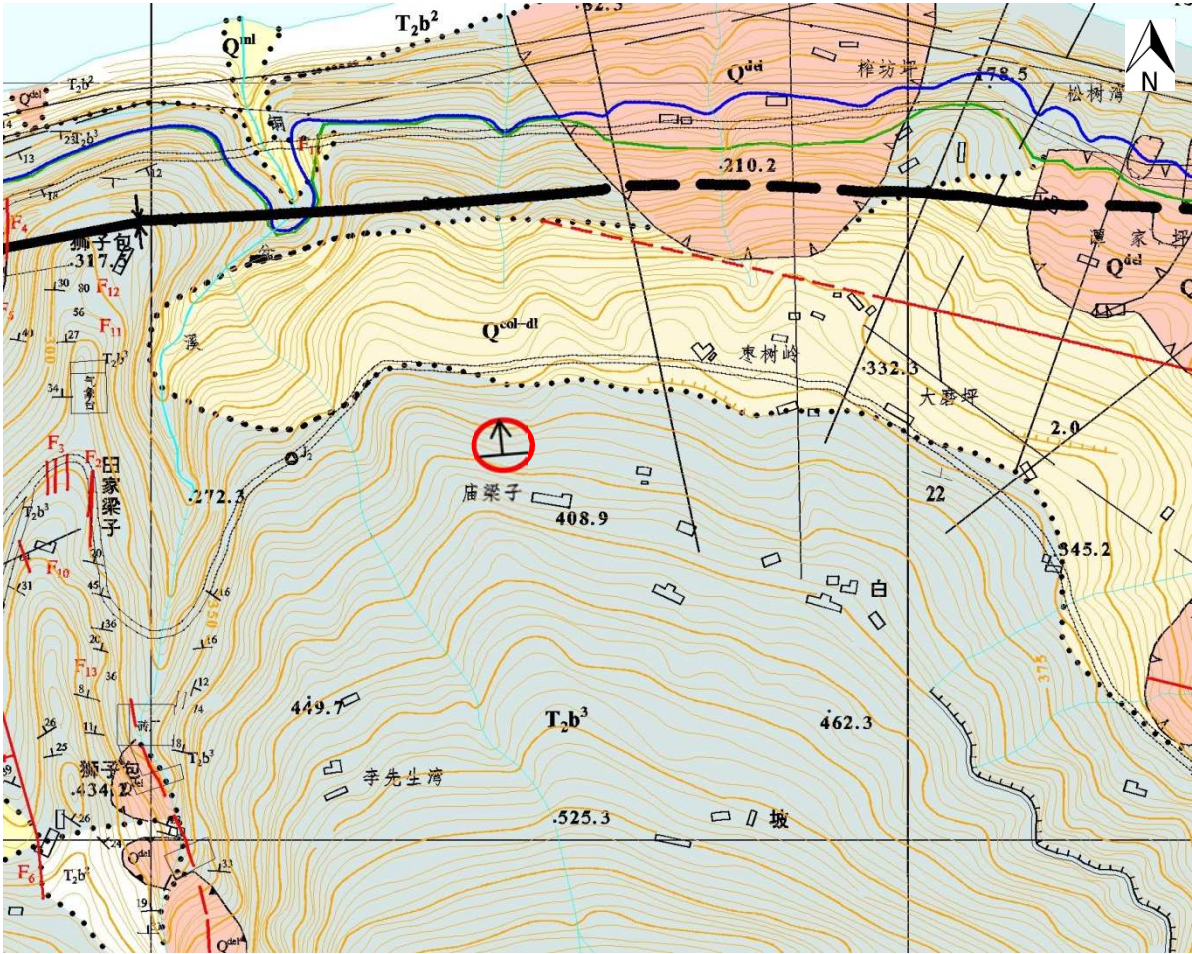


Figure 62: Geological map of  $T_2b^3$  (red circle indicates the investigated site); blue line: water level at 175 m.a.s.l.

### 3.3.2 Field Investigation

The field investigations on the  $T_2b^3$  site show that several layers of marlstone are exposed (see Figure 63). The whole cutting is 5.5 m perpendicular in height to the described layer. The quaternary deposits are not available on this site. Estimating for the surroundings, the layer of quaternary deposits is about 5 to 10 m thick (in patches more) and is mainly composed of yellowish-grey soil with gravel contents.

The marlstones are of a bright- brown to greyish- grey colour. Cracks are distributed over every 2- 3 m. There are some spots with 3 cracks per meter. The cracks are along the dip direction as well as along the main trend almost perpendicular to the interlayer.

Compass measurements of several interlayers display a dip direction of  $10^\circ$  and a dip angle of  $35^\circ$ . This accompanies the former reported dip angle of the south wing of the Guandukou syncline (Wang 2009, p. 25).



Figure 63: Exposure of  $T_2b^3$  (Photo: Mayrhofer 2012)

#### 3.3.2.1 Artificial opening profile

The general incline of the shear zone, weak zone and interlayer, displayed in the following images, has approximately a north-ward direction and dips with a maximum of  $35^\circ$  down.

1



The first layer of the Artificial opening is a brown- grey coloured marlstone with a scratch hardness of 1-2. The total dimension is 0.4 m. The fracture plane appears rough. Smith hammer measurements show strength of 41 MPa. The transmission zone of layer 1 and 2 is undisturbed.

2



This grey interbedding has a dimension of 1.7 m. The fracture plane is between smooth and slightly rough. A slight reaction of HCl shows a medium carbonate content. The scratch hardness reaches 4 with a measured strength of 52.7 MPa.

3



A weak interlayer of two centimetre thickness is between layer 2 and 4. It consists of flattened small gravel as the main grain size with sand and silt/clay in between. The granular skeleton of the gravel is not blasted.

4



A 27 cm thick grey layer is similar to layer 2 but a bit darker grey coloured. It also displays a slow HCl reaction. The scratch hardness of 4 and the slightly rough fracture plane indicates similar properties like layer 2. Just the measured strength is with 52.5 MPa a bit higher.

5



Layer 5 is a similar thin weak layer like interlayer 3 of 4 cm thickness. It consists mainly of gravel and sand with silt/clay in between. The granular skeleton of the gravel is not blasted.

6-8



Layer 6 is a grey 95 cm thick layer, similar to layer 4 and 2. The fracture plane appears smooth like a wood plate- The scratch hardness reaches 5. The measurements with the Schmidt hammer display a higher strength of 59.5 MPa.

There is a smooth transition (Layer 7) between the layer 6 and 8. The colour changes into grey-brown of a thickness of 10 cm.

Layer 8 is a 50 cm thick grey layer with similar properties as layer 6. Measurements with the Schmidt hammer display strength of 49.3 MPa.

9



Layer 9 is a reddish, 60 cm thick layer of mudstone. With strength of 14.4 MPa it has a weak appearance as also the scratch hardness is only 1. It is interposed with cracks and loose rock topples out. The HCl test displays a slow reaction. The fracture plane appears from soft to slightly rough.

10



The transition between layer 9 and 10 is blurred.

Layer number 10 is a weak layer of 10 cm. With a main content of clay and silt (T,u'). Calcareous concretions with intense HCl-reaction are noticeable.

11



The following layer is grey coloured. Similar to the aforementioned grey layer but the scratch hardness reaches just 4. Here the measurements with the Schmidt hammer show strength of 36.2 MPa. It is the last possible layer to assess.

#### 3.3.2.1.1 Crushed beds

Nr.3 and 5 are typical crushed beds in the member of  $T_2b^3$  as they consist mainly of gravel and sand. The gravel content and cementation material have a significant effect on the strength. Gravel has a climbing effect as rock joint shear shows. Results of a paper by Chai et al. (2012) have shown that the shear strength of a sand interface is with about  $28^\circ$  internal friction angle and 120 kPa cohesion, which seems relatively low. But test samples of crushed layers can display a friction angle of  $49^\circ$  and cohesion of 72 kPa. Crushed beds are cemented by calcite with low moisture content and this explains the high shear strength. If disturbed samples are taken and the sand with a grain size of 2 mm is used for a direct shear test, the shear strength is very low ( $\varphi$  of  $21.6^\circ$  and  $c$  of 10kPa). Crushed beds have also a strong infiltration capacity. Therefore it can be deduced that crushed beds can easily deform and fail when they are affected by groundwater and lose their calcite cementation which will be replaced by clay minerals (Chai et al. 2012, p. 10). The crushed beds of Nr. 3 and 5 have already a certain amount of silt and clay which means that there is already an influence of water decomposing the material.

#### 3.3.2.1.2 Clay interlayer

Nr 10 is a typical clay interlayer of  $T_2b^3$ . That is because of the unstable sediment environment of  $T_2b^3$  with its different mineral contents and strengths. Clay interlayers are easily generated. Between the soft and hard rock those crushed beds are developed with the Guandukou syncline deformation. When the river cuts to the corresponding elevation, the crushed beds are rebuilt, calcareous minerals are partly dissolved and the content of clay is relatively increased. Through further cutting of the river, the incompetent beds are subsequently formed (Chai et al. 2012, p. 10).

### 3.3.3 Laboratory tests

#### 3.3.3.1 Shear test of weak zones between the layers

The shear strength is one of the most important parameters with which to estimate whether the slope's stability is endangered through slip zones or weak layers such as those present in the T<sub>2</sub>b<sup>3</sup> site investigated.

A quick shear test on the taken samples under different vertical pressures shows shear strength parameters  $\phi$  of 5.97 degree and  $c$  of 21.95 kPa (see Figure 64 and Figure 65).

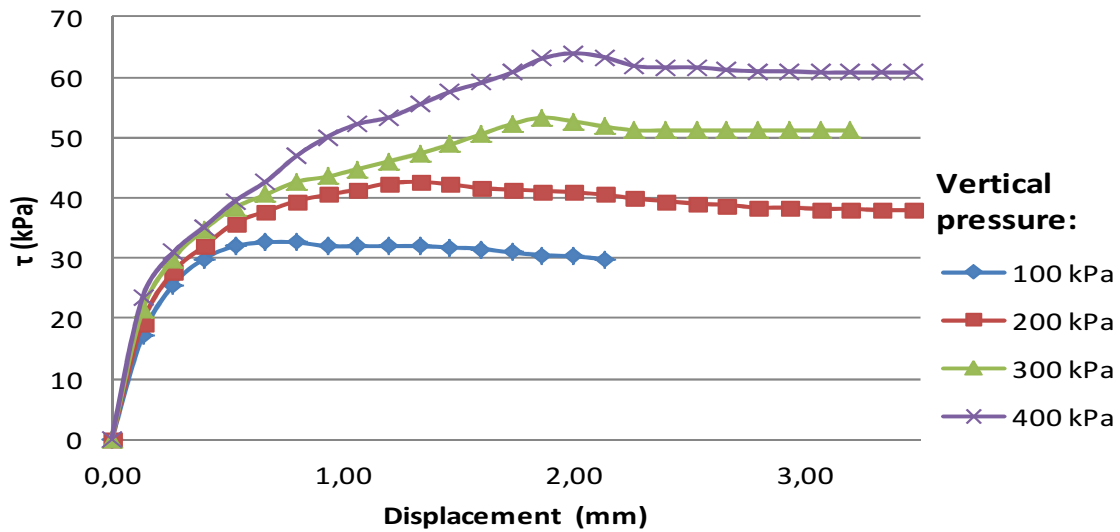


Figure 64: Relation curve of shear stress and shearing displacement

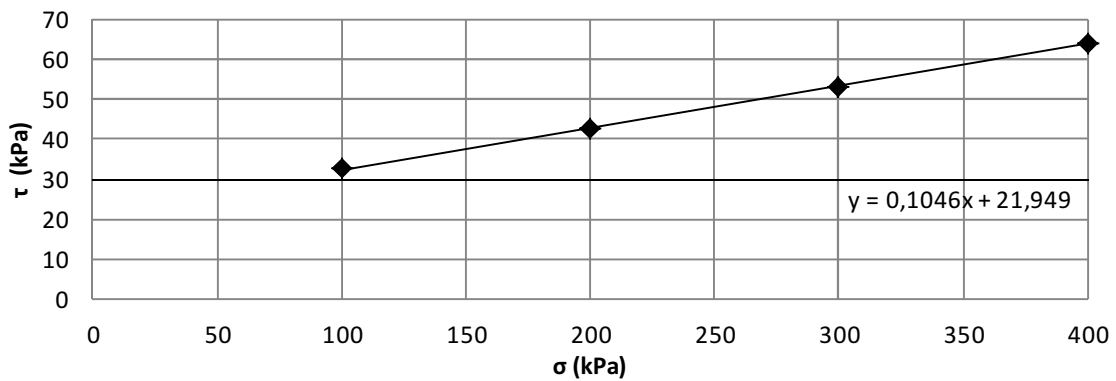


Figure 65: Relation of shear strength and vertical pressure

The internal friction angle is far less than expected for such material. One important reason might be that the procedure of the quick shear test is too fast for material with high clay content. As a result, the pore pressure is too high and the material cannot establish shear strength, as it could under normal conditions. But it is obvious that no reasonable shear force can be transmitted by this layer.

However, other results of slow shear tests show that a clay interlayer similar to the present material has friction angle of 29° and cohesion of 20 kPa; when measuring the residual shear strength of the clay interlayer, by repeated slow shear tests, lower results are given. So if the rock strata are affected by tectonic deformation or gravitation creep, the shear strength descends and comes down to residual strength, and the internal friction angle lowers to 10° (Chai et al. 2012, p. 9). So due to the disturbed sample taken in the present investigation, the residual strength alone is reflected by the test: this is another possible factor of the low internal shear angle.

Nevertheless, with a material without gravel, and containing just fine particles, the friction angle can be estimated, due to its content of fine particles (see Figure 66 and Figure 67). So as this material consists just of fine particles, it can be deduced that the friction angle must be about 10° or even lower (Wen et al. 2007, p. 94).

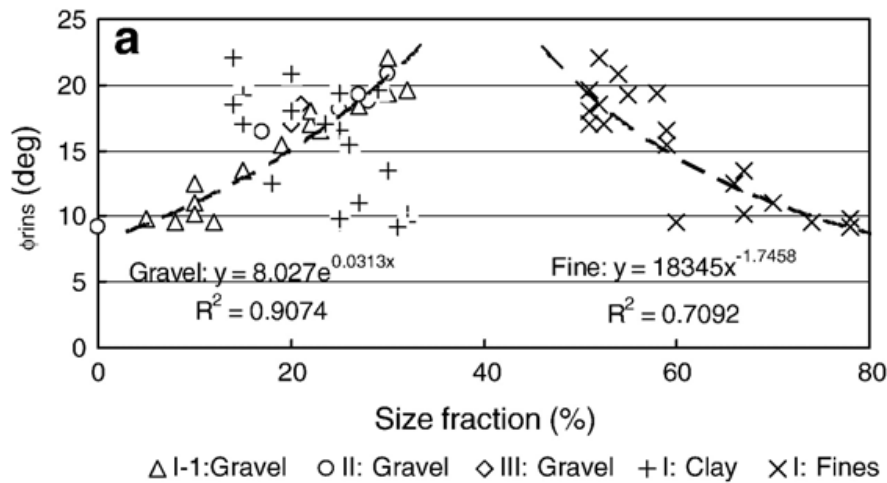


Figure 66 Relationship between residual friction angle and particle size fractions (Wen et al. 2007, p. 93)

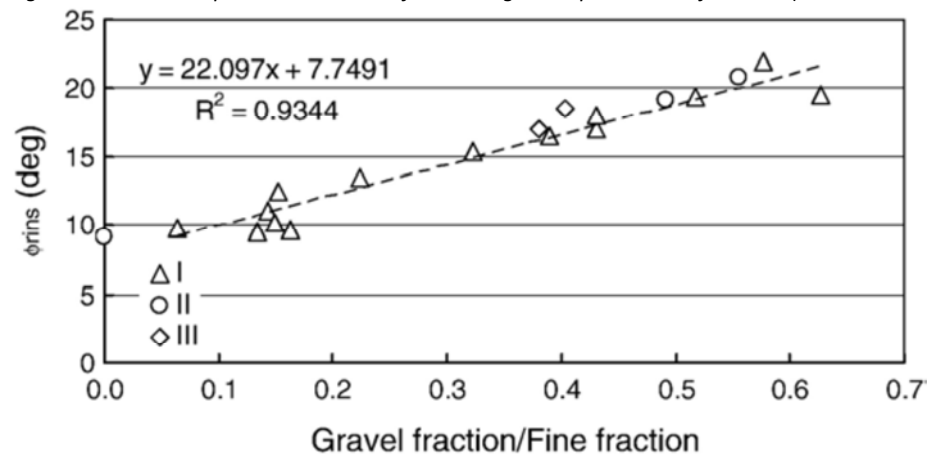


Figure 67: Relationship between residual friction angle and ratio of gravel of fine contents (Wen et al. 2007, p. 94)

### 3.3.3.2 XRD-Test

A XRD- Test was carried out in the Laboratory of the China University of Geoscience, Wuhan. The results match with reported results of marlstone in this area and display no new features. In this study cannot made relations between the calcite content and the compressive strength. However, also the cementation of the rock structure is an important factor of the strength.

	Montmorillonite	Clinochlore	Illite	Kaolinite	Quartz	Feldspar	Calcite	Dolomite	Hematite
样品编号	蒙脱石	绿泥石	伊利石	高岭石	石英	长石	方解石	白云石	赤铁矿
Nr01	15	10	10	15	19	2	27	2	0
Nr02	5	15	0	35	18	3	24	0	0
Nr06	15	15	15	5	12	2	36	0	0
Nr09	20	10	15	5	19	2	29	0	0
Nr10	20	10	5	10	17	3	33	2	0
Nr11	20	5	5	10	18	2	40	0	0

Table 12: XRD-Test of  $T_2b^3$  rock

### 3.3.3.3 Mineral content of the weak layer

**Clay minerals are the main components** of incompetent beds and slip zones. The results of the XRD-Test display a clay mineral content of 45% (see layer 10 in Table 12). On this observation point mineral compositions of the weak layer are montmorillonite (20%), chlorite (10%), illite (5 %), kaolinite (10%), quartz (17 %) and calcite (33 %). This indicates the typical mineral composition of a clay interlayer of calcareous marlstone. Another type of weak layer in respect of mineral content is that with **carbonate mineral as the main** mineral. This has the same mineral composition as marlite of  $T_2b^3$ . Mineral compositions of these incompetent beds are montmorillonite (15 %), illite (5 %), quartz (10 %) and calcite (70 %). Chlorite and illite are the main clay minerals of original  $T_2b^3$ . The difference in clay minerals between incompetent beds and original strata is that illite transits to montmorillonite gradually under the long- term action of groundwater (Chai B 2010, quoted in Chai et al. 2012, p. 7). However, in this test, this transition of illite displays too weak to be interpreted, but the weak layer is mainly composed of clay minerals, quartz and calcite.

### 3.3.3.4 Watercontent w:

The measured water content is 58%. This high content may be one reason for the weak results of strength parameter of the quick shear test (Table 13).

Box No.	Wet soil mass (g)	Dry soil mass (g)	Water ratio (%)
37	5,645	3,518	60%
30	5,487	3,457	59%
1-1-2	4,871	3,105	57%
274	5,355	3,396	58%
Mean	5,340	3,369	58%

Table 13: Water content of weak layer of T2b<sup>3</sup> (Dec. 2012)

### 3.3.4 Rock mass rating (RMR)

Geomechanics classification or the Rock Mass Rating (RMR) system is used to obtain the shear parameter of the rock mass (compare Table 5).

#### A- Classification parameters and their ratings

Parameter / Value	Rating	
1. Uniaxial comp. Strength: 100 Mpa	9	
2. Drill core Quality RQD: $RQD = 115 - 3.3 J_v$ 115 -3,3 7 = 92 %	18	
3. Spacing of discontinuities: 0,6-2 m	15	
4. Condition of discontinuities /Rating		
Length: 1-3 m	4	
Aperture: 1-5mm	1	
Roughness: very rough	6	
Infilling: Soft <5 mm	2	
Weathering: Slightly	5	
Sum	18	
5. Groundwater: General conditions: damp	10	
Intermediate rating:	70	
<b>B- Rating adjustment for discontinuity orientations</b>		
fair (drive against dip 45-90°)	-7	
<b>Total rock mass rating</b>	<b>63</b>	
<u>Class number:</u>	II	
<u>Description:</u>	Good rock	
<u>Cohesion of rock mass:</u>	315 kPa	
<u>Friction angle of rock mass:</u>	36.5 °	

An indoor shear test of the structural plane on T<sub>2</sub>b<sup>3</sup> pelmicrite shows shear strength of  $\phi$  30- 38°, and cohesion of c 50-100 kPa Wang 2009, p. 96. So the friction angle  $\phi$  of the RMR is very close to this result and the cohesion might be overestimated by the method of RMR.

**3.3.5 Simulation of slope stability under different boundary conditions**

The following sections lay out different simulations of slope stability of the slightly weathered rock explored in the T<sub>2</sub>b<sup>3</sup> site in Badong. To do this, a diameter of 150 mm is taken, as this is usual in anchor technics (Wichter et al. 2000, p. 46). The marlstone is slightly weathered, so the service carcass friction can be assumed as 500 kN/m<sup>2</sup> (Wichter et al. 2000, p. 48). The anchors should not be arranged parallel to the joint face; an angle >15° of the friction angle of the joint face should be respected. The section of force transition is on rocks up to 6 m (Prinz et al. 2011, p. 302).

**3.3.5.1 Simulation: Excavation on T<sub>2</sub>b<sup>3</sup> slightly weathered rock**

The simulations carried out seek to explore the potential effect on slope stability of cutting, current stabilisation methods and also construction on the examined site using the data gathered. For the rock mass, the material properties of the RMR (see chapter 3.3.4) are taken. The quick shear test, carried out in the laboratory of the China University of Geoscience, provides the material properties for the weak clay layer (see chapter 3.3.3.1). The possible sliding zone is expected in the weak layer, therefore the estimated slip surface is defined by the option “Block Specified”. This provides a calculation of a planar failure along the weak layer.

**Material Properties:**

Marlstone rock mass

Cohesion:.....315 kPa  
 φ: .....36.5°  
 Unit Weight: .....26 kN/m<sup>3</sup> } blue

Clay layer

Cohesion:.....21.95 kPa  
 φ: .....5.97°  
 Unit Weight: .....17.4 kN/m<sup>3</sup> } thin  
 } yellow  
 } line

**Setting:**

Analysis Type: ..... Morgenstern-Price  
 PWP-Condition:..... (none)  
 Side Function: ..... Constant function  
 Slip Surface Option: ..... Block Specified

The simulated condition is a cutting in a slightly weathered marlstone. The toe of the slope (in the cutting) is essential. In this case the thickness of the intact rock mass between the cutting and the weak layer is not thick enough. The factor of safety reaches only 0.706 (see Figure 68); therefore the slope above the cutting is not stable.

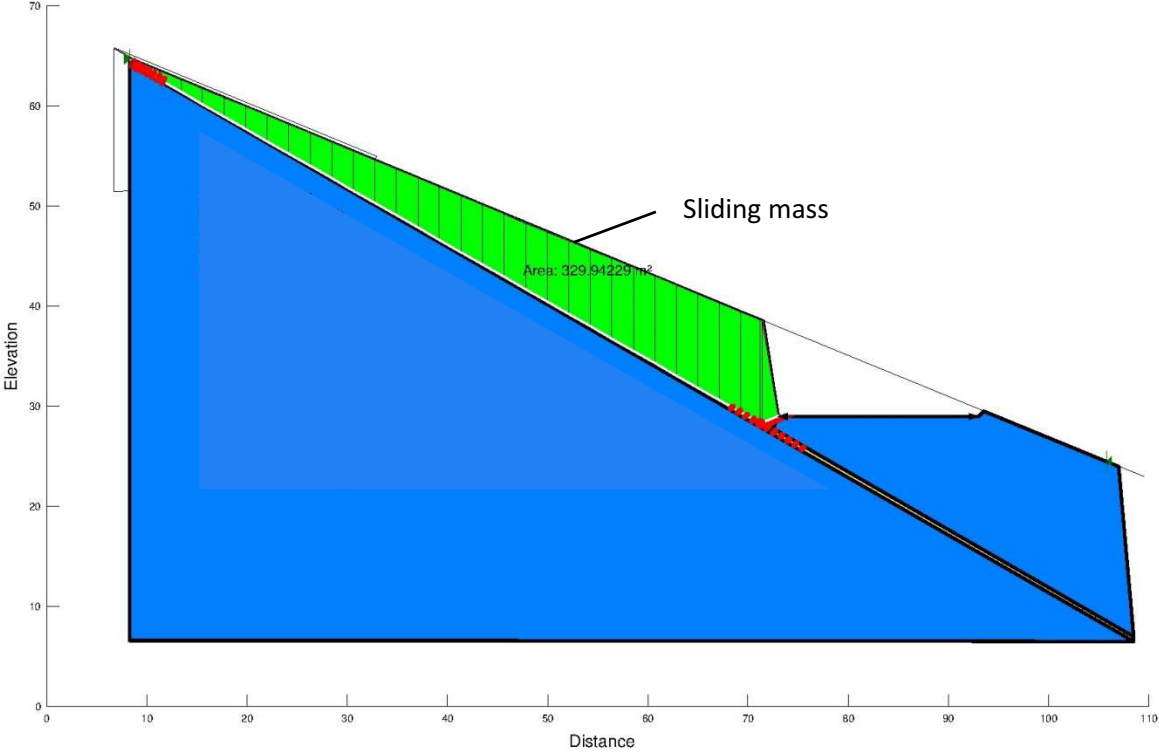


Figure 68: Simulation:  $T_2b^3$  slightly weathered rock with a weak clay layer; FOS: 0.706

Pile reinforcement is a frequently observed reinforcement method in Badong area. Two pile rows of a spacing of 3 m and a maximal shear force bearing capacity of 2800 kN increases the factor of safety to 1.111 (see Figure 69).

**Pile reinforcement settings:**

Length:.....19 m

Spacing: .....3 m

Shear force: .....2800 kN

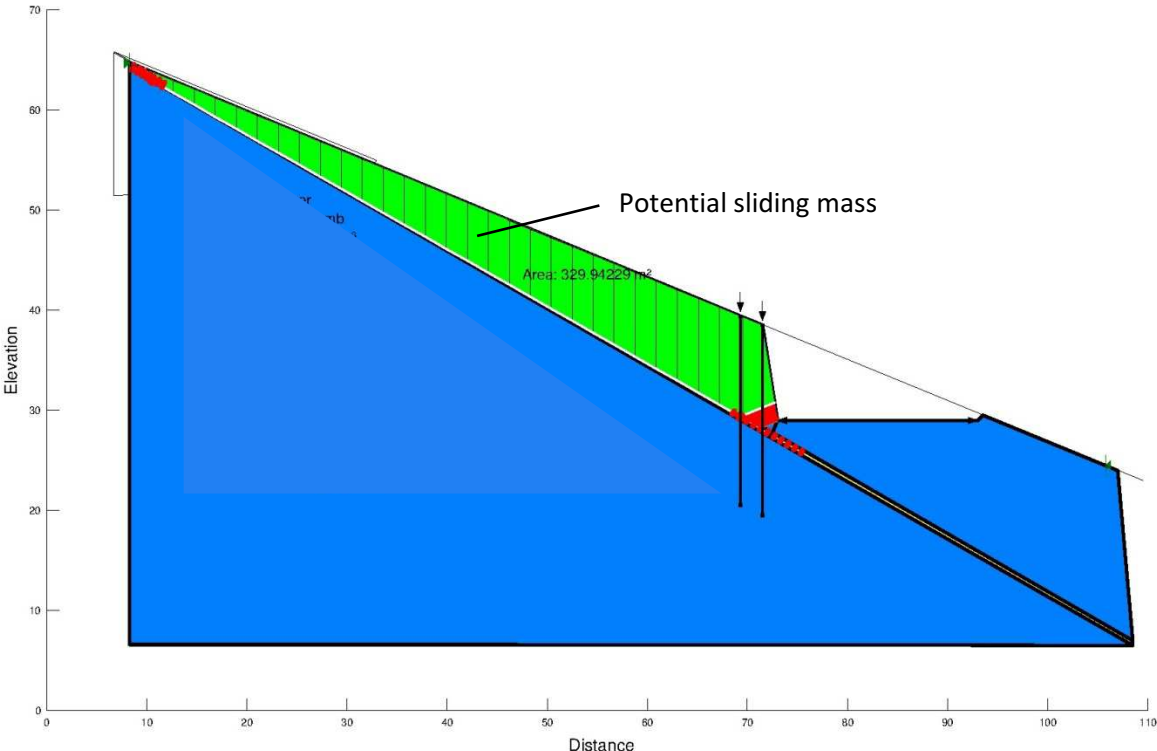


Figure 69: Simulation: Stabilisation piles on  $T_2b^3$  slightly weathered rock with a weak clay layer; FOS: 1.111

With two rows of anchors of a spacing of 3 m (see Figure 70) and the below listed settings, the anchor increases the factor of safety to 1.101, almost the same as that of the pile stabilisation. So the effects of both stabilisation methods can be compared.

**Anchor reinforcement settings:**

- Total Length:.....24.2 m
- Bond Length: .....8 m
- Bond Diameter: .....0.15 m
- Bond Skin Friction:.....500 kPa
- Anchor Spacing: ..... 3 m
- Bar Capacity ..... 1900 kN
- Shear Capacity: ..... 500 kN

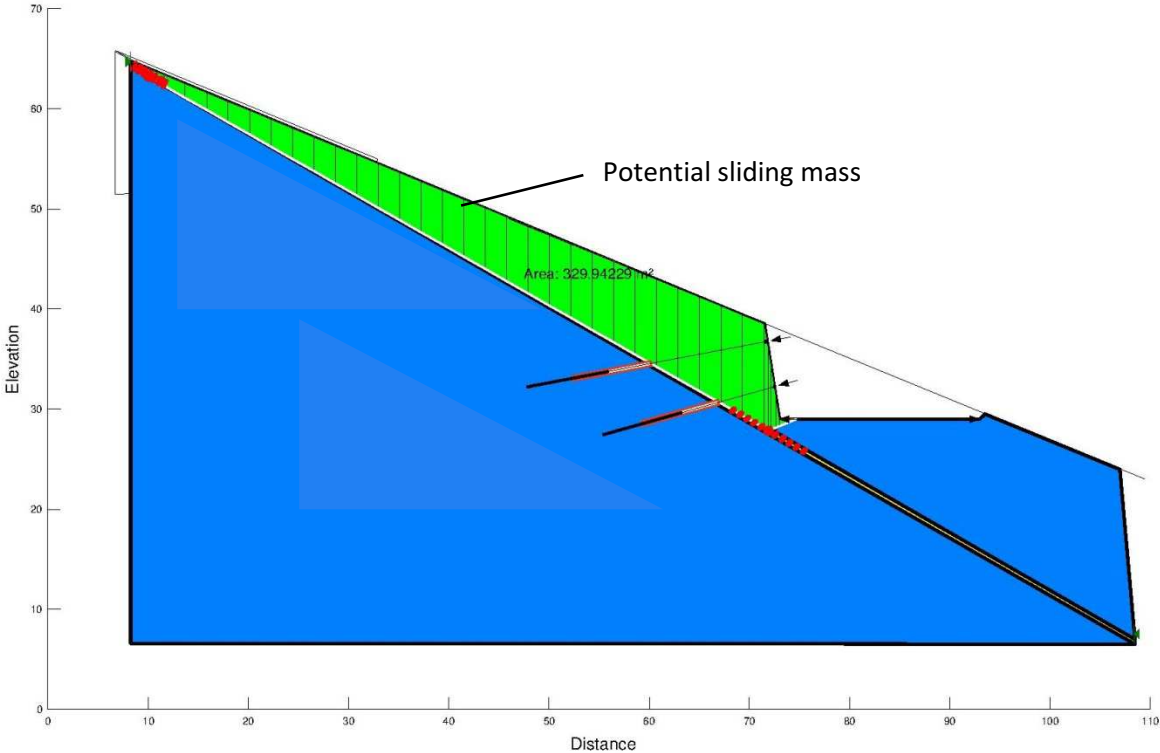


Figure 70: Simulation: Anchor stabilisation in  $T_2b^3$  slightly weathered rock with a weak clay layer; FOS: 1.101

An applied load (450 kN/m<sup>2</sup>) gives a slight improvement in stability (an increasing factor of safety from 0.706 to 0.710). The failure would develop right under the edge of the building. But due to the pressure of the building, a local improvement of the material capacity takes place.

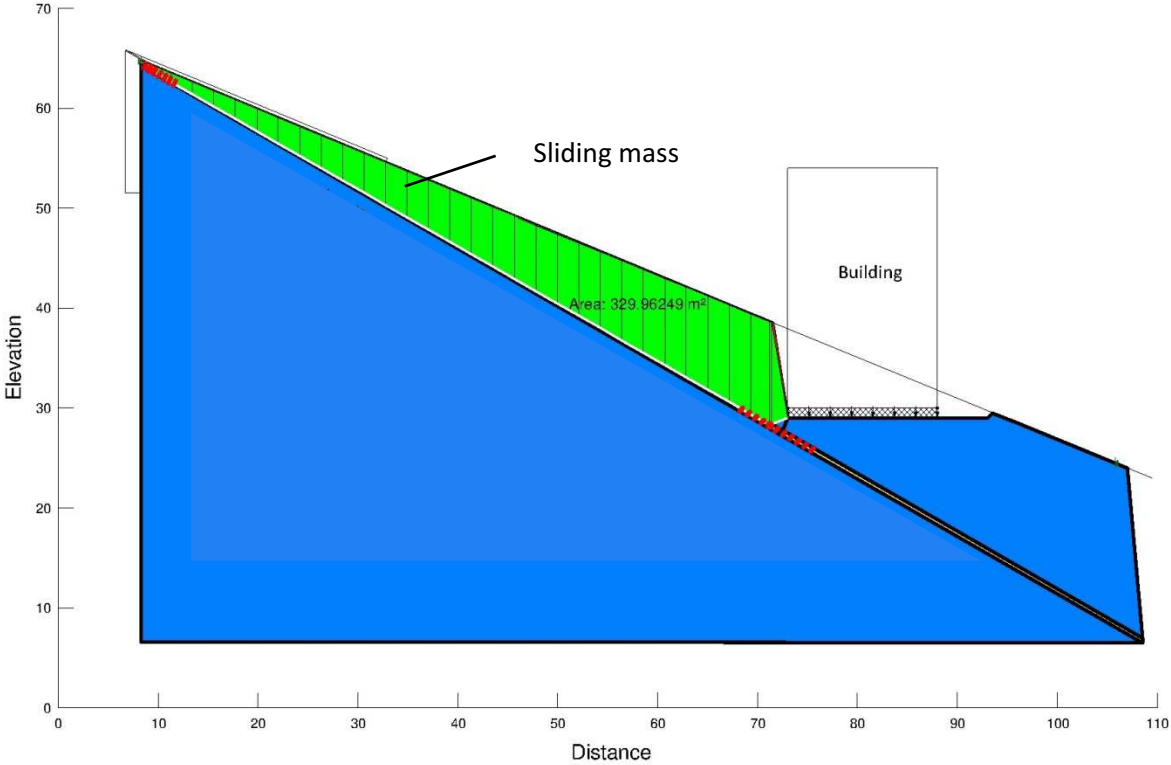


Figure 71: Simulation: Building on T<sub>2</sub>b<sup>3</sup> slightly weathered rock with a weak clay layer; FOS: 0.710

Both, anchor reinforcement and pile stabilisation increases the factor of safety to a degree, that the slope can be considered as stable. The building has the same effect as visible in Figure 71. In this case the factor of safety increases from 1.101 to 1.116 (compare Figure 70 and Figure 72).

**Anchor reinforcement settings:**

Total Length:.....17.6 m; 24.2 m	Anchor Spacing: ..... 3 m
Bond Length: .....8 m	Bar Capacity ..... 1900 kN
Bond Diameter: .....0.15 m	Shear Capacity: ..... 500 kN
Bond Skin Friction:.....500 kPa	

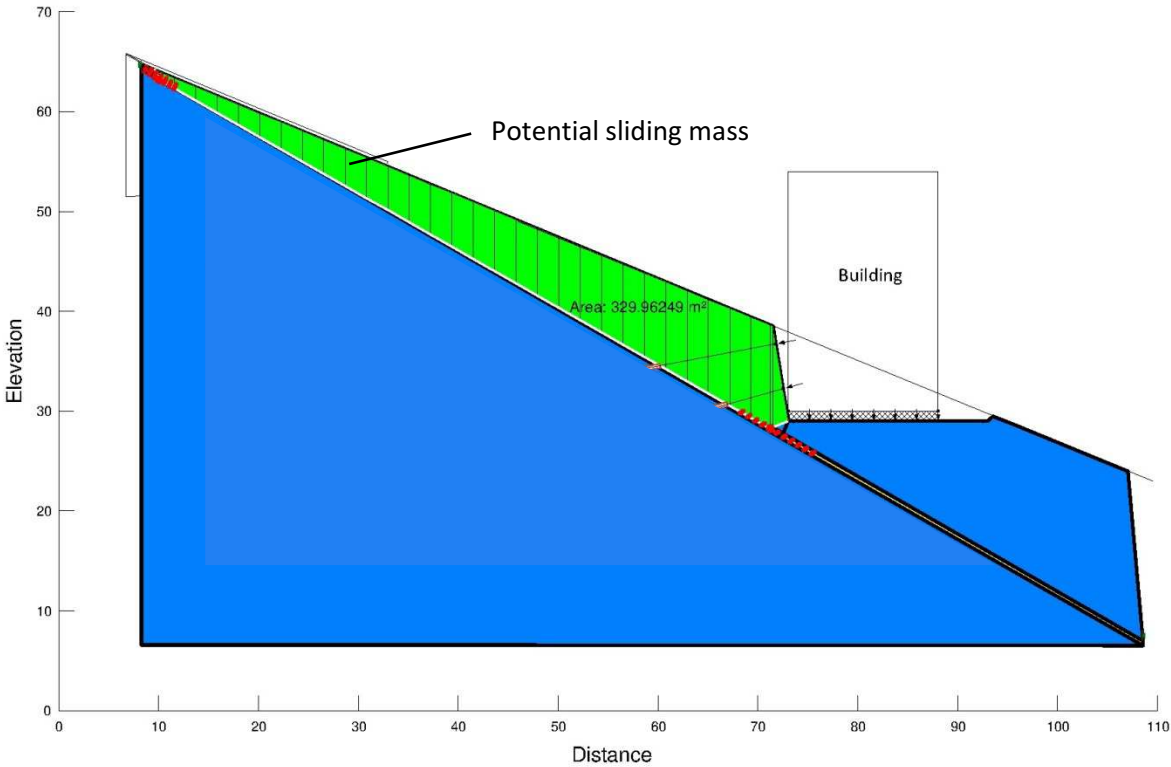


Figure 72: Simulation: Building and anchor stabilisation on  $T_2b^3$  slightly weathered rock with a weak clay layer; FOS: 1.116

By stabilising with pile foundation, the factor of safety does not increase; as on this simulation the failure plane does not develop through the bottom of the foundation (compare Figure 69 and Figure 73).

**Pile reinforcement settings:**

Length:.....19 m

Spacing: .....3 m

Shear force: .....2800 kN

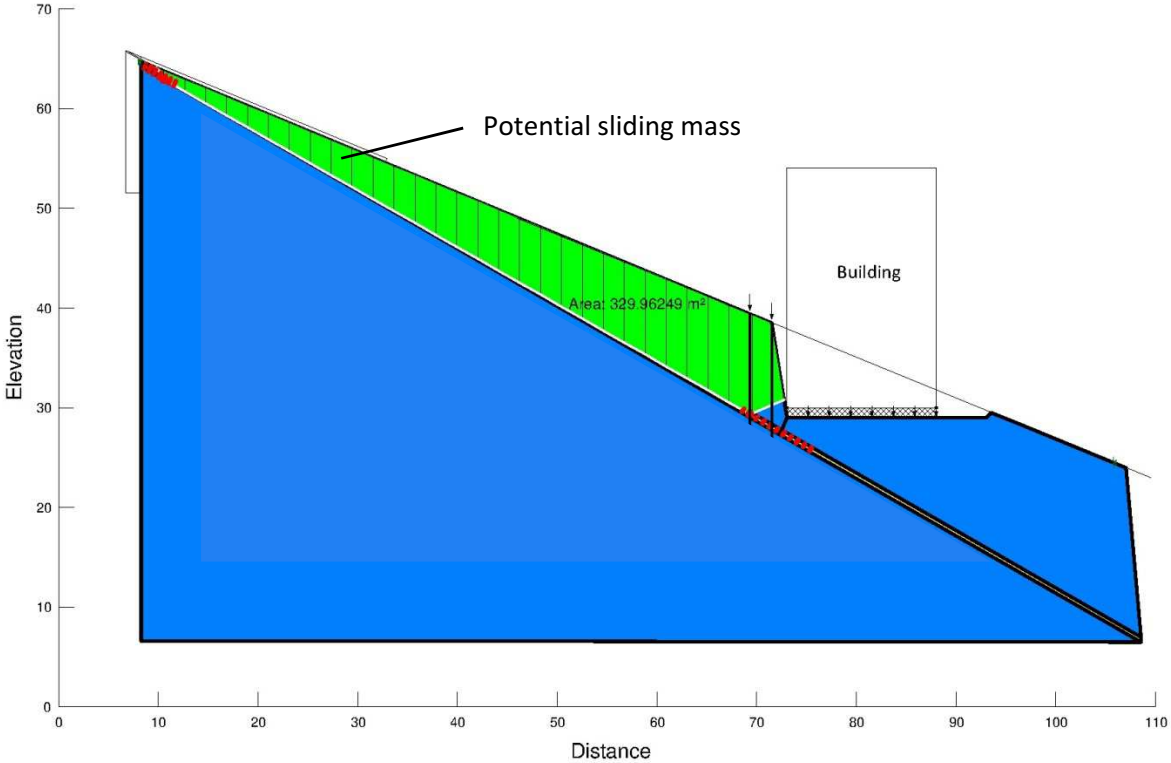


Figure 73: Simulation: Building and pile stabilisation on  $T_2b^3$  slightly weathered rock with a weak clay layer; FOS: 1.111

A main problem of the Member of  $T_2b^3$  is the high decay rate, once the rock is exposed to the environment. The following simulation displays these conditions. A site was chosen, in which the safety factor would be  $>1$  in the initial stadium (see Figure 74 and Figure 75). The rock mass properties are equal to those of the present construction site, assessed during the fieldwork.

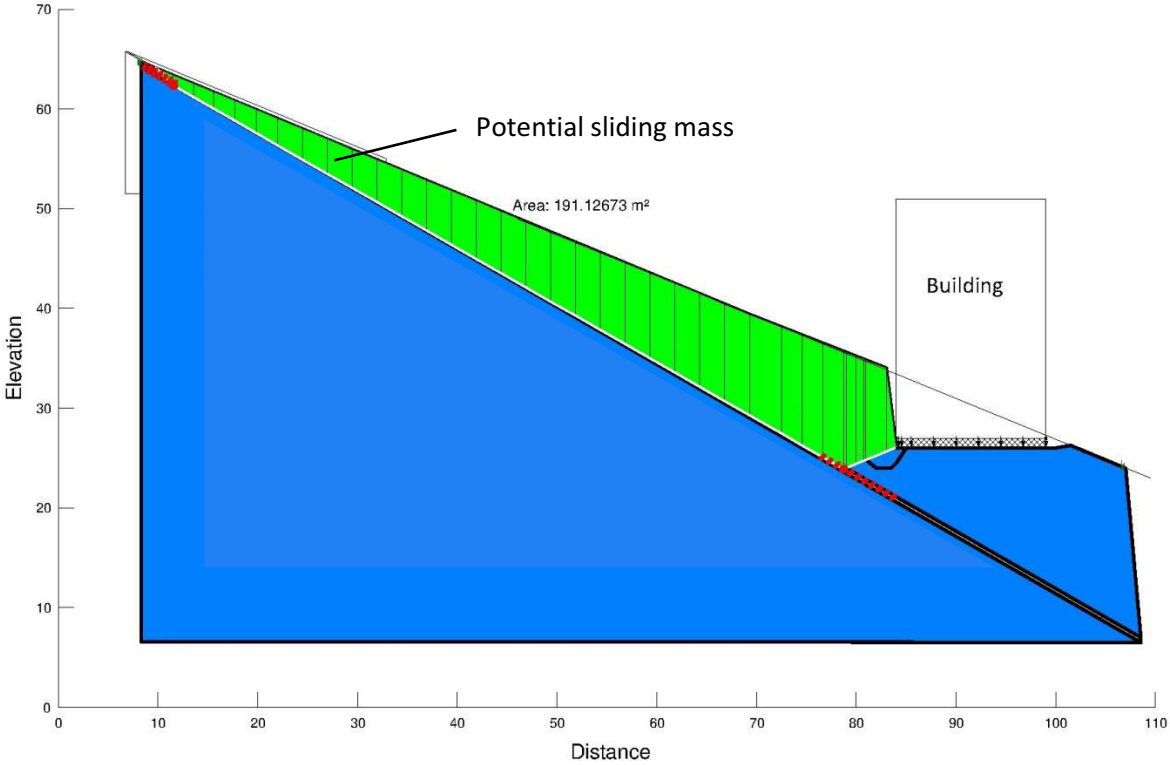


Figure 74: Simulation: Building on  $T_2b^3$  slightly weathered rock with a weak clay layer; FOS: 1.244

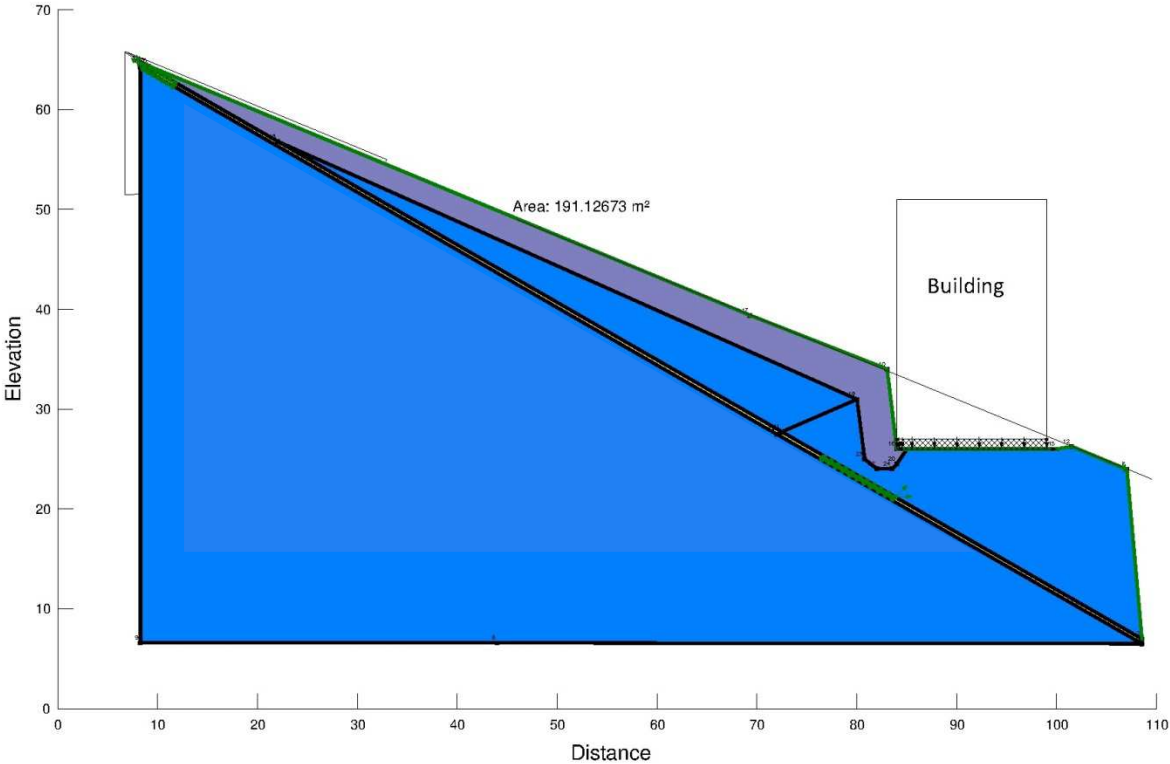


Figure 75: Building on  $T_2b^3$  highly weathered rock on the surface, and a weak clay layer under ground.

The friction angle of the weathered rock mass decreases from 36.5° to 15°. The remaining cohesion is 20 kPa. In the simulation without reinforcement, the factor of safety decreases to 0.884 (compare Figure 74 and Figure 76) and the slope uphill of the foundation is no longer stable.

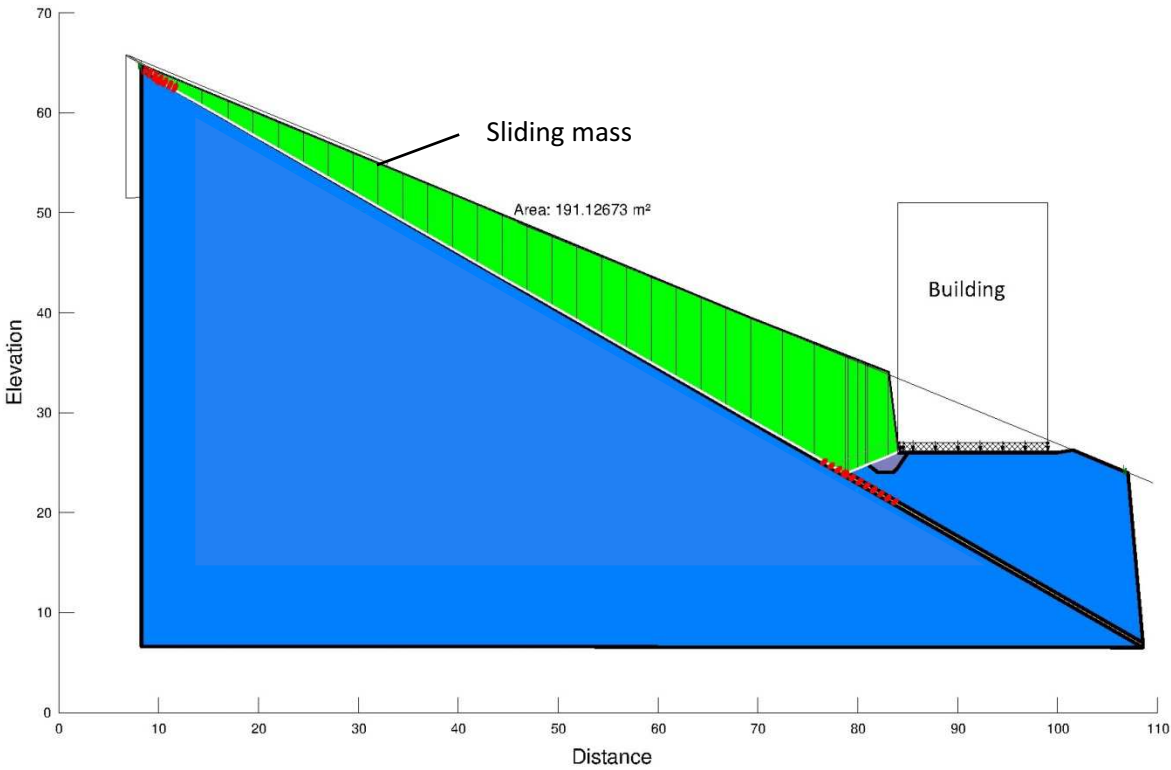


Figure 76: Simulation: Building on  $T_2b^3$  highly weathered rock on the surface, and a weak clay layer under ground.; FOS:0.884

## 4 Discussion and Conclusions

Throughout Badong, different geological conditions are clearly defined and the borders are easily visible by field inspection. The most frequent spots in this area are the type of an ancient landslide, the geological setting of  $T_2b^2$  and  $T_2b^3$ . The characteristics of each condition are very regular. The tests, carried out for this thesis, match well to former published literature. However, of course this research can neither replace nor reduces the need for a careful investigation on every future planned construction. But it can improve the focus in investigations on the foundations of planned constructions in the Badong area. The simulations give a first impression of the features in the different settings. However, 2-D software, such as Geoslope used for these simulations, is taken with caution. This is because the pressure line, especially in intact rock mass, should be considered in three dimensions. The following sections discuss the results found in the three different sites researched, namely the ancient landslide, the soil foundations of  $T_2b^2$  and the rock foundations of  $T_2b^3$ .

### 4.1 Ancient landslide soil

Compared to foundations on  $T_2b^2$  and  $T_2b^3$ , the foundations on ancient landslide soil have very low strength properties. The reported results on the Huangtupo landslide match with the measured results of the triaxial test in respect of the friction angle (see Table 14). However, the unfavourable test procedure of the performed triaxial test, as reported in chapter 3.1.3.2, does not allow a reliable comparison. Considering the visual assessment of the grain distribution, a range of  $18^\circ$  to  $28^\circ$  of the friction angle can be assumed. The cohesion ranges between 24 kPa to over 30 kPa. The cohesion result of the performed triaxial test (48 kPa) can be considered as an outlier as it does not match to any other results.

		$\varphi$ ( $^\circ$ )	c (kPa)
Xirangpo ancient landslide mass	upper mass:	23	48
	Table by Schnell:	28	30
Huangtupo ancient landslide mass	Upper part:	18	24
	middle part:	23	31

Table 14: Comparison of reported shear parameter of Huangtupo sliding mass and measured parameter of Xirangpo ancient landslide mass Zhou et al. 2001,

The simulations of the slope stability, as represented by the calculations produced in 3.3.5, show that if the slope is under initial conditions, no hazards of small failures are likely under the given slope angle. The weakest slip surface would be along the whole slope, which is not the focus in this thesis.

Applying a surcharge load, like a building, reduces the factor of safety slightly, but the weakest slip surface is the size of smaller landslides. This matches with the observations on-site and reports of local people that after additional loads on the slope, the occurrence of small landslides is an issue. Stabilisation piles are noticeably improving the stability of the slope. However, the function of the stabilising pile as a pile foundation, to distribute the load of a building through the pile skin friction (and the point bearing pressure), is not considered with this software and would improve the stability even more.

## **4.2 Decayed rock and soil on geological environment of T<sub>2</sub>b<sup>2</sup>**

The soil in the T<sub>2</sub>b<sup>2</sup> site researched is made up of purple red mudstone which is mainly already decayed into angular stones and gravel. The remaining parts which could be considered as rock are full of cracks and joints filled with loam.

Compass measurements on the structure planes of the surface do not correspond to the reported geometry of former published literature (see page 61). The weathering degree is highly advanced and the discontinuities are not following a regular regime such as normally develops on less weathered sedimentary rock of this type. So this rock can be considered as soil and calculated/estimated as elastic-isotropic half-space. The parameters of former published results of this material vary in a high range (compare Table 10). Further investigation on this soil, with reported research methods, would be recommendable. For calculation in this thesis, the strength parameters were estimated by means of the table by Schnell (Smolczyk et al. 2001, p. 122). This estimation allows assumption of soil strength parameter in a range of 35° to 43° friction angle and cohesion of 10 kPa to 0 kPa. Even when the calculation on the safe side of this range is searched (35°), the friction angle is suggested to be raised in a modest degree, as the gravel is angular. The water situation cannot be obtained through existing wells as there are no wells reported or accessible. But wet spots at a depth of aprox. 20 meter under the surface provide an indication of retained water (without capillary connection to the groundwater) in the decayed rock. However, the water distribution is very inhomogeneous, which indicates also that the soil properties are spatially highly variable, as water is a main driving force for the decay rate.

Assuming a friction angle of 38°, there are no hazards of small landslides under conditions of a slope angle of 25°. Stabilisation piles would be not necessary for the slope stability in this case. However, with further decay, there would be a higher content of fine particles, which leads to a weaker strength parameter.

### 4.3 Rock on geological environment of T<sub>2</sub>b<sup>3</sup>

Rock foundations in this environment have to be carefully chosen and assessed. Initially, the rock mass seems stable, even if there is already a slightly progressed weathering rate. But due to the high solubility, the strength decreases rapidly, once exposed to the environment. Many different separation planes are accelerating this process. The hazard of toppling from cut slopes is a common observed failure.

The observations on the investigated site match to the characteristics cited in previous published literature (compare Table 15). According to the observations and the XRD-test, the predominant rock is marl with an intercalated calcareous weak clay layer. The reported strata in this environment have a dip angle of 20° to 48°; however in this case the measured dip angle is 35°. The dip of the natural slope is 20° according to the geological map. This implies that there are no failure hazards downhill of a cutting into the slope, as the friction angle of the rock mass is, with 38°, enough for these conditions.

	Strata dip angle	Friction angle of rock mass	
		RMR	indoor shear test
Field work (2012)	35°	36°	
Literature	20°-48°	38°	38°
Map	Slope angle: 20°		

Table 15: Comparison of results of literature and fieldwork in respect of friction angle of rock mass, strata dip and slope dip

When cut, then the foot of the new profile is set to endure more stress caused by the upper rock mass. Especially when the next underlying layer is close, the layer of the stressed rock mass is thin. With the weakening due to weathering, the risk of failure rises and the upper slope would slide down. Crushed beds are also well developed in this area and display the same hazards as clay layers in terms of a weak layer in the rock mass. However, especially with ground water influence, these crushed beds can deform easily due to the loss of calcite cementation. Therefore the actual measured shear strength is taken with caution and a reasonable factor of safety is prudent, as it will lower with time.

The scratch hardness is a first good estimation of the rock strength (see Figure 77). The coefficient of determination ( $R^2$ ) is 0,703). However, it is not recommendable to make direct quantitative relations, so additional measurements of the rock strength are essential. For a more advanced statistical statement the sample number is too low.

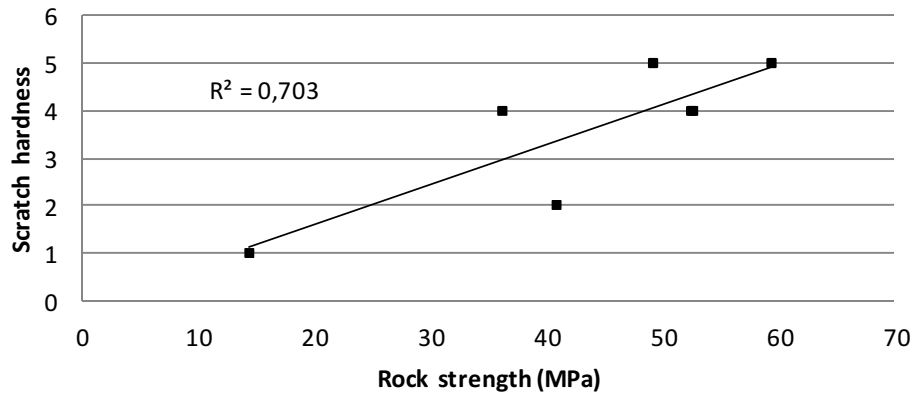


Figure 77: Comparison of scratch hardness and rock strength (measured by Schmidt hammer)

Simulation on  $T_2b^3$  rock foundation makes clear, that on this setting weak layers are one main factor of slope stability. Stabilisation measures are indispensable. Piles and/or anchors for stabilisation represent an effective method. On the assessed site the dip angle of the weak layer is steeper than the slope angle, so an applied surcharge load (building) improves the stability due to local enhancement of the shear parameter of the rock mass. A simulated weathering, on the surface and along the joints around the cutting of the rock mass, displays a remarkable decrease of the slope stability.

## 5 Literature

1. Alberts, H. C., R. M. Alberts, et al. (2004). "The Three Gorges Dam Project from a systems viewpoint." Systems Research and Behavioral Science **21**(6): 585-602.
2. Austrian-Standard (1981). "ÖNORM B 4401-3, Geotechnical engineering (foundation engineering); exploration by test pits and borings; sampling; recording."
3. Austrian-Standard (1981). ÖNORM B 4490, Geotechnical engineering (foundation engineering); terms, symbols and units.
4. Bernhard Pipkin, D. D. T., Richard Hazlett, Paul Biermann (2008). *Geology and Environment*. P. Adams. Belmont, Thompsons Brooks/Cole.
5. Bieniawski, H. (1979). "Geomechanics classification in rock engineering applications : Proc 4th Congress International Society for Rock Mechanics, Montreux,," International Journal of Rock Mechanics and Mining Sciences & Geomechanics Abstracts **17**(6): A111.
6. Bieniawski, H. (1994). "Classification of rock masses for engineering: the RMR system and future trends " International Journal of Rock Mechanics and Mining Sciences & Geomechanics Abstracts **31**(4): 192.
7. Borja, R. I., J. A. White, et al. (2010). "Factor of safety in a partially saturated slope inferred from hydro-mechanical continuum modeling." International Journal for Numerical and Analytical Methods in Geomechanics **36**(2): 236-248.
8. Chai, B., K. Yin, et al. (2012). "Correlation between incompetent beds and slope deformation at Badong town in the Three Gorges reservoir, China." Environmental Earth Sciences: 1-15.
9. Chai B, Y. K., Xiao YJ (2010). "Characteristics of weak-soft zones of Three Gorges reservoir shoreline slope in new Badong county." Rock Soil Mechanics **31**: 2501-2506 (in Chinese).
10. China National Standard, T. M. o. C. o. t. P. s Republic of C. (1999). National Standard of the People's Republic of China. Standard for Soil Test Method. Beijing, China-State Bureau of Quality and Technical Supervision; The Ministry of Construction of the People's Republic of China: 220.
11. Dai Huichao, P. Y. (2005). "Study on relationship between TGP and the eco-environment of the middle & lower Yangtze." Journal of Hydroelectric Engineering **24**(4): 26-30.
12. Dai Huichao, Z. T., Liu Defu (2010). "Effects of Reservoir Impounding on Key Ecological Factors in the Three Gorges Region." Procedia Environmental Sciences **2**(0): 15-24.
13. Dam, C. o. G. H. P. i. t. T. G. and A. CGHPTGDA (2006). "Annual Report on Geological Hazard Prevention in the Three Gorges Dam Area." Open file report: 2005.
14. Deere D.U., H. A. J., Patton F.D., Cording E.J. (1967). "Design of surface and near surface construction in rock." Failure and breakage of rock, proc. 8th U.S. symposium of rock mechanics(237-302).
15. Deji, C. (1999). "Engineering geological problems in the Three Gorges Project on the Yangtze, China." Engineering Geology **51**(3): 183-193.
16. Fuchsberger, M. (2008). Slope Failure at a Major Cut for a Motorway in Austria; its Cause and Its Stabilisation. From Research to Practice in Geotechnical Engineering: 616-625.
17. Geo-Slope (2012). Stability Modeling with Slope/W; An Engineering Methodology. Calgary, Geo-Slope International Ltd.
18. Gudehus, G. (2011). *Physical soil mechanics*. Heidelberg, Springer.
19. He, M., H. Zheng, et al. (2012). "Yangtze River sediments from source to sink traced with clay mineralogy." Journal of Asian Earth Sciences(0).
20. He, Y. R. (2003). "Purple Soil in China." Science Press, Beijing **2**(In Chinese).
21. Jackson, S. and A. Sleigh (2000). "Resettlement for China's Three Gorges Dam: socio-economic impact and institutional tensions." Communist and Post-Communist Studies **33**(2): 223-241.
22. Jiang, H.-T., F.-F. Xu, et al. (2006). "Weathering Characteristics of Sloping Fields in the Three Gorges Reservoir Area, China." Pedosphere **16**(1): 50-55.

23. Keqiang, H., Y. Guangming, et al. (2009). "The regional distribution regularity of landslides and their effects on the environments in the Three Gorges Reservoir Region, China." Environmental Geology **57**(8): 1925-1931.
24. Li, L. R. (2002). "Geological hazards and prevention in the Three Gorges dam area." Land and Resources **4**(4-7).
25. Liu, J., J. Zuo, et al. (2013). "Sustainability in hydropower development - A case study." Renewable and Sustainable Energy Reviews **19**(0): 230-237.
26. Meteorological-Services-section. (2013). "Rainfall data." Retrieved 02.05.2013, 2013, from <http://zdz.hbqx.gov.cn/>.
27. Morgenstern, N. R. and V. E. Price (1965) "The Analysis of the Stability of General Slip Surfaces." Geotechnique, 79-93.
28. Mulder, M. B., S. Bowles, et al. (2009). "Intergenerational Wealth Transmission and the Dynamics of Inequality in Small-Scale Societies." Science **326**(5953): 682-688.
29. Palmström A. (1982). "The volumetric joint count: a useful and simple measure of the degree of rock mass jointing." Proc. of the 4th Congr. Int. Assoc. of Engng. Geology **5**: 221-228.
30. Polynov, B. B. (1937). The cycle of weathering. London, Thomas Murby and Co.
31. Prinz, H. and R. Strauß (2011). Ingenieurgeologie. [s.l.], Spektrum Akademischer Verlag.
32. Proceq. (2013). "Original Schmidt." Retrieved 02.05, 2013, from <http://www.proceq.com>.
33. Qi, S., Z. Yue, et al. (2009). "Significance of outward dipping strata in argillaceous limestones in the area of the Three Gorges reservoir, China." Bulletin of Engineering Geology and the Environment **68**(2): 195-200.
34. Qi, S. W., Y. Z. Qi, et al. (2009). "Deep weathering of a group of thick argillaceous limestone rocks near Three Gorges Reservoir, Central China." International Journal of Rock Mechanics and Mining Sciences **46**(5): 929-939.
35. Rock-science. (2013). "Rock mass classification." Retrieved 05.06., 2013, from [http://www.rocscience.com/hoek/corner/3\\_Rock\\_mass\\_classification.pdf](http://www.rocscience.com/hoek/corner/3_Rock_mass_classification.pdf).
36. Schwingenschlögl, R. (1991). Bruchhafte Deformation im Gebirgskörper und im Gründungsgestein von Ingenieurbauwerken.
37. Scintag (1999). Basis of X-ray Diffraction. Scintag. Cupertino: 25.
38. Sheng, Q., Z. Q. Yue, et al. (2002). "Estimating the excavation disturbed zone in the permanent shiplock slopes of the Three Gorges Project, China." International Journal of Rock Mechanics and Mining Sciences **39**(2): 165-184.
39. Smolczyk, U., H. Schröder, et al. (2001). Geotechnische Grundlagen; Grundbau-Taschenbuch. Berlin [u.a.], Ernst.
40. Statistics-China, N. B. o. (2008). NSBC. Energy yearbook 2008. Beijing.
41. Sun, H.-Y., Y. Zhao, et al. (2012). "Deep-Seated Slope Failures Induced by Inappropriate Cutting in China." Rock Mechanics and Rock Engineering **45**(6): 1103-1111.
42. Sun, K., K. Li, et al. (2011). "The environmental assessment of the sediment after preliminary impounding of Three Gorges Reservoir." Energy Procedia **5**(0): 377-381.
43. Tullos, D. (2009). "Assessing the influence of environmental impact assessments on science and policy: An analysis of the Three Gorges Project." Journal of Environmental Management **90**, Supplement **3**(0): S208-S223.
44. Wang, F. (2009). Landslide disaster mitigation in Three Gorges Reservoir, China. Dordrecht [u.a.], Springer.
45. Wang, P., J. P. Lassoie, et al. (2013). "A framework for social impact analysis of large dams: A case study of cascading dams on the Upper-Mekong River, China." Journal of Environmental Management **117**(0): 131-140.
46. Wang, P., S. A. Wolf, et al. (2013). "Compensation policy for displacement caused by dam construction in China: An institutional analysis." Geoforum **48**(0): 1-9.

47. Wang, X., Y. Chen, et al. (2013). "Analysis of lengths, water areas and volumes of the Three Gorges Reservoir at different water levels using Landsat images and SRTM DEM data." Quaternary International(0).
48. Wang, Y., M. Liao, et al. (2005). "Analysis of the water volume, length, total area and inundated area of the Three Gorges Reservoir, China using the SRTM DEM data." International Journal of Remote Sensing **26**(18): 4001-4012.
49. Wei, Z., Yin, Guangzhi, Zhang, Dongming, Li, Dongwei (2003). "Comprehensive dynamical control of the landslide disaster at the northern Zhetou Mountain." Chinese Journal of Rock Mechanics and Engineering **22** (8)(in Chinese): 1367-1371.
50. Wen, B.-P. and L. He (2012). "Influence of lixiviation by irrigation water on residual shear strength of weathered red mudstone in Northwest China: Implication for its role in landslides' reactivation." Engineering Geology **151**(0): 56-63.
51. Wen, B. P., A. Aydin, et al. (2007). "Residual strength of slip zones of large landslides in the Three Gorges area, China." Engineering Geology **93**(34): 82-98.
52. Wichter, L. and W. Meiniger (2000). Verankerungen und Vernagelungen im Grundbau. Berlin, Ernst.
53. World-Bank. (2013). "World Bank national accounts data, and OECD National Accounts data files." Retrieved 25. May, 2013, from <http://data.worldbank.org/indicator/NY.GDP.MKTP.KD.ZG/countries/1W-CN-AT-EU?display=graph>.
54. Wu, F. Q., Y. H. Luo, et al. (2011). "Slope reinforcement for housing in Three Gorges reservoir area." Journal of Mountain Science **8**(2): 314-320.
55. Xinhua-News-Agency. (2003). "Background of the Three Gorges Project." Retrieved 05.03, 2013, from [http://news.xinhuanet.com/ziliao/2003-05/30/content\\_894678.htm](http://news.xinhuanet.com/ziliao/2003-05/30/content_894678.htm).
56. Yi, Y., Z. Yang, et al. (2010). "Ecological influence of dam construction and river-lake connectivity on migration fish habitat in the Yangtze River basin, China." Procedia Environmental Sciences **2**(0): 1942-1954.
57. Zhang, D., A. Chen, et al. (2012). "Effect of moisture and temperature conditions on the decay rate of a purple mudstone in southwestern China." Geomorphology **182**(0): 125-132.
58. Zhang, J. G. (2004). "Variation of mechanical property of marlite in process of karstification and weathering in Three Gorges region." Chinese Journal of Rock Mechanics and Engineering **23**(7):1073-7(in Chinese with English abstract).
59. Zhou, Y., H. Huang, et al. (2001). Study report of the engineering characteristics of  $T_2b^2$  of Badong County, Three Gorges Area, Changjinag institute of survey, planning, design and research (in Chinese).
60. Zuolan, W., L. Shihai, et al. (2006). "A dynamic comprehensive method for landslide control." Engineering Geology **84**(1-2): 1-11.

## 6 Figures

Figure 1: Overview of Badong Town (Google Earth 2005).....	2
Figure 2: Three rivers (Jinshajiang, Lanchangjiang(Mekong) and Nujiang(Salween river)) flow to the north until Jinshajiang turns towards east to form the Yangtze River (Wang 2009, p. 22); Small Figure: Structural outline map in the connected area between Chuan and Xiajiang rivers. 1 Anticline; 2 sincline; 3 faults; 4 Qutang Gorge at present; 5 water system (Wang 2009, p. 16).....	3
Figure 3: Areal structure sketch of Badong slope in the Three Gorges of the Yangtze River; .....	4
Figure 4: Two typical stratigraphic columns showing the group of argillaceous limestone rocks (Qi et al. 2009, p. 933).....	5
Figure 5: Mineral contents of different members of the Badong formation.....	10
Figure 6: Transitional zone between residual soil of $T_2b^3$ (left) and $T_2b^2$ (right) (Photo: Mayrhofer 2012).....	11
Figure 7: $T_2b^2$ decomposed into soil (Photo: Mayrhofer 2012).....	11
Figure 8: Thickly dotted pores of $T_2b^2$ (Photo: Mayrhofer 2012) .....	11
Figure 9: Highly weathered $T_2b^3$ (Photo: Mayrhofer 2012).....	12
Figure 10: Highly weathered $T_2b^3$ (Photo: Mayrhofer 2012) .....	12
Figure 11: Weak layer in $Tb_3$ (Photo: Mayrhofer 2012).....	12
Figure 12: Distinction of claystone, marlstone and limestone by means of content of clay- and $CaCO_3$ .....	13
Figure 13: Relationship between uniaxial compressive strength (UCS) and calcite content of weathered argillaceous limestone rocks (Qi et al. 2009, p. 938).....	14
Figure 14: Climate graph of Yichang (Data from: NOAA Station Id: PC57461; Latitude: 30°42'N; Longitude: 111°18'E; Elevation: 133m) .....	16
Figure 15: Energy use per capita and GDP growth (World-Bank 2013) .....	18
Figure 16: Sketch of ancient landslide revivification (Wang 2009, p. 151 modified by the author).....	24
Figure 17: Sketch of surficial slip of thick loose deposit material (Wang 2009, p. 151 modified by the author).....	25
Figure 18: Sketch of a slide along the bed- deposit interface (Wang 2009, p. 151 modified by the author).....	25
Figure 19: Sketch of bed rock sliding along the weak accordant layer (Wang 2009, p. 151 modified by the author).....	26
Figure 20: Hourly rainfall at 29.10.2012 in millimetre in Badong (Meteorological-Services-section 2013).....	28

Figure 21: Slope failure in urban area of Badong (Photo: Mayrhofer 2012).....	28
Figure 22: Example of a small landslide on the site of an ancient landslide: Erdaogou landslide developed in the debris accumulation (June 10, 1995)(Wang 2009, p. 368).....	29
Figure 23: Shi-jia-po landslide; black line: row of stabilising piles foundation (Photo: Mayrhofer 2012) .....	32
Figure 24: Sketch of the Shijiapo landslide.....	33
Figure 25: Shijiapo landslide (rest of concreted path and stabilising pile (Photo: Mayrhofer 2012 )	33
Figure 26: Control measures for landslide control (Zuoan et al. 2006, p. 9).....	33
Figure 27: Design procedures for landslide control (Zuoan et al. 2006, p. 9).....	33
Figure 28: Geological map of Badong area (China University of Geosciences, Wuhan).....	35
Figure 29: Mapping of the selected sites (China University of Geosciences, Wuhan).....	36
Figure 30: Readout scale of the Schmidt hammer (Photo: Mayrhofer 2012).....	38
Figure 31: Cutting ring (Photo: Mayrhofer 2012).....	41
Figure 32: Prepared sample for triaxial test (Photo: Mayrhofer 2012).....	43
Figure 33: Fixed sample on the triaxial device (Photo: Mayrhofer 2012).....	43
Figure 34: Sheared sample at an axial strain of 15% (Photo: Mayrhofer 2012) .....	43
Figure 35: Devise for quick shear test (Photo: Mayrhofer 2012).....	44
Figure 36: Specimen after shearing (Photo: Mayrhofer 2012) .....	44
Figure 37: An example of a relation curve of shear stress and shearing displacement (China National Standard 1999) .....	44
Figure 38: Relation-curve of shearing strength and vertical pressure (China National Standard 1999) .....	45
Figure 39: Ground sample (Photo: Mayrhofer 2013).....	45
Figure 40: Sample between two small glass plates (Photo Mayrhofer: 2013).....	45
Figure 41: Sample holder of the X-Ray Diffractometer (Photo: Mayrhofer 2013).....	46
Figure 42: X-Ray Diffractometer of China University of Geoscience (Photo: Mayrhofer 2013) .....	46
Figure 43: Free body of constant function (Geo-Slope 2012, p. 40).....	50
Figure 44: Free body of half- sine function (Geo-Slope 2012, p. 42) .....	50
Figure 45: Geological map of the ancient landslide at Xirangpo (pink area) (China University of Geosciences, Wuhan); the red circle indicates the investigated site; the blue line indicates the water level at 175 m.a.s.l. ....	52
Figure 46: Setting of the investigated ancient landslide (Photo: Mayrhofer 2012).....	53
Figure 47: Triaxialtest (2012).....	55
Figure 48: Mohr circles of the triaxial test .....	55

Figure 49: Simulation: Slide mass of ancient landslide on Xirangpo; FOS: 1.699 .....	57
Figure 50: Simulation: Slide mass of ancient landslide at Xirangpo with wide entry-exit ranges; FOS: 1.022 .....	58
Figure 51: Simulation: Building on slide mass of ancient landslide on Xirangpo; FOS: 1.341.....	58
Figure 52: Simulation: Building and stabilisation piles on slide mass of ancient landslide at Xirangpo; FOS: 1.605.....	59
Figure 53: Geological map of $T_2b^2$ (China University of Geosciences, Wuhan); the red circle indicates the investigated site .....	60
Figure 54: Exposure of $T_2b^2$ (Photo: Mayrhofer 2012) .....	61
Figure 55: Red calcareous mudstone with grey bed sets (Photo: Mayrhofer 2012) .....	61
Figure 56: Black spots on red mudstone (Photo: Mayrhofer 2012).....	62
Figure 57: New Houses for people of Huangtupo slope, under construction (on $T_2b^2$ ) (Photo: Mayrhofer 2012).....	64
Figure 58: Simulation: $T_2b^2$ highly decayed rock; FOS: 2.316.....	65
Figure 59: Simulation: $T_2b^2$ highly decayed rock with wide entry-exit ranges; FOS: 1.728.....	66
Figure 60: Simulation: Building on $T_2b^2$ highly decayed rock; FOS: 2.225.....	66
Figure 61: Simulation: Building with stabilisation pile on $T_2b^2$ highly decayed rock; FOS: 2.396 .....	67
Figure 62: Geological map of $T_2b^3$ (red circle indicates the investigated site); blue line: water level at 175 m.a.s.l. ....	68
Figure 63: Exposure of $T_2b^3$ (Photo: Mayrhofer 2012) .....	69
Figure 64: Relation curve of shear stress and shearing displacement.....	73
Figure 65: Relation-curve of shear strength and vertical pressure.....	73
Figure 66 Relationship between residual friction angle and particle size fractions (Wen et al. 2007, p. 93).....	74
Figure 67: Relationship between residual friction angle and ratio of gravel of fine contents (Wen et al. 2007, p. 94).....	74
Figure 68: Simulation: $T_2b^3$ slightly weathered rock with a weak clay layer; FOS: 0.706 .....	78
Figure 69: Simulation: Stabilisation piles on $T_2b^3$ slightly weathered rock with a weak clay layer; FOS: 1.111 .....	79
Figure 70: Simulation: Anchor stabilisation in $T_2b^3$ slightly weathered rock with a weak clay layer; FOS: 1.101.....	80
Figure 71: Simulation: Building on $T_2b^3$ slightly weathered rock with a weak clay layer; FOS: 0.710 ..	81
Figure 72: Simulation: Building and anchor stabilisation on $T_2b^3$ slightly weathered rock with a weak clay layer; FOS: 1.116.....	82

Figure 73: Simulation: Building and pile stabilisation on T<sub>2</sub>b<sup>3</sup> slightly weathered rock with a weak clay layer; FOS: 1.111..... 83

Figure 74: Simulation: Building on T<sub>2</sub>b<sup>3</sup> slightly weathered rock with a weak clay layer; FOS: 1.244 .. 84

Figure 75: Building on T<sub>2</sub>b<sup>3</sup> highly weathered rock on the surface, and a weak clay layer under ground. .... 84

Figure 76: Simulation:Building on T<sub>2</sub>b<sup>3</sup> highly weathered rock on the surface, and a weak clay layer under ground.; FOS:0.884 ..... 85

Figure 77: Comparison of scratch hardness and rock strength (measured by Schmidt hammer)..... 89

## 7 Tables

Table 1: Recommended parametric values for mechanical calculation of rock masses (Wang 2009, p. 98).....	8
Table 2: Recommended parametric values for calculation of structure planes (Wang 2009, p. 98).....	9
Table 3: Relationship of frequency landslide occurrence with precipitation in the Three Gorges Reservoir (Figure by Keqiang et al. 2009, p. 1928).....	27
Table 4: The maximum particle size of specimen soil grain (mm) .....	42
Table 5: Rock Mass Rating System (Bieniawski 1979).....	48
Table 6: Density and water ratio of the ancient landslide soil (Dec. 2012) .....	54
Table 7: Data from “Investigation report of Huangtupo landslide in Badong County” Hubei geo-hazard prevention and investigation institute, December, 2011 .....	56
Table 8: XRD-Test of T <sub>2</sub> b <sup>2</sup> rock.....	63
Table 9: Grain distribution after sieving ( Zhou et al. 2001) .....	63
Table 10: Results of a large scale triaxial test of weatered material on T <sub>2</sub> b <sup>2</sup> (Zhou et al. 2001).....	63
Table 11: Strength parameter of joints in T <sub>2</sub> b <sup>2</sup> (Zhou et al. 2001).....	64
Table 12: XRD-Test of T <sub>2</sub> b <sup>3</sup> rock.....	75
Table 13: Water content of weak layer of T <sub>2</sub> b <sup>3</sup> (Dec. 2012).....	76
Table 14: Comparison of reported shear parameter of Huangtupo sliding mass and measured parameter of Xirangpo ancient landslide mass Zhou et al. 2001,.....	86
Table 15: Comparison of results of literature and fieldwork in respect of friction angle of rock mass, strata dip and slope dip .....	88
Table 16: Measured Schmidt hammer values.....	102
Table 17: Modified values (MPa) converted by means of the table of the manual of the Schmidt hammer (Table A). The used column of the Table is 0.0 (0.0 mm calcification of concrete). 103	103
Table 18: Measured and converted Schmidt hammer values .....	103

## 8 Annex

### 8.1 Triaxial test data

1	样高(cm)	直径(cm)	围压(kPa)	剪切速率	轴向位移(mm)	轴向应变(%)	轴向力(N)	轴向应力(kPa)	大主应力(kPa)	序号	
Nr.	Hight	diameter	confining pressure $\sigma_3$	load speed	axial displacement	axial strain	axial force	axial stress	sigma 1		$\sigma_1-\sigma_3$
1-1	8	3,91	50	0,6	0,070	0,088	14,727	12,262	62,262	1	12,262
1-1	8	3,91	50	0,6	0,130	0,162	16,568	13,784	63,784	2	13,784
1-1	8	3,91	50	0,6	0,185	0,231	20,250	16,836	66,836	3	16,836
1-1	8	3,91	50	0,6	0,256	0,320	23,932	19,879	69,879	4	19,879
1-1	8	3,91	50	0,6	0,311	0,389	27,613	22,922	72,922	5	22,922
1-1	8	3,91	50	0,6	0,516	0,645	44,181	36,580	86,580	6	36,580
1-1	8	3,91	50	0,6	0,722	0,903	51,545	42,566	92,566	7	42,566
1-1	8	3,91	50	0,6	0,942	1,177	62,590	51,544	101,544	8	51,544
1-1	8	3,91	50	0,6	1,162	1,452	73,635	60,472	110,472	9	60,472
1-1	8	3,91	50	0,6	1,370	1,713	84,681	69,359	119,359	10	69,359
1-1	8	3,91	50	0,6	1,495	1,869	88,363	72,259	122,259	11	72,259
1-1	8	3,91	50	0,6	1,619	2,024	95,726	78,157	128,157	12	78,157
1-1	8	3,91	50	0,6	1,743	2,179	99,408	81,035	131,035	13	81,035
1-1	8	3,91	50	0,6	1,867	2,334	104,931	85,401	135,401	14	85,401
1-1	8	3,91	50	0,6	1,976	2,470	110,453	89,771	139,771	15	89,771
1-1	8	3,91	50	0,6	2,194	2,743	117,817	95,488	145,488	16	95,488
1-1	8	3,91	50	0,6	2,413	3,016	121,499	98,195	148,195	17	98,195
1-1	8	3,91	50	0,6	2,621	3,276	127,021	102,383	152,383	18	102,383
1-1	8	3,91	50	0,6	2,849	3,561	134,385	107,999	157,999	19	107,999
1-1	8	3,91	50	0,6	3,058	3,823	139,907	112,133	162,133	20	112,133
1-1	8	3,91	50	0,6	3,276	4,095	145,430	116,229	166,229	21	116,229
1-1	8	3,91	50	0,6	3,494	4,367	150,953	120,300	170,300	22	120,300
1-1	8	3,91	50	0,6	3,712	4,640	161,998	128,734	178,734	23	128,734
1-1	8	3,91	50	0,6	3,945	4,931	169,362	134,175	184,175	24	134,175
1-1	8	3,91	50	0,6	4,153	5,191	173,043	136,717	186,717	25	136,717
1-1	8	3,91	50	0,6	4,656	5,820	184,089	144,479	194,479	26	144,479
1-1	8	3,91	50	0,6	5,187	6,484	195,134	152,068	202,068	27	152,068
1-1	8	3,91	50	0,6	5,715	7,144	208,020	160,967	210,967	28	160,967
1-1	8	3,91	50	0,6	6,215	7,769	215,384	165,543	215,543	29	165,543
1-1	8	3,91	50	0,6	6,742	8,428	226,429	172,789	222,789	30	172,789
1-1	8	3,91	50	0,6	7,256	9,070	233,793	177,156	227,156	31	177,156
1-1	8	3,91	50	0,6	7,763	9,704	242,997	182,848	232,848	32	182,848
1-1	8	3,91	50	0,6	8,265	10,331	248,520	185,704	235,704	33	185,704
1-1	8	3,91	50	0,6	8,786	10,983	257,724	191,183	241,183	34	191,183
1-1	8	3,91	50	0,6	9,294	11,617	261,406	192,531	242,531	35	192,531
1-1	8	3,91	50	0,6	9,804	12,255	265,088	193,834	243,834	36	193,834
1-1	8	3,91	50	0,6	10,309	12,886	272,451	197,785	247,785	37	197,785
1-1	8	3,91	50	0,6	10,827	13,534	277,974	200,295	250,295	38	200,295
1-1	8	3,91	50	0,6	11,330	14,162	283,497	202,789	252,789	39	202,789
1-1	8	3,91	50	0,6	11,835	14,794	290,860	206,526	256,526	40	206,526
1-1	8	3,91	50	0,6	12,363	15,454	294,542	207,520	257,520	41	207,520

1	样高(cm)	直径 (cm)	围压 (kPa)	剪切速率	轴向位移(mm)	轴向应变(%)	轴向力(N)	轴向应力 (kPa)	大主应力(kPa)	序号	
Nr.	Hight	diameter	confining pressure $\sigma_3$	load speed	axial displacement	axial strain	axial force	axial stress	sigma 1		$\sigma_1-\sigma_3$
1-2	8	3,91	100	0,6	0,056	0,070	13,600	11,325	111,325	1	11,325
1-2	8	3,91	100	0,6	0,107	0,134	23,800	19,807	119,807	2	19,807
1-2	8	3,91	100	0,6	0,178	0,223	44,200	36,751	136,751	3	36,751
1-2	8	3,91	100	0,6	0,248	0,310	57,800	48,017	148,017	4	48,017
1-2	8	3,91	100	0,6	0,299	0,374	61,200	50,809	150,809	5	50,809
1-2	8	3,91	100	0,6	0,519	0,649	85,000	70,374	170,374	6	70,374
1-2	8	3,91	100	0,6	0,734	0,918	120,700	99,660	199,660	7	99,660
1-2	8	3,91	100	0,6	0,939	1,174	139,400	114,803	214,803	8	114,803
1-2	8	3,91	100	0,6	1,159	1,449	171,700	141,010	241,010	9	141,010
1-2	8	3,91	100	0,6	1,377	1,721	195,500	160,112	260,112	10	160,112
1-2	8	3,91	100	0,6	1,488	1,860	207,400	169,619	269,619	11	169,619
1-2	8	3,91	100	0,6	1,605	2,006	215,900	176,307	276,307	12	176,307
1-2	8	3,91	100	0,6	1,722	2,153	227,800	185,747	285,747	13	185,747
1-2	8	3,91	100	0,6	1,839	2,299	238,000	193,774	293,774	14	193,774
1-2	8	3,91	100	0,6	1,951	2,439	248,200	201,789	301,789	15	201,789
1-2	8	3,91	100	0,6	2,170	2,713	263,500	213,627	313,627	16	213,627
1-2	8	3,91	100	0,6	2,384	2,980	282,200	228,159	328,159	17	228,159
1-2	8	3,91	100	0,6	2,613	3,266	297,500	239,819	339,819	18	239,819
1-2	8	3,91	100	0,6	2,822	3,528	312,800	251,472	351,472	19	251,472
1-2	8	3,91	100	0,6	3,031	3,789	323,000	258,969	358,969	20	258,969
1-2	8	3,91	100	0,6	3,251	4,064	333,200	266,383	366,383	21	266,383
1-2	8	3,91	100	0,6	3,462	4,327	343,400	273,783	373,783	22	273,783
1-2	8	3,91	100	0,6	3,683	4,604	351,900	279,750	379,750	23	279,750
1-2	8	3,91	100	0,6	3,894	4,868	365,500	289,758	389,758	24	289,758
1-2	8	3,91	100	0,6	4,115	5,144	377,400	298,323	398,323	25	298,323
1-2	8	3,91	100	0,6	4,636	5,795	394,400	309,620	409,620	26	309,620
1-2	8	3,91	100	0,6	5,157	6,446	413,100	322,059	422,059	27	322,059
1-2	8	3,91	100	0,6	5,675	7,094	431,800	334,308	434,308	28	334,308
1-2	8	3,91	100	0,6	6,201	7,751	447,100	343,703	443,703	29	343,703
1-2	8	3,91	100	0,6	6,733	8,416	459,000	350,308	450,308	30	350,308
1-2	8	3,91	100	0,6	7,254	9,068	469,200	355,546	455,546	31	355,546
1-2	8	3,91	100	0,6	7,754	9,693	477,700	359,499	459,499	32	359,499
1-2	8	3,91	100	0,6	8,268	10,335	489,600	365,833	465,833	33	365,833
1-2	8	3,91	100	0,6	8,782	10,977	501,500	372,040	472,040	34	372,040
1-2	8	3,91	100	0,6	9,296	11,620	508,300	374,363	474,363	35	374,363
1-2	8	3,91	100	0,6	9,820	12,275	515,100	376,560	476,560	36	376,560
1-2	8	3,91	100	0,6	10,334	12,917	523,600	379,970	479,970	37	379,970
1-2	8	3,91	100	0,6	10,858	13,572	533,800	384,458	484,458	38	384,458
1-2	8	3,91	100	0,6	11,390	14,238	540,600	386,360	486,360	39	386,360
1-2	8	3,91	100	0,6	11,913	14,891	544,000	385,826	485,826	40	385,826
1-2	8	3,91	100	0,6	12,427	15,534	547,400	385,307	485,307	41	385,307

1	样高(cm)	直径 (cm)	围压(kPa)	剪切速率	轴向位移(mm)	轴向应变(%)	轴向力(N)	轴向应力(kPa)	大主应力(kPa)	序号	
Nr.	Hight	diameter	confining pressure $\sigma_3$	load speed	axial displacement	axial strain	axial force	axial stress	sigma 1		$\sigma_1-\sigma_3$
1-3	8	3,91	150	0,6	0,075	0,094	18,409	15,326	165,326	1	15,326
1-3	8	3,91	150	0,6	0,135	0,169	27,613	22,972	172,972	2	22,972
1-3	8	3,91	150	0,6	0,206	0,258	36,818	30,602	180,602	3	30,602
1-3	8	3,91	150	0,6	0,266	0,333	40,500	33,637	183,637	4	33,637
1-3	8	3,91	150	0,6	0,321	0,401	44,181	36,670	186,670	5	36,670
1-3	8	3,91	150	0,6	0,546	0,683	66,272	54,850	204,850	6	54,850
1-3	8	3,91	150	0,6	0,777	0,971	92,044	75,959	225,959	7	75,959
1-3	8	3,91	150	0,6	0,982	1,227	106,771	87,884	237,884	8	87,884
1-3	8	3,91	150	0,6	1,201	1,501	119,658	98,218	248,218	9	98,218
1-3	8	3,91	150	0,6	1,435	1,794	136,226	111,485	261,485	10	111,485
1-3	8	3,91	150	0,6	1,554	1,943	149,112	121,846	271,846	11	121,846
1-3	8	3,91	150	0,6	1,678	2,097	160,157	130,665	280,665	12	130,665
1-3	8	3,91	150	0,6	1,802	2,253	169,362	137,956	287,956	13	137,956
1-3	8	3,91	150	0,6	1,906	2,383	174,884	142,265	292,265	14	142,265
1-3	8	3,91	150	0,6	2,020	2,525	180,407	146,543	296,543	15	146,543
1-3	8	3,91	150	0,6	2,229	2,786	196,975	159,572	309,572	16	159,572
1-3	8	3,91	150	0,6	2,432	3,040	206,179	166,593	316,593	17	166,593
1-3	8	3,91	150	0,6	2,645	3,306	220,906	178,002	328,002	18	178,002
1-3	8	3,91	150	0,6	2,869	3,586	230,111	184,882	334,882	19	184,882
1-3	8	3,91	150	0,6	3,080	3,850	242,997	194,701	344,701	20	194,701
1-3	8	3,91	150	0,6	3,288	4,110	252,201	201,530	351,530	21	201,530
1-3	8	3,91	150	0,6	3,492	4,365	261,406	208,330	358,330	22	208,330
1-3	8	3,91	150	0,6	3,715	4,644	272,451	216,499	366,499	23	216,499
1-3	8	3,91	150	0,6	3,919	4,899	285,337	226,133	376,133	24	226,133
1-3	8	3,91	150	0,6	4,122	5,153	294,542	232,805	382,805	25	232,805
1-3	8	3,91	150	0,6	4,648	5,810	316,633	248,530	398,530	26	248,530
1-3	8	3,91	150	0,6	5,151	6,439	338,835	264,182	414,182	27	264,182
1-3	8	3,91	150	0,6	5,670	7,088	355,908	275,569	425,569	28	275,569
1-3	8	3,91	150	0,6	6,170	7,713	371,084	285,386	435,386	29	285,386
1-3	8	3,91	150	0,6	6,693	8,366	384,362	293,505	443,505	30	293,505
1-3	8	3,91	150	0,6	7,220	9,025	397,641	301,461	451,461	31	301,461
1-3	8	3,91	150	0,6	7,727	9,659	410,920	309,358	459,358	32	309,358
1-3	8	3,91	150	0,6	8,248	10,310	422,301	315,635	465,635	33	315,635
1-3	8	3,91	150	0,6	8,765	10,956	431,786	320,399	470,399	34	320,399
1-3	8	3,91	150	0,6	9,268	11,585	445,065	327,920	477,920	35	327,920
1-3	8	3,91	150	0,6	9,773	12,216	448,859	328,354	478,354	36	328,354
1-3	8	3,91	150	0,6	10,273	12,841	456,447	331,528	481,528	37	331,528
1-3	8	3,91	150	0,6	10,796	13,495	462,137	333,143	483,143	38	333,143
1-3	8	3,91	150	0,6	11,313	14,141	467,828	334,726	484,726	39	334,726
1-3	8	3,91	150	0,6	11,813	14,766	475,416	337,679	487,679	40	337,679
1-3	8	3,91	150	0,6	12,328	15,410	479,210	337,803	487,803	41	337,803
1-3	8	3,91	150	0,6	12,828	16,035	484,901	339,289	489,289	42	339,289

1	样高(cm)	直径 (cm)	围压 (kPa)	剪切速率	轴向位移(mm)	轴向应变(%)	轴向力(N)	轴向应力 (kPa)	大主应力 (kPa)	序号	
Nr.	Hight	diameter	confining pressure $\sigma_3$	load speed	axial displacement	axial strain	axial force	axial stress	sigma 1		$\sigma_1-\sigma_3$
1-4	8	3,91	200	0,6	0,065	0,081	28,900	24,064	224,064	1	24,064
1-4	8	3,91	200	0,6	0,117	0,146	37,400	31,121	231,121	2	31,121
1-4	8	3,91	200	0,6	0,173	0,216	44,200	36,754	236,754	3	36,754
1-4	8	3,91	200	0,6	0,224	0,280	51,000	42,381	242,381	4	42,381
1-4	8	3,91	200	0,6	0,280	0,350	56,100	46,586	246,586	5	46,586
1-4	8	3,91	200	0,6	0,509	0,636	74,800	61,937	261,937	6	61,937
1-4	8	3,91	200	0,6	0,710	0,887	100,300	82,842	282,842	7	82,842
1-4	8	3,91	200	0,6	0,935	1,169	119,000	98,008	298,008	8	98,008
1-4	8	3,91	200	0,6	1,164	1,455	136,000	111,684	311,684	9	111,684
1-4	8	3,91	200	0,6	1,392	1,740	158,100	129,458	329,458	10	129,458
1-4	8	3,91	200	0,6	1,504	1,880	170,000	139,003	339,003	11	139,003
1-4	8	3,91	200	0,6	1,616	2,020	178,500	145,745	345,745	12	145,745
1-4	8	3,91	200	0,6	1,748	2,185	188,700	153,814	353,814	13	153,814
1-4	8	3,91	200	0,6	1,864	2,330	195,500	159,121	359,121	14	159,121
1-4	8	3,91	200	0,6	1,991	2,489	200,600	163,006	363,006	15	163,006
1-4	8	3,91	200	0,6	2,200	2,750	215,900	174,969	374,969	16	174,969
1-4	8	3,91	200	0,6	2,409	3,011	232,900	188,239	388,239	17	188,239
1-4	8	3,91	200	0,6	2,614	3,268	246,500	198,705	398,705	18	198,705
1-4	8	3,91	200	0,6	2,828	3,535	258,400	207,721	407,721	19	207,721
1-4	8	3,91	200	0,6	3,042	3,803	272,000	218,048	418,048	20	218,048
1-4	8	3,91	200	0,6	3,258	4,072	282,200	225,590	425,590	21	225,590
1-4	8	3,91	200	0,6	3,465	4,331	294,100	234,468	434,468	22	234,468
1-4	8	3,91	200	0,6	3,681	4,601	306,000	243,267	443,267	23	243,267
1-4	8	3,91	200	0,6	3,902	4,877	312,800	247,953	447,953	24	247,953
1-4	8	3,91	200	0,6	4,108	5,135	321,300	254,001	454,001	25	254,001
1-4	8	3,91	200	0,6	4,624	5,780	343,400	269,626	469,626	26	269,626
1-4	8	3,91	200	0,6	5,140	6,425	368,900	287,665	487,665	27	287,665
1-4	8	3,91	200	0,6	5,662	7,078	382,500	296,190	496,190	28	296,190
1-4	8	3,91	200	0,6	6,179	7,724	401,200	308,510	508,510	29	308,510
1-4	8	3,91	200	0,6	6,710	8,388	416,500	317,972	517,972	30	317,972
1-4	8	3,91	200	0,6	7,218	9,022	435,200	329,945	529,945	31	329,945
1-4	8	3,91	200	0,6	7,747	9,684	443,700	333,944	533,944	32	333,944
1-4	8	3,91	200	0,6	8,252	10,315	457,300	341,775	541,775	33	341,775
1-4	8	3,91	200	0,6	8,761	10,951	469,200	348,181	548,181	34	348,181
1-4	8	3,91	200	0,6	9,266	11,582	484,500	356,986	556,986	35	356,986
1-4	8	3,91	200	0,6	9,771	12,214	496,400	363,142	563,142	36	363,142
1-4	8	3,91	200	0,6	10,290	12,862	506,600	367,865	567,865	37	367,865
1-4	8	3,91	200	0,6	10,799	13,499	520,200	374,983	574,983	38	374,983
1-4	8	3,91	200	0,6	11,316	14,145	533,800	381,912	581,912	39	381,912
1-4	8	3,91	200	0,6	11,825	14,781	547,400	388,740	588,740	40	388,740
1-4	8	3,91	200	0,6	12,335	15,419	559,300	394,219	594,219	41	394,219

## 8.2 Shear test data

Project Number T2b3 SampleNr.10 for quick direct sh Calculator  
 Test Date 17.12.12 Checker  
 Available Loads (kg): 1,274 2,549  
 Principal stress (kPa): 50  
 C (kPa/0,01mm): 2,131

Time (s)	Specimen No.							
	022		99		10		2-2	
	1,274 kg Load 100 kPa		3,823 kg Load 200 kPa		6,372 kg Load 300 kPa		8,921 kg Load 400 kPa	
0	0	0,00	0	0,00	0	0,00	0	0,00
10	8	17,05	9	19,18	10	21,31	11	23,44
20	12	25,57	13	27,70	14	29,83	14,5	30,90
30	14	29,83	15	31,97	16,3	34,74	16,5	35,16
40	15	31,97	16,8	35,80	18	38,36	18,5	39,42
50	15,3	32,60	17,7	37,72	19	40,49	20	42,62
60	15,3	32,60	18,5	39,42	20	42,62	22	46,88
70	15	31,97	19	40,49	20,4	43,47	23,5	50,08
80	15	31,97	19,4	41,34	21	44,75	24,5	52,21
90	15	31,97	19,9	42,41	21,6	46,03	25	53,28
100	15	31,97	20	42,62	22,2	47,31	26	55,41
110	14,9	31,75	19,8	42,19	22,9	48,80	27	57,54
120	14,8	31,54	19,5	41,55	23,7	50,50	27,7	59,03
130	14,5	30,90	19,4	41,34	24,5	52,21	28,5	60,73
140	14,3	30,47	19,3	41,13	25	53,28	29,6	63,08
150	14,2	30,26	19,2	40,92	24,7	52,64	30	63,93
160	14	29,83	19	40,49	24,3	51,78	29,7	63,29
170			18,7	39,85	24	51,14	29	61,80
			18,5	39,42	24	51,14	28,9	61,59
			18,3	39,00	24	51,14	28,9	61,59
			18,2	38,78	24	51,14	28,7	61,16
			18	38,36	24	51,14	28,6	60,95
			18	38,36	24	51,14	28,6	60,95
			17,9	38,14	24	51,14	28,5	60,73
			17,9	38,14	24	51,14	28,5	60,73
			17,8	37,93			28,5	60,73
			17,8	37,93			28,5	60,73
$\tau$ (kPa)	32,6043		42,62		53,275		63,93	

## 8.3 Schmidt Hammer records

### 8.3.1 Records and conversion of $T_2b^3$

Nr.	Rejected	Ranked values												Rejected	Mean	Stand. devi.	
1	32 32 37	38	38	38	38	40	40	40	41	42	42	42	42	43	44	39,7	1,6
2	5 28 40	42	42	42	42	44	44	45	48	50	52	54	55	58	58	46,1	4,6
4	22 30 32	40	40	40	44	44	44	48	48	50	50	50	52	54	54	45,4	4,3
6	32 34 40	46	48	48	52	54	55	56	56	58	58	58	58	59	59	53,1	4,4
8	30 38 38	38	40	40	43	44	44	45	45	47	48	48	50	54		43,4	3,2
9	10 10 10	10	11	12	13	14	16	28	28	28	30	32	32	33		19,0	8,4
11	22 25 28	28	28	30	38	39	39	40	42	42	43	44	44	47		36,9	5,9

Table 16: Measured Schmidt hammer values

Nr.	Ranked values	Mean	Stand. devi.	
1	37,5 37,5 37,5 37,5 41,6 41,6 41,6 43,7 45,9	45,9	41,0	3,4
2	45,9 45,9 45,9 45,9 50,4 52,7 60,0 60,0 60,0	60,0	52,7	6,7
4	41,6 41,6 41,6 50,4 50,4 60,0 60,0 60,0 60,0	60,0	52,6	8,5
6	55,0 60,0 60,0 60,0 60,0 60,0 60,0 60,0 60,0	60,0	59,5	1,6
8	37,5 41,6 41,6 48,1 50,4 50,4 52,7 52,7 57,5	60,0	49,3	7,2
9	10,0 10,0 10,0 10,0 10,0 10,0 20,3 20,3 20,3	23,3	14,4	5,8
11	20,3 20,3 23,3 37,5 39,5 39,5 41,6 45,9 45,9	48,1	36,2	10,8

Table 17: Modified values (MPa) converted by means of the table of the manual of the Schmidt hammer (Table A). The used column of the Table is 0.0 (0.0 mm calcification of concrete)

### 8.3.2 Records and conversion of $T_2b^2$

Site	Rejected			Ranked values										Rejected			Mean	Stand. devi.
	1	2	3	4	5	6	7	8	9	10	11	12	13	14	15	16		
C1	12	14	16	17	18	19	20	20	20	21	21	21	21	22	22	23	19,8	1,4
*				9	9	10,3	10	10	10	11,4	11,4	11,4	11,4				10,4	1,0
RS1	33	33	33	34	35	36	35	36	38	38	38	38	38	38	40	40	36,6	1,6
*				30	31,8	33,6	31,8	33,6	37,5	37,5	37,5	37,5	37,5				34,8	3,0
RS4	40	41	43	43	44	45	46	47	47	48	48	49	49	49	50	51	46,6	2,1
*				48,1	50,4	52,7	55	57,5	57,5	60	60	60	60				56,1	4,4

\* Modified values (MPa) converted by means of the table of the manual of the Schmidt hammer (Table A). The used column of the Table is 0.0 (0.0 mm calcification of concrete)

Table 18: Measured and converted Schmidt hammer values

### 8.3.3 Conversion table

附录 A 测区混凝土强度换算表

表 A

平均回弹值 R <sub>m</sub>	测区混凝土强度换算值 $f_{cu,i}^c$ (MPa)															
	平均碳化深度值 $d_{av}$ (mm)															
	0.0	0.5	1.0	1.5	2.0	2.5	3.0	3.5	4.0	4.5	5.0	5.5	>6			
20.0	10.3	10.1	—	—	—	—	—	—	—	—	—	—	—			
20.2	10.5	10.3	10.0	—	—	—	—	—	—	—	—	—	—			
20.4	10.7	10.5	10.2	—	—	—	—	—	—	—	—	—	—			
20.6	11.0	10.8	10.4	10.1	—	—	—	—	—	—	—	—	—			
20.8	11.2	11.0	10.6	10.3	—	—	—	—	—	—	—	—	—			
21.0	11.4	11.2	10.8	10.5	10.0	—	—	—	—	—	—	—	—			
21.2	11.6	11.4	11.0	10.7	10.2	—	—	—	—	—	—	—	—			
21.4	11.8	11.6	11.2	10.9	10.4	10.0	—	—	—	—	—	—	—			
21.6	12.0	11.8	11.4	11.0	10.6	10.2	—	—	—	—	—	—	—			
21.8	12.3	12.1	11.7	11.3	10.8	10.5	10.1	—	—	—	—	—	—			
22.0	12.5	12.3	11.9	11.5	11.0	10.6	10.2	—	—	—	—	—	—			
22.2	12.7	12.4	12.1	11.7	11.2	10.8	10.4	10.0	—	—	—	—	—			
22.4	13.0	12.7	12.4	12.0	11.4	11.0	10.7	10.3	10.0	—	—	—	—			
22.6	13.2	12.9	12.5	12.1	11.6	11.2	10.8	10.4	10.2	—	—	—	—			
22.8	13.4	13.1	12.7	12.3	11.8	11.4	11.0	10.6	10.3	—	—	—	—			
23.0	13.7	13.4	13.0	12.6	12.1	11.6	11.2	10.8	10.5	10.1	—	—	—			
23.2	13.9	13.6	13.2	12.8	12.2	11.8	11.4	11.0	10.7	10.3	10.0	—	—			
23.4	14.1	13.8	13.4	13.0	12.4	12.0	11.6	11.2	10.9	10.4	10.2	—	—			
23.6	14.4	14.1	13.7	13.2	12.7	12.2	11.8	11.4	11.1	10.7	10.4	10.1	—			
23.8	14.6	14.3	13.9	13.4	12.8	12.4	12.0	11.5	11.2	10.8	10.5	10.2	—			
24.0	14.9	14.6	14.2	13.7	13.1	12.7	12.2	11.8	11.5	11.0	10.7	10.4	10.1			
24.2	15.1	14.8	14.3	13.9	13.3	12.8	12.4	11.9	11.6	11.2	10.9	10.6	10.3			
24.4	15.4	15.1	14.6	14.2	13.6	13.1	12.6	12.2	11.9	11.4	11.1	10.8	10.4			
24.6	15.6	15.3	14.8	14.4	13.7	13.3	12.8	12.3	12.0	11.5	11.2	10.9	10.6			
24.8	15.9	15.6	15.1	14.6	14.0	13.5	13.0	12.6	12.2	11.8	11.4	11.1	10.7			
25.0	16.2	15.9	15.4	14.9	14.3	13.8	13.3	12.8	12.5	12.0	11.7	11.3	10.9			

平均回弹值 R <sub>m</sub>	测区混凝土强度换算值 $f_{cu,i}^c$ (MPa)															
	平均碳化深度值 $d_{av}$ (mm)															
	0.0	0.5	1.0	1.5	2.0	2.5	3.0	3.5	4.0	4.5	5.0	5.5	>6			
25.2	16.4	16.1	15.6	15.1	14.4	13.9	13.4	13.0	12.6	12.1	11.8	11.5	11.0			
25.4	16.7	16.4	15.9	15.4	14.7	14.2	13.7	13.2	12.9	12.4	12.0	11.7	11.2			
25.6	16.9	16.6	16.1	15.7	14.9	14.4	13.9	13.4	13.0	12.5	12.2	11.8	11.3			
25.8	17.2	16.9	16.3	15.8	15.1	14.6	14.1	13.6	13.2	12.7	12.4	12.0	11.5			
26.0	17.5	17.2	16.6	16.1	15.4	14.9	14.4	13.8	13.5	13.0	12.6	12.2	11.6			
26.2	17.8	17.4	16.9	16.4	15.7	15.1	14.6	14.0	13.7	13.2	12.8	12.4	11.8			
26.4	18.0	17.6	17.1	16.6	15.8	15.3	14.8	14.2	13.9	13.3	13.0	12.6	12.0			
26.6	18.3	17.9	17.4	16.8	16.1	15.6	15.0	14.4	14.1	13.5	13.2	12.8	12.1			
26.8	18.6	18.2	17.7	17.1	16.4	15.8	15.3	14.6	14.3	13.8	13.4	12.9	12.3			
27.0	18.9	18.5	18.0	17.4	16.6	16.1	15.5	14.8	14.6	14.0	13.6	13.1	12.4			
27.2	19.1	18.7	18.1	17.6	16.8	16.2	15.7	15.0	14.7	14.1	13.8	13.3	12.6			
27.4	19.4	19.0	18.4	17.8	17.0	16.4	15.9	15.2	14.9	14.3	14.0	13.4	12.7			
27.6	19.7	19.3	18.7	18.0	17.2	16.6	16.1	15.4	15.1	14.5	14.1	13.6	12.9			
27.8	20.0	19.6	19.0	18.2	17.4	16.8	16.3	15.6	15.3	14.7	14.2	13.7	13.0			
28.0	20.3	19.7	19.2	18.4	17.6	17.0	16.5	15.8	15.4	14.8	14.4	13.9	13.2			
28.2	20.6	20.0	19.5	18.6	17.8	17.2	16.7	16.0	15.6	15.0	14.6	14.0	13.3			
28.4	20.9	20.3	19.7	18.8	18.0	17.4	16.9	16.2	15.8	15.2	14.8	14.2	13.5			
28.6	21.2	20.6	20.0	19.1	18.2	17.6	17.1	16.4	16.0	15.4	15.0	14.3	13.6			
28.8	21.5	20.9	20.0	19.4	18.5	17.8	17.3	16.6	16.2	15.6	15.2	14.5	13.8			
29.0	21.8	21.1	20.5	19.6	18.7	18.1	17.5	16.8	16.4	15.8	15.4	14.6	13.9			
29.2	22.1	21.4	20.8	19.9	19.0	18.3	17.7	17.0	16.6	16.0	15.6	14.8	14.1			
29.4	22.4	21.7	21.1	20.2	19.3	18.6	17.9	17.2	16.8	16.2	15.8	15.0	14.2			
29.6	22.7	22.0	21.3	20.4	19.5	18.8	18.2	17.5	17.0	16.4	16.0	15.1	14.4			
29.8	23.0	22.3	21.6	20.7	19.8	19.1	18.4	17.7	17.2	16.6	16.2	15.3	14.5			
30.0	23.3	22.6	21.9	21.0	20.0	19.3	18.6	17.9	17.4	16.8	16.4	15.4	14.7			
30.2	23.6	22.9	22.2	21.2	20.3	19.6	18.9	18.2	17.6	17.0	16.6	15.6	14.9			
30.4	23.9	23.2	22.5	21.5	20.6	19.9	19.2	18.5	17.9	17.3	16.9	15.9	15.1			
30.6	24.3	23.6	22.8	21.9	20.9	20.2	19.5	18.8	18.2	17.6	17.2	16.8	15.8			
30.8	24.6	23.9	23.1	22.1	21.2	20.4	19.7	19.0	18.4	17.8	17.4	16.4	15.7			
31.0	24.9	24.2	23.4	22.4	21.4	20.7	19.9	19.2	18.4	17.9	17.4	16.4	15.8			
31.2	25.2	24.4	23.7	22.7	21.7	20.9	20.2	19.4	18.6	18.1	17.6	16.6	15.9			

平均回弹值 $R_a$	测区混凝土强度换算值 $f_{cu}^c$ (MPa)												
	平均碳化深度值 $d_a$ (mm)												
	0.0	0.5	1.0	1.5	2.0	2.5	3.0	3.5	4.0	4.5	5.0	5.5	>6
31.4	25.6	24.8	24.1	23.0	22.0	21.2	20.5	19.7	18.9	18.4	17.8	16.9	15.8
31.6	25.9	25.1	24.3	23.3	22.3	21.5	20.7	19.9	19.2	18.6	18.0	17.1	16.0
31.8	26.2	25.4	24.6	23.6	22.5	21.7	21.0	20.2	19.4	18.9	18.2	17.3	16.2
32.0	26.5	25.7	24.9	23.9	22.8	22.0	21.2	20.4	19.6	19.1	18.4	17.5	16.4
32.2	26.9	26.1	25.3	24.2	23.1	22.3	21.5	20.7	19.9	19.4	18.6	17.7	16.6
32.4	27.2	26.4	25.6	24.5	23.4	22.6	21.8	20.9	20.1	19.6	18.8	17.9	16.8
32.6	27.6	26.8	25.9	24.8	23.7	22.9	22.1	21.3	20.4	19.9	19.0	18.1	17.0
32.8	27.9	27.1	26.2	25.1	24.0	23.2	22.3	21.5	20.6	20.1	19.2	18.3	17.2
33.0	28.2	27.4	26.5	25.4	24.3	23.4	22.6	21.7	20.9	20.3	19.4	18.5	17.4
33.2	28.6	27.7	26.8	25.7	24.6	23.7	22.9	22.0	21.2	20.5	19.6	18.7	17.6
33.4	28.9	28.0	27.1	26.0	24.9	24.0	23.1	22.3	21.4	20.7	19.8	18.9	17.8
33.6	29.3	28.4	27.4	26.4	25.2	24.2	23.3	22.6	21.7	20.9	20.0	19.1	18.0
33.8	29.6	28.7	27.7	26.6	25.4	24.4	23.5	22.8	21.9	21.1	20.2	19.3	18.2
34.0	30.0	29.1	28.0	26.8	25.6	24.6	23.7	23.0	22.1	21.3	20.4	19.5	18.3
34.2	30.3	29.4	28.3	27.0	25.8	24.8	23.9	23.2	22.3	21.5	20.6	19.7	18.4
34.4	30.7	29.8	28.6	27.2	26.0	25.0	24.1	23.4	22.5	21.7	20.8	19.8	18.6
34.6	31.1	30.2	28.9	27.4	26.2	25.2	24.3	23.6	22.7	21.9	21.0	20.0	18.8
34.8	31.4	30.5	29.2	27.6	26.4	25.4	24.5	23.8	22.9	22.1	21.2	20.2	19.0
35.0	31.8	30.8	29.6	28.0	26.7	25.8	24.8	24.0	23.2	22.3	21.4	20.4	19.2
35.2	32.1	31.1	29.9	28.2	27.0	26.0	25.0	24.2	23.4	22.5	21.6	20.6	19.4
35.4	32.5	31.5	30.2	28.6	27.3	26.3	25.4	24.4	23.7	22.8	21.8	20.8	19.6
35.6	32.9	31.9	30.6	29.0	27.6	26.6	25.7	24.7	24.0	23.0	22.0	21.0	19.8
35.8	33.3	32.3	31.0	29.3	28.0	27.0	26.0	25.0	24.3	23.3	22.2	21.2	20.0
36.0	33.6	32.6	31.2	29.6	28.2	27.2	26.2	25.2	24.5	23.5	22.4	21.4	20.2
36.2	34.0	33.0	31.6	29.9	28.6	27.5	26.5	25.5	24.8	23.8	22.6	21.6	20.4
36.4	34.4	33.4	32.0	30.3	28.9	27.9	26.8	25.8	25.1	24.1	22.8	21.8	20.6
36.6	34.8	33.8	32.4	30.6	29.2	28.2	27.1	26.1	25.4	24.4	23.0	22.0	20.8
36.8	35.2	34.1	32.7	31.0	29.6	28.6	27.5	26.4	25.7	24.6	23.2	22.2	21.1
37.0	35.6	34.4	33.0	31.2	29.8	28.8	27.7	26.6	25.9	24.8	23.4	22.4	21.3
37.2	35.9	34.8	33.4	31.6	30.2	29.1	28.0	26.9	26.2	25.1	23.7	22.6	21.5
37.4	36.3	35.2	33.8	31.9	30.5	29.4	28.3	27.2	26.6	25.4	24.0	22.9	21.8
37.6	36.7	35.6	34.1	32.3	30.8	29.7	28.6	27.5	26.8	25.7	24.2	23.1	22.0

12

平均回弹值 $R_a$	测区混凝土强度换算值 $f_{cu}^c$ (MPa)												
	平均碳化深度值 $d_a$ (mm)												
	0.0	0.5	1.0	1.5	2.0	2.5	3.0	3.5	4.0	4.5	5.0	5.5	>6
37.8	37.1	36.0	34.5	32.6	31.2	30.0	28.9	27.8	27.1	26.0	24.5	23.4	22.3
38.0	37.5	36.4	34.9	33.0	31.5	30.3	29.2	28.1	27.4	26.2	24.8	23.6	22.5
38.2	37.9	36.8	35.2	33.4	31.8	30.6	29.5	28.4	27.7	26.5	25.0	23.9	22.7
38.4	38.3	37.2	35.6	33.7	32.1	30.9	29.8	28.7	28.0	26.8	25.3	24.1	23.0
38.6	38.7	37.5	36.0	34.1	32.4	31.2	30.1	29.0	28.3	27.0	25.5	24.2	23.2
38.8	39.1	37.9	36.4	34.4	32.7	31.5	30.4	29.3	28.5	27.2	25.8	24.6	23.5
39.0	39.5	38.2	36.7	34.7	33.0	31.8	30.6	29.6	28.8	27.4	26.0	24.8	23.7
39.2	39.9	38.5	37.0	35.0	33.3	32.1	30.8	29.8	29.0	27.6	26.2	25.0	23.9
39.4	40.3	38.8	37.3	35.3	33.6	32.4	31.0	30.0	29.2	27.8	26.4	25.2	24.2
39.6	40.7	39.1	37.6	35.6	33.9	32.7	31.2	30.2	29.4	28.0	26.6	25.4	24.4
39.8	41.2	39.6	38.0	35.9	34.2	33.0	31.4	30.5	29.7	28.2	26.8	25.6	24.7
40.0	41.6	39.9	38.3	36.2	34.5	33.3	31.7	30.8	30.0	28.4	27.0	25.8	24.9
40.2	42.0	40.3	38.6	36.5	34.8	33.6	32.0	31.1	30.2	28.6	27.3	26.0	25.2
40.4	42.4	40.7	39.0	36.9	35.1	33.9	32.3	31.4	30.5	28.8	27.6	26.2	25.4
40.6	42.8	41.1	39.4	37.2	35.4	34.2	32.6	31.7	30.8	29.1	27.8	26.5	25.7
40.8	43.3	41.6	39.8	37.7	35.7	34.5	32.9	32.0	31.2	29.4	28.1	26.8	26.0
41.0	43.7	42.0	40.2	38.0	36.0	34.8	33.2	32.3	31.5	29.7	28.4	27.1	26.2
41.2	44.1	42.3	40.6	38.4	36.3	35.1	33.5	32.6	31.8	30.0	28.7	27.3	26.5
41.4	44.5	42.7	40.9	38.7	36.6	35.4	33.8	32.9	32.0	30.3	28.9	27.6	26.7
41.6	45.0	43.2	41.4	39.2	36.9	35.7	34.2	33.3	32.4	30.6	29.2	27.9	27.0
41.8	45.4	43.6	41.8	39.5	37.2	36.0	34.5	33.6	32.7	30.9	29.5	28.1	27.2
42.0	45.9	44.1	42.2	39.9	37.6	36.3	34.9	34.0	33.0	31.2	29.8	28.5	27.5
42.2	46.3	44.4	42.6	40.3	38.0	36.6	35.2	34.3	33.3	31.5	30.1	28.7	27.8
42.4	46.7	44.8	43.0	40.6	38.3	36.9	35.5	34.6	33.6	31.8	30.4	29.0	28.0
42.6	47.2	45.3	43.4	41.1	38.7	37.3	35.9	34.9	34.0	32.1	30.7	29.3	28.3
42.8	47.6	45.7	43.8	41.4	39.0	37.6	36.2	35.2	34.3	32.4	30.9	29.5	28.6
43.0	48.1	46.2	44.2	41.8	39.4	38.0	36.6	35.6	34.6	32.7	31.3	29.8	28.9
43.2	48.5	46.6	44.6	42.2	39.8	38.3	36.9	35.9	34.9	33.0	31.5	30.1	29.1
43.4	49.0	47.0	45.1	42.6	40.2	38.7	37.2	36.3	35.3	33.3	31.8	30.4	29.4
43.6	49.4	47.4	45.4	43.0	40.5	39.0	37.5	36.6	35.6	33.6	32.1	30.6	29.6
43.8	49.9	47.9	45.9	43.4	40.9	39.4	37.9	36.9	35.9	33.9	32.4	30.9	29.9
44.0	50.4	48.4	46.4	43.8	41.3	39.8	38.3	37.3	36.3	34.3	32.8	31.2	30.2

13

平均回弹值 $R_a$	测区混凝土强度换算值 $f_{cu}^c$ (MPa)												
	平均碳化深度值 $d_a$ (mm)												
	0.0	0.5	1.0	1.5	2.0	2.5	3.0	3.5	4.0	4.5	5.0	5.5	>6
44.2	50.8	48.8	46.7	44.2	41.7	40.1	38.6	37.6	36.6	34.5	33.0	31.5	30.5
44.4	51.3	49.2	47.2	44.6	42.1	40.5	39.0	38.0	36.9	34.9	33.3	31.8	30.8
44.6	51.7	49.6	47.6	45.0	42.4	40.8	39.3	38.3	37.2	35.2	33.6	32.1	31.0
44.8	52.2	50.1	48.0	45.4	42.8	41.2	39.7	38.6	37.6	35.5	33.9	32.4	31.3
45.0	52.7	50.6	48.5	45.8	43.2	41.6	40.1	39.0	37.9	35.8	34.3	32.7	31.6
45.2	53.2	51.1	48.9	46.3	43.6	42.0	40.4	39.4	38.3	36.2	34.6	33.0	31.9
45.4	53.6	51.5	49.4	46.6	44.0	42.3	40.7	39.7	38.6	36.4	34.8	33.2	32.2
45.6	54.1	51.9	49.8	47.1	44.4	42.7	41.1	40.0	39.0	36.8	35.2	33.5	32.5
45.8	54.6	52.4	50.2	47.5	44.8	43.1	41.5	40.4	39.3	37.1	35.5	33.9	32.8
46.0	55.0	52.8	50.6	47.9	45.2	43.5	41.9	40.8	39.7	37.5	35.8	34.2	33.1
46.2	55.5	53.3	51.1	48.3	45.5	43.8	42.2	41.1	40.0	37.7	36.1	34.4	33.3
46.4	56.0	53.8	51.5	48.7	45.9	44.2	42.6	41.4	40.3	38.1	36.4	34.7	33.6
46.6	56.5	54.2	52.0	49.2	46.3	44.6	42.9	41.8	40.7	38.4	36.7	35.0	33.9
46.8	57.0	54.7	52.4	49.6	46.7	45.0	43.3	42.2	41.0	38.8	37.0	35.3	34.2
47.0	57.5	55.2	52.9	50.0	47.2	45.2	43.7	42.6	41.4	39.1	37.4	35.6	34.5
47.2	58.0	55.7	53.4	50.5	47.6	45.8	44.1	42.9	41.8	39.4	37.7	36.0	34.8
47.4	58.5	56.2	53.8	50.9	48.0	46.2	44.5	43.3	42.1	39.8	38.0	36.3	35.1
47.6	59.0	56.6	54.3	51.3	48.4	46.6	44.8	43.7	42.5	40.1	38.3	36.6	35.4
47.8	59.5	57.1	54.7	51.8	48.8	47.0	45.2	44.0	42.8	40.5	38.7	36.9	35.7
48.0	60.0	57.6	55.2	52.2	49.2	47.4	45.6	44.4	43.2	40.8	39.0	37.2	36.0
48.2	—	58.0	55.7	52.6	49.6	47.8	46.0	44.8	43.6	41.1	39.3	37.5	36.3
48.4	—	58.6	56.1	53.1	50.0	48.2	46.4	45.1	43.9	41.5	39.6	37.8	36.6
48.6	—	59.0	56.6	53.5	50.4	48.6	46.7	45.5	44.3	41.8	40.0	38.1	36.9
48.8	—	59.5	57.1	54.0	50.9	49.0	47.1	45.9	44.6	42.2	40.3	38.4	37.2
49.0	—	60.0	57.5	54.4									

平均回弹值 R <sub>a</sub>	测区混凝土强度换算值 $f_{cu,i}$ (MPa)												
	平均碳化深度值 $d_a$ (mm)												
	0.0	0.5	1.0	1.5	2.0	2.5	3.0	3.5	4.0	4.5	5.0	5.5	>6
57.0	—	—	—	—	—	—	—	—	—	57.6	58.1	52.5	50.8
57.2	—	—	—	—	—	—	—	—	—	58.0	55.5	52.9	51.2
57.4	—	—	—	—	—	—	—	—	—	58.4	55.9	53.3	51.6
57.6	—	—	—	—	—	—	—	—	—	58.9	56.3	53.7	51.9
57.8	—	—	—	—	—	—	—	—	—	59.3	56.7	54.0	52.3
58.0	—	—	—	—	—	—	—	—	—	59.7	57.0	54.4	52.7
58.2	—	—	—	—	—	—	—	—	—	60.0	57.4	54.8	53.0
58.4	—	—	—	—	—	—	—	—	—	—	57.8	55.2	53.4
58.6	—	—	—	—	—	—	—	—	—	—	58.2	55.6	53.8
58.8	—	—	—	—	—	—	—	—	—	—	58.6	55.9	54.1
59.0	—	—	—	—	—	—	—	—	—	—	59.0	56.3	54.5
59.2	—	—	—	—	—	—	—	—	—	—	59.4	56.7	54.9
59.4	—	—	—	—	—	—	—	—	—	—	59.8	57.1	55.2
59.6	—	—	—	—	—	—	—	—	—	—	60.0	57.5	55.6
59.8	—	—	—	—	—	—	—	—	—	—	—	57.9	56.0
60.0	—	—	—	—	—	—	—	—	—	—	—	58.3	56.4

注：表中未注明的测区混凝土强度换算值为小于 10 MPa 或大于 60MPa。

### 8.4 Table of Schnell (Smoltczyk et al. 2001, p. 122)

Spalte	a		b		c				d			e		f			g			h		i
	Bodenart		Boden- gruppe nach DIN 18196		Korngrößen- verteilung		Ungleich- körnig- keitszahl		Zustandsgrenzen des Kornanteils <0,4 mm			Wichte		Proctor- werte		Zusammendrückbarkeit $E_s = a \left( \frac{\sigma}{\sigma_b} \right)^c$			Scherparameter			Durch- lässigkeits- beiwert
Zeile Nr.			<0,06 mm [%]	<2,0 mm [%]	U [-]	w <sub>L</sub> [%]	w <sub>p</sub> [%]	ψ [%]	γ [kN/m³]	γ' [kN/m³]	w [%]	p <sub>p1</sub> [t/m²]	w <sub>Pr</sub> [%]	a [MN/m²]	c [-]	Δu	φ [°]	c [kN/m²]	φ <sub>r</sub> [°]	k [m/s]		
1	Kies, gleichkörnig		<5	<60	2 5	-	-	-	16,0 19,0	9,5 10,5	5 2	1,70 1,90	8 5	40 90	0,6 0,4	0	34 42	- -	32 35	2.10 <sup>-1</sup> 1.10 <sup>-2</sup>		
2	Kies, sandig, mit wenig Feinkorn		<5	<60	10 100	-	-	-	21,0 23,0	11,5 13,5	7 3	2,00 2,25	7 4	40 110	0,7 0,5	0	35 45	- -	32 35	1.10 <sup>-2</sup> 1.10 <sup>-6</sup>		
3	Kies, sandig, mit Schluff- oder Tonbeimengungen, die das Korngerüst nicht sprengen		8 15	<60	30 300	20 45	16 25	4 25	21,0 24,0	11,5 14,5	9 3	2,10 2,35	7 3	40 120	0,7 0,5	0 +	35 43	10 0	32 35	1.10 <sup>-5</sup> 1.10 <sup>-8</sup>		
4	Kies-Sand-Feinkornmisch. Das Feinkorn sprengt das Korngerüst		20 40	<60	100 1000	20 50	16 25	4 30	20,0 22,5	10,5 13,0	13 5	1,90 2,20	10 5	15 40	0,9 0,7	++	28 35	30 5	22 30	1.10 <sup>-8</sup> 1.10 <sup>-11</sup>		
5	Sand, gleichkörnig	Feinsand	<5	100	1,2 3	-	-	-	16,0 19,0	9,5 11,0	22 8	1,60 1,75	15 10	15 30	0,75 0,60	0	32 40	- -	30 32	2.10 <sup>-4</sup> 1.10 <sup>-5</sup>		
		Grobsand	<5	100	1,2 3	-	-	-	16,0 19,0	9,5 11,0	16 6	1,60 1,75	13 8	25 70	0,70 0,55	0	34 42	- -	30 34	5.10 <sup>-3</sup> 2.10 <sup>-4</sup>		
6	Sand, gut abgestuft und Sand, kiesig		<5	<60	6 15	-	-	-	18,0 21,0	10,0 12,0	11 5	1,90 2,15	10 6	20 60	0,70 0,55	0	33 41	- -	32 34	5.10 <sup>-4</sup> 2.10 <sup>-5</sup>		
7	Sand mit Feinkorn, das das Korngerüst nicht sprengt		8 15	>60	10 50	20 45	16 25	4 25	19,0 22,5	10,5 13,0	15 4	2,00 2,20	13 7	15 50	0,80 0,65	+	32 40	10 0	30 32	1.10 <sup>-5</sup> 1.10 <sup>-7</sup>		
8	Sand mit Feinkorn, das das Korngerüst sprengt		20 40	>60	30 300	20 50	16 30	4 30	18,0 21,5	9,0 11,0	20 8	1,70 2,00	18 12	5 25	0,90 0,75	++	25 32	50 10	22 30	1.10 <sup>-7</sup> 1.10 <sup>-10</sup>		
9	Schluff, gering plastisch		>50	>80	5 50	25 35	20 26	4 11	17,5 21,0	9,5 11,0	28 15	1,60 1,80	22 15	4 11	0,80 0,60	+	28 35	20 5	25 30	1.10 <sup>-5</sup> 1.10 <sup>-8</sup>		
10	Schluff, mittel- und hoch plastisch		>80	100	5 50	35 50	22 23	7 20	17,0 20,0	8,5 10,5	35 20	1,55 1,75	23 16	3 7	0,90 0,70	++	25 33	30 10	22 29	2.10 <sup>-6</sup> 1.10 <sup>-9</sup>		
11	Ton, gering plastisch		>60	100	6 20	25 35	15 22	7 16	19,0 22,0	9,5 12,0	28 14	1,65 1,85	20 14	2 5	1,00 0,90	++	24 32	60 15	20 26	1.10 <sup>-7</sup> 2.10 <sup>-9</sup>		
12	Ton, mittel plastisch		>90	100	5 40	40 50	18 25	16 28	18,0 21,0	8,5 11,0	38 18	1,55 1,75	23 17	1 3	1,00 0,95	++	20 30	80 20	10 20	5.10 <sup>-8</sup> 1.10 <sup>-10</sup>		

